

**Effects of Subsurface Physical Barrier
and Artificial Recharge on Seawater
Intrusion in Coastal Aquifers**

(海岸帯水層における海水侵入に及ぼす
地下止水壁と人工涵養の効果)

Roger Apuntar Luyun Jr.

(ロジャー アプンタールユン ジュニア)

A dissertation presented to the United Graduate School of
Agricultural Sciences, Kagoshima University
in partial fulfillment of the requirements
for the degree of
Doctor of Philosophy

2010

*To my loving wife, Lov, our children Iya, Isa, JM, Ana
and my mother, Patricia, my eternal source of
love, joy and inspiration*

Biographical Sketch

The author was born on April 18, 1972 at Tanauan, Batangas as the second among four children of his namesake Roger Luyun (†) and the former Patricia Apuntar. He finished his elementary education at the Our Lady of Fatima Academy in 1984 and his high school at the Colegio de San Juan de Letran, Manila in 1988. He entered the University of the Philippines Los Baños that same year and graduated with a B.S. Agricultural Engineering degree in 1993. After passing the government licensure exam he worked at the university as an Engineer, then University Researcher. He was a part of various national projects such as the STW Irrigation Project and the Comprehensive Irrigation Research and Development Umbrella Program of the Department of Agriculture. He pursued graduate studies part-time and obtained his M.S. Agricultural Engineering degree at the same university in 2003 with the thesis “Evaluation of the effects of partially penetrating shallow tubewells in a confined aquifer.” He became a faculty member at the Land and Water Resources Division, Institute of Agricultural Engineering, College of Engineering and Agro-Industrial Technology in 2005.

He obtained a Japanese Ministry of Education, Culture, Sports, Science and Technology (Monbukagakusho) scholarship to study in Japan in 2006 and entered the United Graduate School of Agricultural Sciences, Kagoshima University. This dissertation presents the author’s research for his Doctor of Philosophy degree.

He is happily married to the former Lov Vasquez, with whom he has four adoring children, Patricia Marie, Elisa Marie, John Matthew and Johanna Marie.

Abstract

Seawater intrusion is often a major constraint to optimal use of fresh groundwater from coastal aquifers. Excessive groundwater abstraction to meet growing demands from an increasing coastal population and the expected rise in mean sea level from global warming will cause seawater to encroach farther inland and threaten the available groundwater supply. The installation of subsurface physical barriers and the application of artificial recharges are among several countermeasures proposed to control seawater intrusion into unconfined coastal aquifers. In this research laboratory-scale experiments and numerical simulations were performed to determine the effectiveness of these control methods. The physical barriers examined were subsurface dams and partially penetrating flow barriers, while the artificial recharge methods included recharge ponds and recharge wells.

In the study of subsurface dams, the dynamics of residual saltwater after cutoff wall installation was investigated. Experimental and numerical results show that the residual saltwater trapped in storage areas of cutoff walls is completely flushed out by the freshwater flow from inland. This phenomenon proves that subsurface dams are very effective not only in preventing saltwater intrusion but also in reclaiming previously saline-intruded coastal aquifers for freshwater storage. Results also show that residual saltwater is flushed if the wall crest exceeds the thickness of the saltwater wedge at that location. These results imply that there is a potential for construction cost savings by installing shorter subsurface dams.

In the study of subsurface flow barriers, the behavior of the saltwater wedge resulting from different barrier penetration depths and locations was analyzed. Results show that more effective saltwater repulsion can be achieved with deeper barrier penetration and at locations closer to the coast. Where the barrier is installed landward of the original toe position, however, saltwater intrusion increases with deeper barrier penetration. Saltwater repulsion due to flow barrier installation was linearly related to the horizontal barrier location and a polynomial function of barrier penetration depth. For the given boundary condition, a generalized equation relating these design parameters was developed. This equation can be used to determine the theoretical saltwater repulsion that could be achieved by subsurface flow barriers of specific depth and location relative to a saltwater wedge toe.

In the artificial recharge studies, the effects of location and mode of application of recharge on saltwater behavior were analyzed. Results show that more effective saltwater repulsion can be achieved if recharge is applied near the saltwater toe. Recharge becomes less effective if applied farther and higher from the toe. These findings imply that, for the same recharge rate, recharge wells are more effective than recharge ponds in repulsing saltwater intrusion. For recharge ponds, the most effective location would be above the toe because of the increased pressure head created by the recharge water. Results from recharge wells also show that for the same recharge rate, point injection achieved about the same saltwater repulsion as line application.

Table of Contents

List of Figures	ix
List of Tables	xii
1 Introduction	1
1.1 Statement of the Problem.....	2
1.2 Seawater Intrusion Control Methods.....	3
1.2.1 Subsurface Physical Barrier.....	5
1.2.2 Artificial Recharge.....	10
1.3 Objectives of the Study.....	14
1.4 Overview of the Dissertation.....	15
2 Groundwater Flow and Solute Transport	17
2.1 Overview.....	18
2.2 Groundwater Flow Equation.....	20
2.3 Solute Transport Equation.....	23
2.4 SEAWAT Code.....	25
2.5 Numerical Simulation Parameters.....	25
3 Effects of Subsurface Physical Barriers on Seawater Intrusion	29
3.1 Introduction.....	30
3.2 Laboratory Approach.....	33
3.2.1 Experimental Setup.....	33

Table of Contents

3.2.2	Experimental Procedure.....	38
3.3	Experimental Results and Discussion.....	40
3.3.1	Subsurface Dam Experiment.....	40
3.3.2	Subsurface Flow Barrier Experiment.....	46
3.4	Numerical Approach.....	50
3.4.1	Subsurface Dam Numerical Parameters.....	50
3.4.2	Subsurface Flow Barrier Numerical Parameters.....	55
3.5	Subsurface Dam Numerical Results and Discussion.....	57
3.5.1	Advancing Saltwater Intrusion Wedge.....	57
3.5.2	Retreating Residual Saltwater.....	60
3.5.3	Discussion of Model Results.....	61
3.5.4	Effect of Cutoff Wall Height.....	67
3.6	Subsurface Flow Barrier Numerical Results and Discussion.....	68
3.7	Conclusion.....	77
4	Effects of Artificial Recharge on Seawater Intrusion	79
4.1	Introduction.....	80
4.2	Laboratory Approach.....	82
4.2.1	Experimental Setup.....	82
4.2.2	Experimental Procedure.....	84
4.3	Experimental Results and Discussion.....	87
4.3.1	Recharge Pond Experiment.....	87
4.3.2	Recharge Well Experiment.....	90
4.4	Numerical Approach.....	96

4.5	Numerical Results and Discussion.....	99
4.6	Conclusion.....	104
5	General Conclusion and Recommendations	105
	References	110
	Acknowledgement	122
	Appendix A Steady State Simulation Results for the Study of Subsurface Flow Barriers.....	124
A.1	Horizontal Barrier Location $x_b = 5$ cm.....	124
A.2	Horizontal Barrier Location $x_b = 10$ cm.....	126
A.3	Horizontal Barrier Location $x_b = 20$ cm.....	127
A.4	Horizontal Barrier Location $x_b = 30$ cm.....	128
A.5	Horizontal Barrier Location $x_b = 40$ cm.....	129
A.6	Horizontal Barrier Location $x_b = 50$ cm.....	130
	Appendix B Steady State Simulation Results for the Study of Recharge Wells	131
B.1	Point Injection at Different Locations.....	131
B.2	Line Injection at Different Horizontal Locations.....	136
	Appendix C Japanese Abstract (日本語要旨)	138

List of Figures

1.1	An illustration of a subsurface dam in an unconfined coastal aquifer with the cutoff wall base imbedded into the impervious layer at the bottom of the aquifer.....	6
1.2	An illustration of a subsurface flow barrier partially imbedded in an unconfined coastal aquifer.....	7
1.3	An illustration of artificial recharge application from a recharge pond in an unconfined coastal aquifer.....	12
1.4	An illustration of artificial recharge injection through a recharge well in an unconfined coastal aquifer.....	13
3.1	Schematic diagram of the experimental setup for the subsurface physical barrier experiments.....	34
3.2	Saltwater in 40 L barrels made from commercial salt dissolved in tap water.....	36
3.3	Red food color used to dye the saltwater.....	36
3.4	Akanuma hydrometers for (a) freshwater and (b) saltwater.....	36
3.5	WTW-LF330 conductivity meter.....	36
3.6	Small centrifugal pumps used to circulate the (a) saltwater and (b) freshwater.....	37
3.7	Experimental subsurface barriers: (a) 20 cm cutoff wall, (b) 40 cm cutoff wall and (c) shutoff wall.....	37
3.8	Behavior of the residual saltwater before and after installation of 40 cm cutoff wall.....	42

List of Figures

3.9	Behavior of the residual saltwater before and after installation of 20 cm cutoff wall.....	43
3.10	Comparison of the transient position of the saltwater wedge toe for the 40 and 20 cm cutoff wall experiments.....	45
3.11	Steady state experimental results after installation of flow barriers at different penetration depths.....	47
3.12	Comparison of repulsion ratio (R) values from experiment ($x_b = 20$ cm) and Equation 3.2 for different penetration ratio, d_b/h_s	51
3.13	Initial and boundary conditions for the subsurface physical barrier numerical simulations.....	52
3.14	Comparison of model-predicted transient positions of the intruding saltwater wedge with experimental data for Case 1 (1.0 cm grid).....	58
3.15	Comparison of model-predicted transient positions of the intruding saltwater wedge with experimental data for Case 2 (0.5 cm grid).....	59
3.16	Comparison of model-predicted transient positions of the residual saltwater with experimental data for Case 1 (1.0 cm grid).....	62
3.17	Comparison of model-predicted transient positions of the residual saltwater with experimental data for Case 2 (0.5 cm grid).....	63
3.18	Comparison of experimental and numerical results for the 20 cm cutoff wall.....	65
3.19	Steady state model results for 20, 10, 9 and 5 cm cutoff walls.....	69
3.20	Numerical simulation of experimental flow barrier with penetration depth of 11 cm.....	70
3.21	Repulsion ratio ($R = (L-L_0)/L_0$) with respect to barrier penetration ratio (d_b/h_s).....	72
3.22	Repulsion ratio ($R = (L-L_0)/L_0$) with respect to barrier horizontal location ($1 - x_b/L_0$).....	73

List of Figures

3.23	Repulsion ratio ($R = (L_0 - L)/L_0$) with respect to horizontal barrier location ($1 - x_b/L_0$) and penetration ratio (d_b/h_s) as computed from Equation 3.4....	76
4.1	Schematic diagram of the experimental setup for the artificial recharge experiments.....	83
4.2	Horiba ES-51 conductivity meter.....	85
4.3	Blue food color used to dye the freshwater recharge.....	85
4.4	Behavior of the saltwater wedge after application of 20% surface recharge (Case 1).....	88
4.5	Behavior of the saltwater wedge after application of 40% surface recharge (Case 2).....	89
4.6	Retreat in saltwater wedge toe position with time after recharge application and the corresponding saltwater repulsion R	91
4.7	Behavior of the saltwater wedge after application of 20% injection recharge (Case 1).....	92
4.8	Behavior of the saltwater wedge after application of 40% injection recharge (Case 2).....	93
4.9	Initial and boundary conditions for the artificial recharge numerical simulations.....	97
4.10	Steady state model results for recharge well (Case 1).....	100
4.11	Percentage repulsion of seawater intrusion based on location of recharge well injection points.....	101

List of Tables

3.1	Numerical simulation parameters for subsurface dam.....	53
3.2	Numerical simulation parameters for subsurface flow barrier.....	56
4.1	Experimental parameters for artificial recharge.....	87
4.2	Numerical simulation parameters for recharge wells.....	98

Chapter

1

Introduction

1.1 Statement of the Problem

Coastal groundwater is a major source of freshwater supplies in many areas around the world. In mountainous, archipelagic places like Japan and the Philippines where major communities and agricultural areas are located near coastlines, coastal groundwater is vital for domestic, agricultural and industrial water supplies. About 70% of the world's population lives in coastal zones (Bear and Cheng, 1999) and this figure is likely to increase in the near future. In response to deteriorating quantity and quality of available surface water resources, the demand for fresh groundwater will increase dramatically. Excessive groundwater abstraction to meet growing demands has led to large-scale lowering of groundwater tables and decreased seaward flow of freshwater. Consequently, the freshwater-saltwater interface advance far enough inland and threaten the available fresh groundwater supply. This mass inflow of saline water in an aquifer system is referred to as seawater or saltwater intrusion.

Seawater intrusion is often a major constraint to optimal utilization of fresh groundwater from coastal aquifers. These aquifers are further threatened by an accelerated rise in global sea level resulting from climate change. The Intergovernmental Panel on Climate Change (IPCC) estimates that global sea level may rise by an additional 0.09 to 0.88 m by 2100 (IPCC, 2001a). Saltwater intrusion would become more serious and threaten Japan coastal zones and sandy beaches. Large delta regions of Bangladesh, Myanmar, Vietnam and Thailand, and the low-lying areas of Indonesia, Malaysia and the Philippines are especially at risk (IPCC, 2001b).

Seawater intrusion occurs in many coastal and deltaic areas around the world. Because it occurs underground and is practically invisible, there is not enough information as to the distribution and extent of encroachment. Most often, the problem is already substantial before actual detection and consequently, there is insufficient planning on measures to be taken and their effects. When saltwater travels inland to production wells, underground water supplies become useless. In agriculture, this could cause soil salinity problems resulting to poor crop yields and the substitution of more salt-tolerant crops over indigenous crops. Once an aquifer is contaminated, corrective measures are difficult and the costs prohibitive. The contaminated aquifer is sometimes abandoned resulting in the loss of a precious groundwater resource. Thus, present-day and future water supply engineers and managers face the challenges of optimal exploitation of fresh groundwater and the control of seawater intrusion (Bear and Cheng, 1999).

1.2 Seawater Intrusion Control Methods

The flows of fresh and saline groundwater in coastal aquifers are determined by boundary conditions, such as surface water levels, and rates of recharge and abstraction. Changes on the boundary conditions, either due to natural causes like relative sea level rise, or human activities such as over-pumping or controlling surface water levels, will affect the degree and control of seawater intrusion. The importance of development and conservation of coastal aquifers have led to researches towards methods for prevention and control of seawater intrusion. Several control strategies to prevent or control seawater intrusion have been suggested (e.g., Todd, 1959; van Dam, 1999; Oude Essink, 2001). These may be summarized into the following methods: (1) reduction or

rearrangement of the pattern of groundwater extraction; (2) artificial recharge from spreading basins or recharge wells; (3) maintenance of a freshwater ridge by freshwater injection along the coast; (4) development of a pumping trough by saltwater extraction adjacent to the coast; (5) construction of artificial subsurface barriers; and (6) land reclamation. Abarca et al. (2006) grouped these countermeasures into demand actions, recharge actions, relocation of pumping wells, and additional engineering solutions.

Voluntary reduction of pumping demand on a coastal aquifer by water users enables the groundwater levels to rise and reduce seawater intrusion. This could be expected only if supplemental water from other sources can be made available at comparable costs. Modifying pumping practice or relocating pumping wells further inland will prevent excessive upconing near the coast and reduce seawater intrusion. The production wells can also be spread throughout the groundwater basin to reduce concentrated drawdown in localized pumping zones. These methods aim to reduce the magnitude of the cone of depression and maintain a groundwater level with seaward hydraulic gradient thus preventing the saltwater flow towards production wells. Extraction of saline or brackish groundwater can be done before it reaches the production wells. However, this could result in undesirably low piezometric heads and the disposal of abstracted saline groundwater can also pose a problem. Another method combines extraction wells that withdraw saline water and injection wells that recharge reclaimed freshwater. Coastal land reclamation is one engineering solution proposed to create a foreland where a freshwater body may develop which could delay the inflow of saline groundwater. Analytical studies show that after reclamation, the water table rises and the saltwater wedge move seaward (Guo and Jiao, 2007).

Two saltwater intrusion control methods applicable to coastal unconfined aquifers are presented in this research. These are the construction of subsurface physical barriers and the application of artificial recharge. These countermeasures are currently applied in Japan and in many parts of the world. Detailed descriptions of these methods are presented in the following sections. The effectiveness of these countermeasures can be assessed through field studies, laboratory experiments and numerical simulations. Field studies however are difficult, time-consuming and prohibitively expensive to perform. Whereas laboratory experiments and numerical simulation models provide a relatively convenient and inexpensive means to locate the freshwater–saltwater interface and examine saltwater behavior after installation of the countermeasures.

1.2.1 Subsurface Physical Barrier

Subsurface physical barriers can be defined as underground semi-impervious or impervious structures constructed in a coastal aquifer to retain groundwater, prevent seawater intrusion, and increase the groundwater storage capacity. They can be of two types depending on the opening for fresh groundwater flow towards the coast. Subsurface dams are storage dams with a base imbedded on the aquifer bedrock and an open crest at the upper part of the aquifer (Figure 1.1). Subsurface flow barriers (Figure 1.2), on the other hand, are not meant for storage but may simply be physical barriers inserted across the flow direction to modify the flow field. Flow barriers partially penetrate the aquifer and have openings at the lower aquifer layer. They are meant primarily for increasing groundwater level and seawater intrusion control.

Subsurface dams were constructed as far back as the Roman times in Sardinia and by ancient civilizations in North Africa (Hanson and Nilsson, 1986). Recently, small–

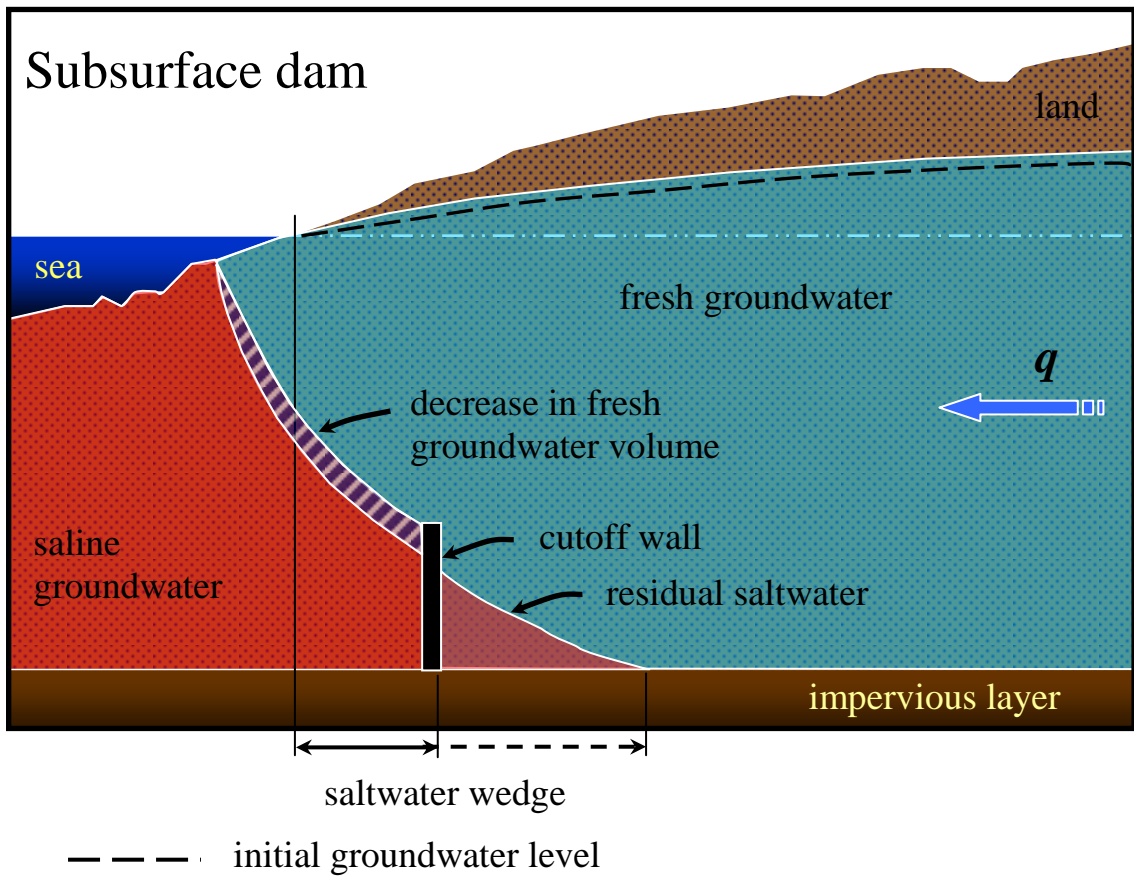


Figure 1.1 An illustration of a subsurface dam in an unconfined coastal aquifer with the cutoff wall base imbedded into the impervious layer at the bottom of the aquifer.

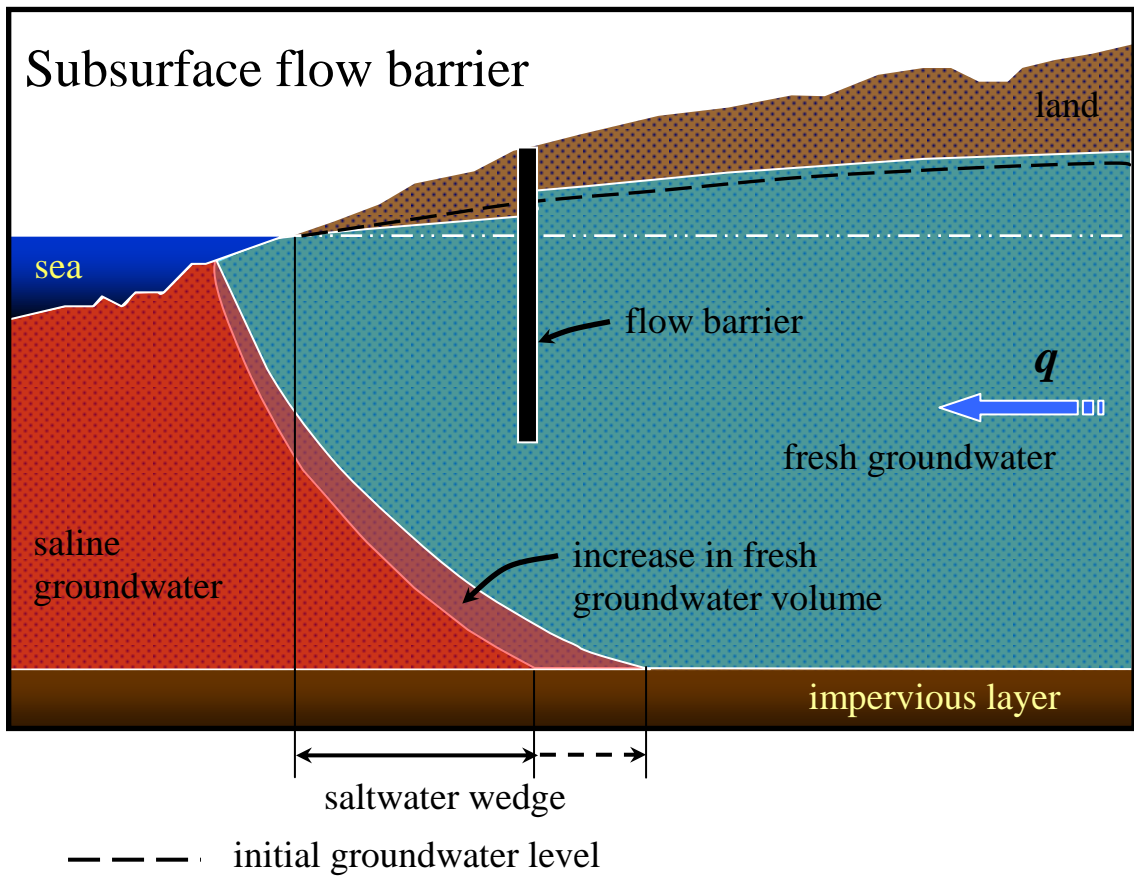


Figure 1.2 An illustration of a subsurface flow barrier partially imbedded in an unconfined coastal aquifer.

scale groundwater dams have been built in Southern and Eastern Africa, India, Brazil and Japan. Japan has become the leading proponent of subsurface dam technology. Prof. Kachi first proposed full-scale subsurface dam development in Japan in 1945 but the first structure was not built until 1974, on Kabashima Island off the coast of Nagasaki (Shibasaki et al., 1995). It had a wall height of 24.8 m, a crest length of 58.5 m, and was installed using grouting methods. Since then the development of subsurface dams has advanced progressively. On Miyakojima Island for example, the Komesu dam has a crest height of 70 m, while the Fukuzato dam has a crest length of 2.9 km and a reservoir capacity of more than 10 million m³. There are now about 15 subsurface dams in Japan, seven of which were specifically constructed to prevent saltwater intrusion into coastal aquifers (Japan Green Resources Agency, 2004). There is a dearth of information on existing partially penetrating flow barriers constructed for seawater control. However, the advantages and disadvantages, as well as, design requirements may be patterned after subsurface dams.

Nishigaki et al. (2004) stated that the advantages of subsurface dams compared to conventional surface dams are: (a) evaporation losses are low; (b) there is no reduction of storage volume due to silting; (c) part of the abstracted water returns to storage since the pumped water is spread upstream; (d) good water quality and less susceptible to pollution and health hazards; (e) there is no submergence of houses and land; (f) there is no danger of dam collapse; and (g) the construction cost can be lowered by thinning the cutoff wall, provided it satisfies the permeability requirements. The disadvantages are: (a) low downstream flow may lead to land subsidence and/or seawater intrusion; (b) groundwater storage and retention may cause liquefaction and other seismic activities in the surrounding aquifer; (c) changes in groundwater levels both upstream and

downstream may cause changes in soil fauna and flora; (d) groundwater storage and retention may cause increase in soil pore pressure resulting to increased uplift pressure on infrastructures; (e) the dam capacity is low compared to surface dams; (f) accurate estimation of groundwater reserve volume could be difficult; and (g) dam construction quality assessment is difficult.

The viability of a subsurface barrier depends upon topographical and hydrogeological factors. Subsurface dams are best sited in well-defined and narrow valleys underlain by a bedrock or low permeability formation. This reduces construction costs and makes it possible to assess storage volumes and to control possible seepage losses. Hanson and Nilsson (1986) reported that areas with 1–5% slope are the most feasible. Subsurface barriers are preferably constructed in high hydraulic conductivity sites such as sand and gravel river beds, weathered zones, and deep alluvial layers.

Since the installation of subsurface barriers involves underground works, the cost of construction becomes fairly high compared to other methods. Although many groundwater engineers believe that construction cost is a major constraint to building a barrier, Japanese engineers have succeeded in reducing the cost by utilizing advanced construction procedures such as the soil mixing wall (SMW) or trench-cutting remixing deep wall (TRD) methods for the cutoff walls. In the long run, low operation expenses and maintenance costs may balance out the high cost of constructing subsurface barriers.

1.2.2 Artificial Recharge

Artificial recharge of groundwater may be defined as man's planned operation of transferring water from ground surface into aquifers (Bear, 1979). This is apart from the natural replenishment. While natural recharge is uncontrolled, artificial recharge is a controlled input such that the quantity, quality, location and time of artificial recharge are decision variables. Artificial recharge of groundwater is applied for many reasons such as to increase the sustainable yield, to control the groundwater table or the piezometric level, to increase the volume of fresh groundwater available for emergencies, and/or as a barrier against inflow of saline groundwater (van Dam, 1999). This can be realized by increased infiltration at the land surface or surface waters through recharge ponds (Figure 1.3), or by recharge wells with well screens in aquifers at any desired depth (Figure 1.4). Both techniques can be applied for the recharge of phreatic aquifers. Confined and semi-confined aquifers can not be recharged from the land surface due to the high hydraulic resistance between the recharge source and the aquifer to be recharged.

The choice of recharge method depends on several factors, such as water availability and its quality, soil and aquifer types, topographical and geological conditions, among others. Recharge ponds and reservoirs are specific surface recharge sources. Stream channels, as well as irrigation and drainage channel networks, are often used in water spreading method. One important factor in the choice of surface spreading basin is the cost and availability of land, particularly in urban areas. Consideration should also be given to the distance between the recharge zone and the areas of groundwater exploitation. For soil type, aquifers with gravel, or gravel and sand are

strongly recommended. The infiltration rate may over time drop below the design value caused by the filling of soil pores by water, swelling, and clogging. Bear (1979) enumerated the causes of clogging in saturated soil as follows: (a) retention of suspended solids; (b) growth of algae and bacteria; (c) release of entrained or dissolved gases from water; and (d) chemical reactions between dissolved solids and soil particles and/or the native water present in the void space. As a result, spreading operation method works effectively only at the outset and the recharge rate even from a recharge ponds with constant water level will almost invariably declines with time (Freeze and Cherry, 1979).

Recharge wells or injection wells may be ordinary pumping wells or one specially designed for this purpose. Recharge wells remove the problem of scarcity and high cost of land as in water spreading techniques but they may also suffer from clogging problems (Bear, 1979). Recharge water more often carries fine material such as silt that may clog the well screen and the aquifer itself. Dissolved air carried together with recharge water may also lessen the aquifer hydraulic conductivity. Bacteria, which can also be found in recharge water, may grow quickly and eventually reduce the filtering area of the well screen. Recharge water also contains chemical constituents that induce flocculation, which is described as a reaction between high sodium-ion content and colloidal soil particles (Bear, 1979). Despite the disadvantages however, this method remains as a primary option in controlling seawater intrusion.

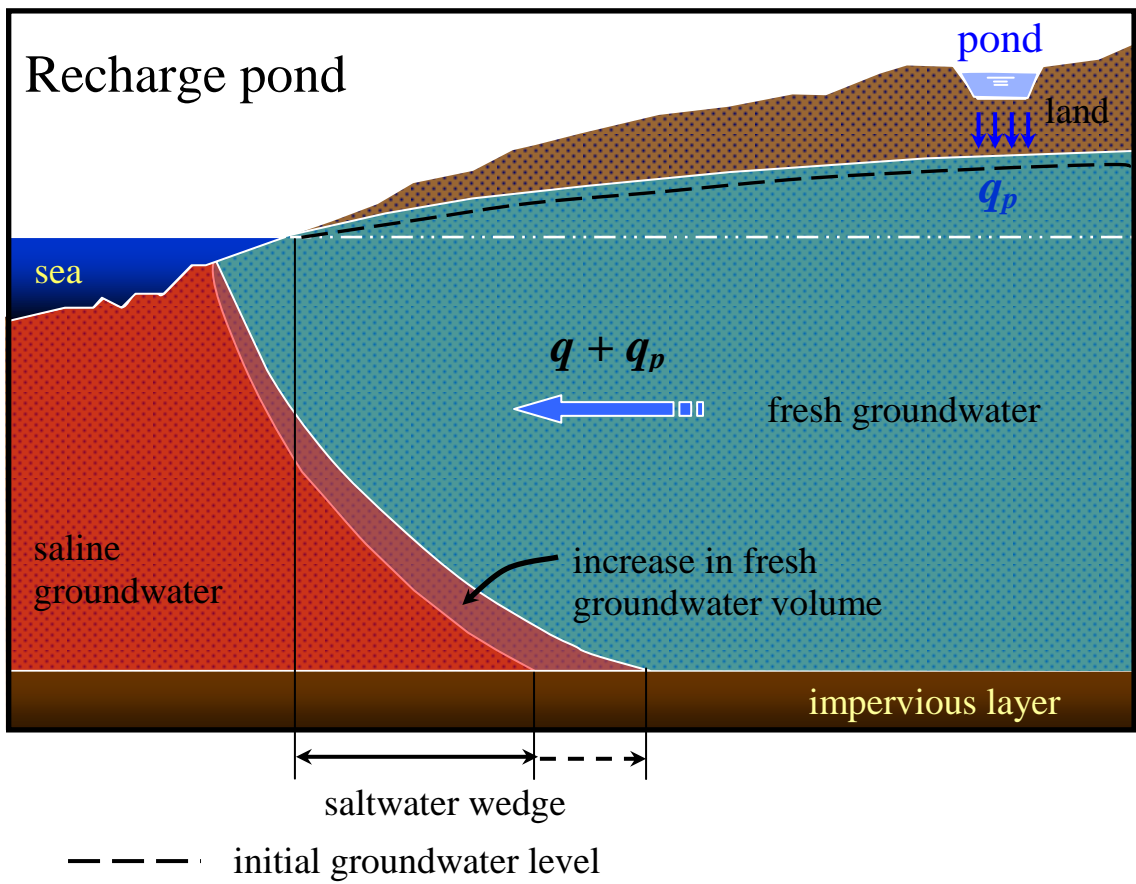


Figure 1.3 An illustration of artificial recharge application from a recharge pond in an unconfined coastal aquifer.

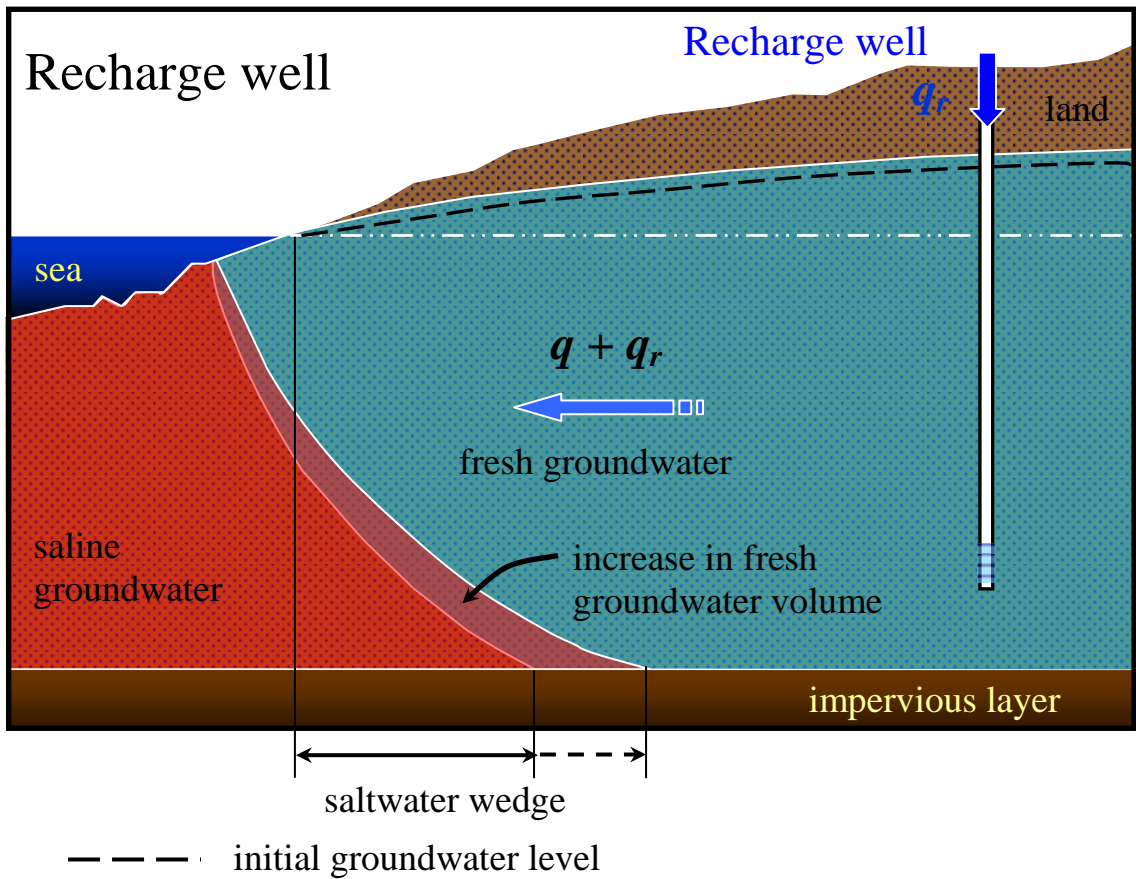


Figure 1.4 An illustration of artificial recharge injection through a recharge well in an unconfined coastal aquifer.

1.3 Objectives of the Study

The main objective of the research is to examine the effectiveness of two general control methods for seawater intrusion. These are the construction of subsurface physical barriers and the application of artificial recharge. from both recharge ponds and recharge wells. The physical barriers examined were subsurface dams and partially penetrating flow barriers, while the artificial recharge methods included recharge ponds and recharge wells. Saltwater dynamics after installation of each control method were investigated. The research involves laboratory-scale experiments on flow tanks specifically constructed to simulate coastal unconfined aquifers with subsurface dams, flow barriers, recharge ponds and recharge wells. Numerical simulations were also performed to simulate the experiments and use the model results to analyze the flow dynamics involved. A state-of-the-art numerical model that permits the solution to equations governing variable-density groundwater flow and solute transport was used for these simulations. Specific design parameters were tested for each control method to achieve the following objectives:

- (1) To study the effect of cutoff wall height on residual saltwater removal in subsurface dams;
- (2) To study the effects of location and penetration depth of flow barriers on seawater repulsion;
- (3) To study the effects of recharge rate from recharge ponds on seawater repulsion, and;
- (4) To study the effects of location and mode of application of recharge wells on seawater repulsion.

1.4 Overview of the Dissertation

The whole manuscript consists of five chapters. Chapter 1 provides a general introduction to the current worldwide problem of seawater intrusion and the need for several countermeasures to control its effects. Several seawater intrusion control methods were discussed with emphasis on the characteristics and advantages of the control methods under consideration in this research. The general objectives of the research and the specific objectives required for each study were then enumerated.

Chapter 2 presents a brief review of relevant contributions to the study of seawater intrusion, including the development of numerical simulations to solve various groundwater problems. Several computer codes currently being used to simulate variable-density groundwater flow were enumerated. The governing mathematical equations for the variable-density groundwater flow and solute transport were discussed. The SEAWAT code, which was used to simulate the experiments in this research, was presented here. The numerical simulation aspect of the research, including the various parameters used in the simulation, was also discussed in this chapter.

Chapter 3 deals with the study on the effects of subsurface physical barriers on seawater intrusion. This main study is further divided into the study of subsurface dams and the study of subsurface flow barriers. A review of related literatures pertaining to the subsurface physical barriers is first presented. The experimental setup and methodology for the two studies are the same and discussed concurrently but the experimental results for each study were discussed separately. The numerical simulation procedures, model results and analyses for each study were also discussed and separately. Finally the conclusions were presented.

Chapter 4 presents the effects of artificial recharge application on seawater intrusion. This chapter is also divided into the study of recharge ponds and the study of recharge wells. A review of related literatures pertaining to artificial recharge application is first presented. The two studies also share a common experimental setup and methodology but in contrast to the previous chapter, the experimental results for the two studies were compared. The numerical procedures, results and analyses for recharge wells were then discussed and thereafter the conclusions were summarized.

The last chapter summarizes the main contributions of this dissertation. Some future research works related to the numerical aspects of the research and on-field investigation were then recommended.

Chapter

2

**Groundwater Flow and
Solute Transport**

2.1 Overview

In general, coastal aquifers have a hydraulic gradient with the sea and fresh groundwater comes in contact with seawater as it discharges into the sea. Because seawater and freshwater have different densities, a boundary surface or interface, is formed wherever the two fluids meet. The denser seawater usually takes the form of a wedge underneath the lighter freshwater flowing to the sea. This wedge develops due to both density driven flow and hydrodynamic dispersion.

Freshwater and seawater are actually miscible fluids and upon contact they form a transition or mixing zone, across which the density of the mixed water varies from that of freshwater to that of seawater. Under certain conditions, the width of this transition zone is small compared to the thickness of the aquifer such that an abrupt or sharp interface can be assumed to separate the regions occupied by the two fluids. The freshwater–saltwater interface position based on the abrupt interface was derived independently by W. Badon Ghyben in 1888 and B. Herzberg in 1901 (Todd, 1959; Bear, 1979). The so-called Ghyben–Herzberg relation assumes static equilibrium and a hydrostatic pressure distribution in a homogenous, unconfined coastal aquifer. This relation usually underestimates the interface position because the assumption of hydrostatic equilibrium with horizontal flow is no longer valid in the vicinity of the coastline near the outflow zone, but it offers a good approximation of the interface position.

Since this famous Ghyben–Herzberg relation, extensive research has been carried out and much progress has been made in understanding the theory of variable-density groundwater flow. Hubbert (1940) introduced the term hydraulic head relating the elevation of a sharp interface to freshwater heads measured on the interface and to the densities of the saltwater and freshwater, and provided a more realistic picture for steady state outflow to the sea. Henry (1964) developed a semi-analytical solution for the steady-state distribution of salt concentration under condition of a constant freshwater flux toward a sea boundary. The original Henry problem has undergone several revisions and corrections (e.g., Bues and Oltean, 2000; Croucher and O’Sullivan, 1995; Segol, 1994; Simpson and Clement, 2004). Several other analytical and semi-analytical solutions have been developed especially on the aspects of flow regime above the saltwater wedge, the variable density flow, and hydrodynamic dispersion (e.g., Bear, 1961; Dagan and Bear, 1968; Harleman and Rumer, 1963; Huyakorn et al., 1987; Ogata, 1970; Pinder and Cooper, 1970; Segol and Pinder, 1976; Segol et al., 1975; Strack, 1976). Numerous field investigations have also been conducted in many coastal aquifers, providing basis for understanding the complicated mechanisms that govern seawater intrusion (e.g., Konikow and Reilly, 1999; Stakelbeek, 1999; Melloul and Zeitoun, 1999; Sherif, 1999; Momii et al., 2005; Kim, 2006). Later on, intensified interest in groundwater quality and the rapid development of computer technology resulted in many numerical simulations relating to various groundwater problems. But despite the large amount of scientific literature about seawater intrusion, many challenges still remain (Simmons et al., 2001; Diersch and Kolditz, 2002; Simmons, 2005).

There is a wide range of computer codes that can be used to simulate variable-density groundwater flow. The United States Geological Survey (USGS) offers the

finite-element SUTRA code (Voss, 1984), and the finite-difference MOCDENISE (Sanford and Konikow, 1985), HST3D (Kipp, 1997) and the SEAWAT (Guo and Langevin, 2002) codes. Many other codes are available: FEFLOW (Diersch and Kolditz, 1998), ROCKFLOW (Kolditz et al., 1998), TVDT3D (Ackerer et al., 1999), METROPOL (Sauter et al., 1993), MVAEM (Strack, 1995), SWICHA (Huyakorn et al., 1987), SWIFT (Ward, 1991), and CODESA (Gambolati et al., 1999). A recent state-of-the-art of density-dependent flow modeling in porous media can be found in Diersch and Kolditz (2002).

The SEAWAT code was used to simulate the experiments in this research. The governing equations describing groundwater flow and solute transport in porous media as used by SEAWAT are presented here. The assumptions are that Darcy's law is valid, the diffusive approach to dispersive transport based on Fick's law can be applied, and isothermal conditions prevail.

2.2 Groundwater Flow Equation

The differential equation of groundwater flow in terms of head in a two-dimensional flow regime may be expressed as:

$$\frac{\partial}{\partial x} \left(K_x \frac{\partial h}{\partial x} \right) + \frac{\partial}{\partial z} \left(K_z \frac{\partial h}{\partial z} \right) + q_s = S_s \frac{\partial h}{\partial t} \quad (2.1)$$

where: h is the hydraulic head [L],

K_x, K_z are the hydraulic conductivities [$L T^{-1}$] aligned with the x and z directions,

q_s is the volumetric flow rate of sinks or sources per unit aquifer volume [T^{-1}],

S_s is the specific storage [L^{-1}], and

t is time [T].

In this equation, the seepage velocity is already accounted for by dividing the Darcy velocity with effective porosity, n [dimensionless]. The differential equation in terms of hydraulic head in Equation 2.1 is based on groundwater of uniform density. For variable-density conditions, the continuity equation is expressed based on mass conservation and can be written in vector form as:

$$\frac{\partial(n\rho)}{\partial t} + \nabla \cdot (\rho \mathbf{q}) = \rho_s \mathbf{q}_s \quad (2.2)$$

where: ∇ is the gradient operator $\frac{\partial}{\partial x} + \frac{\partial}{\partial z}$,

ρ and ρ_s are the densities of the fluid and solute, respectively [ML^{-3}], and

\mathbf{q} is the specific discharge [LT^{-1}], and

The general form of Darcy's law for variable-density conditions is (Bear, 1979):

$$\mathbf{q} = -\frac{k}{\mu} (\nabla p + \rho \mathbf{g} \nabla z) \quad (2.3)$$

where: k is the permeability tensor [L^2],

μ is the dynamic viscosity [$\text{ML}^{-1}\text{T}^{-1}$],

p is pressure [$\text{ML}^{-1}\text{T}^{-2}$],

\mathbf{g} is acceleration due to gravity [LT^{-2}] and

z is the vertical coordinate aligned with gravity.

SEAWAT follows the existing MODFLOW structure which is based on the equivalent freshwater head in a saline-groundwater environment. The head h [L]

expressed in terms of the saline aquifer and the equivalent freshwater head h_f [L] from the same level z above a given datum are given by:

$$h = \frac{p}{\rho g} + z \quad (2.4)$$

$$h_f = \frac{p}{\rho_f g} + z \quad (2.5)$$

Conversion between h and h_f can be made using the relation:

$$h_f = \frac{\rho}{\rho_f} h - \frac{\rho - \rho_f}{\rho_f} z \quad (2.6)$$

By solving Equation 2.5 for p and introducing the freshwater hydraulic conductivity tensor as $\mathbf{K}_f = k\rho_f g / \mu_f$ [LT^{-1}], Equation 2.3 may be rewritten as:

$$\mathbf{q} = -\mathbf{K}_f \frac{\mu_f}{\mu} \left(\nabla h_f + \frac{\rho - \rho_f}{\rho_f} \nabla z \right) \quad (2.7)$$

SEAWAT 2000 neglects the viscosity differences by approximating μ_f / μ to be

1. The final form of the flow equation solved by SEAWAT is obtained by substituting Equation 2.7 into Equation 2.2 and expanding the time derivative into the storage term and a term that accounts for volumetric expansion due to solute concentration changes (Guo and Langevin, 2002):

$$\nabla \cdot \left[\rho \mathbf{K}_f \left(\nabla h_f + \frac{\rho - \rho_f}{\rho} \nabla z \right) \right] = \rho S_{sf} \frac{\partial h_f}{\partial t} + n \frac{\partial \rho}{\partial C} \frac{\partial C}{\partial t} - \rho_s q_s \quad (2.8)$$

where: ρ_f is the freshwater density [ML^{-3}],

S_{sf} is the freshwater specific storage [L^{-1}] and

C is the concentration of the solute mass per unit volume of fluid [ML^{-3}].

2.3 Solute Transport Equation

The transport of solutes in the groundwater is described by the two-dimensional solute transport or advective–dispersive equation:

$$\begin{aligned} \frac{\partial(nC)}{\partial t} = & \frac{\partial}{\partial x} \left(nD_{xx} \frac{\partial C}{\partial x} + nD_{xz} \frac{\partial C}{\partial z} \right) - \frac{\partial(q_x C)}{\partial x} \\ & + \frac{\partial}{\partial z} \left(nD_{zx} \frac{\partial C}{\partial x} + nD_{zz} \frac{\partial C}{\partial z} \right) - \frac{\partial(q_z C)}{\partial z} + q_s C_s \end{aligned} \quad (2.9)$$

where: C_s is the concentration at the source or sink [ML^{-3}],

q_x and q_z are components of the Darcy velocity [LT^{-1}], and

D_{xx} , D_{xz} , D_{zz} and D_{zx} are the components of the hydrodynamic dispersion coefficient [L^2T^{-1}] expressed as:

$$D_{xx} = \alpha_L \frac{v_x^2}{|v|} + \alpha_T \frac{v_z^2}{|v|} + D^* \quad (2.10)$$

$$D_{zz} = \alpha_L \frac{v_z^2}{|v|} + \alpha_T \frac{v_x^2}{|v|} + D^* \quad (2.11)$$

$$D_{xz} = D_{zx} = (\alpha_L - \alpha_T) \frac{v_x v_z}{|v|} \quad (2.12)$$

where: α_L is the longitudinal dispersivity [L] in the direction of flow,

α_T is the transverse dispersivity [L] normal to the flow,

v_x and v_z are the seepage velocity components [LT^{-1}],

$|v| = \sqrt{v_x^2 + v_z^2}$, and

D^* is the molecular diffusion coefficient [L^2T^{-1}].

For a given principal direction, the first term on the right-hand side of Equation 2.9 represents the change in concentration of solutes due to hydrodynamic dispersion. The second term represents the effect of advective transport which is the movement of solute due to groundwater seepage flow. The last term represents the addition or removal of solutes due to sources or sinks.

Hydrodynamic dispersion is defined as the combined effect of mechanical dispersion and molecular diffusion. Mechanical dispersion is the spreading of solute caused by velocity variations in the macroscopic scale and depends on both fluid flow and pore characteristics through which the fluid flow. Molecular diffusion is caused by the random movement of molecules in a fluid and depends on concentration gradient, and the properties of both the fluid and the soil.

The MT3DMS program (Zheng and Wang, 1999) is used by SEAWAT to solve the solute transport equation shown in Equation 2.9 expressed here in vector form as:

$$\frac{\partial(nC)}{\partial t} = \nabla \cdot (nD \cdot \nabla C) - \nabla \cdot (qC) - q_s C_s \quad (2.13)$$

Equation 2.8 and 2.13 are coupled in variable-density groundwater systems since fluid density is a function of solute concentration, transport is dependent on the flow field, and the flow equation incorporates changes in concentration. The relationship between fluid density and solute concentration expressed as a linear function was developed by Baxter and Wallace (Guo and Langevin, 2002):

$$\rho = \rho_f + \frac{\partial \rho}{\partial C} C \quad (2.14)$$

More detailed discussions on the derivations of the above equations using different nomenclatures can be found in groundwater texts (e.g. Bear, 1972; Freeze and Cherry, 1979; Zheng and Bennet, 2002).

2.4 SEAWAT Code

The finite difference SEAWAT 2000 (Langevin et al., 2003), developed to simulate three-dimensional, variable-density, transient groundwater flow in porous media, was used to numerically simulate the experiments. SEAWAT combines the modified MODFLOW (Harbaugh, et al., 2000) and MT3DMS (Zheng and Wang, 1999) into a single program that solves the coupled groundwater flow and solute-transport equations. The SEAWAT code has been tested and proven to simulate common benchmark problems involving variable-density groundwater flow, such as the two box problems, the Henry problem, the Elder problem, and the HYDROCOIN problem (Guo and Langevin, 2002; Langevin et al., 2003). Two additional tests, the modified Henry problem (Simpson and Clement, 2004) and the saltpool problem (Johannsen et al., 2002; Oswald and Kinzelbach, 2004), were presented by Langevin and Guo (2006). Bakker et al. (2004) and Goswami and Clement (2007) have tested SEAWAT for their proposed benchmark problems for density-dependent groundwater flow and transport software code. Examples of SEAWAT applications have been presented in Langevin (2003) and Bauer et al. (2006), among others.

2.5 Numerical Simulation Parameters

The purpose of the numerical simulations was to check whether the experimental results were consistent with SEAWAT predictions, perform numerical simulations that

are not applicable in the experimental setup, and then use the model results to help explain the underlying phenomena. For each study, the simulation area in the two-dimensional vertical cross section was consistent with the flow tank dimensions. Constant head boundary conditions corresponding to hydrostatic pressure conditions were set at the freshwater and saltwater sides. A zero mass flux boundary condition was set at the top and bottom of the simulation area with no recharge at the top and an impermeable bottom. The saltwater concentration was specified as the point source concentration at the saltwater boundary in the Source/Sink Mixing (SSM) package. The block-centered finite-difference grid interval was set at $\Delta x = \Delta z = 0.5$ cm, except in the subsurface dam study where a grid interval of $\Delta x = \Delta z = 1.0$ cm was also used.

Parameter values for the numerical simulations are patterned from values measured during the experiments. A longitudinal dispersivity (α_L) of 0.12 cm, the nominal diameter of the glass beads, was set for the porous medium. The transverse dispersivity (α_T) was assumed to be 1/10 the longitudinal dispersivity (Johannsen et al., 2002; Langevin, 2003; Shoemaker, 2004; and Goswami and Clement, 2007). Two transient stress periods were set for all simulations. The first stress period involved the advancing front of the intruding saltwater wedge until it reach steady state. The head and concentration values obtained at each cell of the calculation domain after this initial simulation were used as the initial condition for the second stress period. This period started with the installation or application of the specific control methods.

Flow and transport were explicitly coupled for all the simulations. Upstream-weighted algorithm was used for internodal density calculation and the variable density water table correction was not applied. The Pre-conditioned Conjugate-Gradient (PCG)

package (Hill, 1990; Harbaugh et al., 2000) was employed for the flow equation where the preconditioning method was set to Cholesky. The Generalized Conjugate-Gradient (GCG) package (Zheng and Wang, 1999) was used for the dispersion and source terms of the transport equation. The third-order total variation diminishing or TVD scheme (Zheng and Wang, 1999) was used to solve the advection term in all simulations. The forward-tracking method of characteristics or MOC (Pinder and Cooper, 1970; Konikow and Bredehoeft, 1978) was also used in the subsurface dam simulations. The initial time step was set at 1×10^{-5} day and time-step lengths were calculated during the simulation using a Courant number of 0.1. In MOC, the 4th order Runge-Kutta algorithm was used for particle tracking near sources and sinks and the 1st order Euler algorithm elsewhere. The concentration weighting factor is 0.5, maximum number of particles is 500,000 and the negligible gradient (DCEPS) is set at 1×10^{-5} . Specifications for the different packages used in the simulations are listed in tables for each study.

The TVD methods are essentially higher-order finite-difference (or finite-volume) methods belonging to the Eulerian family of solution techniques. The term TVD refers to the property shared by these methods that the sum of concentration differences between adjacent nodes diminishes over successive transport steps. They are inherently mass conservative without excessive numerical dispersion, and essentially oscillation-free. In this method, the interface concentrations are determined through a third-order polynomial interpolation of nodal concentrations, supplemented by a universal flux limiting procedure to minimize unphysical oscillations which may occur if sharp concentration fronts are involved (Zheng and Wang, 1999).

MOC is based on the mixed Eulerian-Lagrangian approach and is well suited for sharp front problems (pure advection or largely advection-dominated problems) because it virtually eliminates numerical dispersion. In this scheme, a set of representative particles are generated in the finite-difference grid (cell), either randomly or in a fixed pattern. Each particle is assigned with spatial coordinates and concentration equal to that of the cell and the particles are tracked forward through the flow field using a particle tracking method. At the end of each time increment, the average concentration in each cell is evaluated from the concentrations of the moving particles located within the cell. Implemented with dynamic particle distribution, MOC is very efficient computationally for many practical problems where the contaminant plume occupies only a small fraction of the finite-difference grid, and the concentration field is changing rapidly only at sharp fronts. When the degree of advection dominance decreases, however, the number of moving particles needed by the MOC scheme can become very large for a three-dimensional simulation, pushing the memory requirement beyond the limits of many personal computers.

Compared to the standard finite-difference method, TVD schemes are generally much more accurate in solving advection-dominated problems, but with a greater computational burden. Compared to MOC, TVD schemes are not as effective in eliminating numerical dispersion while preserving concentration “peaks”, but their mass conservation property, smaller memory requirements, and some other advantages, make TVD schemes arguably the best compromise between the standard finite-difference method and the particle tracking based Lagrangian or mixed Eulerian-Lagrangian methods (Zheng and Wang, 1999; Zheng and Bennet, 2002).

Chapter

3

**Effects of Subsurface
Physical Barriers on
Seawater Intrusion**

3.1 Introduction

Subsurface dams are planned and constructed to store and control groundwater for effective use and to ensure a consistent extraction of freshwater without causing intrusion of seawater into coastal aquifers. Subsurface dams have found use in Japan, particularly on small islands and in archipelagos. In these areas, geological conditions not only limit the construction of conventional water supply systems but also favor the construction of subsurface dams for alternative water sources. Subsurface flow barriers, in contrast to subsurface dams, are not meant for storage but are merely impervious physical barriers inserted across the flow direction to modify the flow field. They partially penetrate the aquifer and have openings at the lower aquifer layer and are meant primarily for seawater intrusion control.

Hanson and Nilsson (1986), Nishigaki et al. (2004), and the Japan Green Resources Agency (2004) have reviewed subsurface dam technology and developments worldwide. Other studies (e.g., Nagata, et al., 1994; Osuga, 1997) have been site-specific and more focused on the design criteria, construction, and environmental impacts of individual dams. These prior researches have identified specific benefits of subsurface dams including sustained irrigation supplies for various crops and prevention of seawater intrusion due to increased freshwater groundwater levels in areas where dams have been constructed. However, there is a dearth of information on the behavior of residual saltwater trapped in the storage area after construction of a cutoff wall. After dam construction, the movement and removal of this residual saltwater is usually not investigated.

Numerous investigators have performed experimental and numerical studies to understand the dynamics of saltwater intrusion into coastal aquifers (e.g., Ataie-Ashtiani et al., 1999; Zhang et al., 2001; Thorenz et al., 2002; Momii et al., 2005; Nakagawa et al., 2005; Illangasekare et al., 2006; Goswami and Clement, 2007). However, these studies do not directly reference saltwater dynamics in cutoff walls. Part of the saltwater intrusion wedge that is trapped as residual saltwater in the storage area of the cutoff wall has been assumed to remain stagnant (Fig.10 of Oude Essink, 2001) but relevant experimental and numerical studies have been conducted to show that saltwater can migrate out of an enclosing barrier. Oswald et al. (2002) and Oswald and Kinzelbach (2004) described results from saltpool experiments that showed saltwater of different densities migrating from a closed system due to freshwater flow from the top. It has been presented as a three-dimensional benchmark problem and results have been reported by Diersch and Kolditz (2002), Johannsen et al. (2002) and Oswald and Kinzelbach (2004). The salt dome problem (HYDROCOIN Level 1 Case 5) was proposed for intercomparison of numerical solutions (OECD, 1988) and also involves salt migration as groundwater flows over a constant-concentration salt source in a closed system. It has been widely used and discussed (e.g. Herbert et al., 1988; Oldenburg and Pruess, 1995; Konikow et al., 1997; Kolditz et al., 1998; Holzbecher, 1998; Youness et al., 1999) for the different boundary condition treatments applied. Both problems offer insights on saltwater migration patterns but the boundary conditions are different from the classic saltwater intrusion problem represented here.

There is a dearth of information on actual application of subsurface flow barrier technology. Anwar (1983) obtained analytical solutions for the free surface and the freshwater–seawater interface produced by a subsurface barrier partially embedded into

an unconfined coastal aquifer. These solutions considered steady flow in an isotropic aquifer, assuming a sharp freshwater–saltwater interface with no tidal effects. He introduced shape factors describing the distribution of mass density and velocity and derived their values from laboratory experiments in a vertical-plane Hele-Shaw model. However, his solutions are based on the assumption of very small hydraulic gradients compared to the thickness of the aquifer such that the flow barrier is far away from the flow patterns being considered.

The design and management of subsurface physical barriers for unconfined coastal groundwater systems requires the prediction of the location and movement of the saltwater–freshwater interface. For the study on subsurface dams, the objective is to examine the dynamics of the residual saltwater trapped in the storage area upon installation of the cutoff wall. Additionally, the effect of cutoff wall height on residual saltwater removal was determined. For the study on subsurface flow barriers, the objective is to examine the behavior of the saltwater intrusion wedge after installation of subsurface flow barriers. Specifically, the effects of penetration depth and horizontal location of flow barriers in achieving the most effective repulsion of saltwater intrusion were determined. For each study, flow tank experiments were performed to model saltwater intrusion in a coastal unconfined aquifer. After the steady state saltwater intrusion wedge was achieved, the cutoff wall or flow barrier was installed and the behavior of residual saltwater was examined. The SEAWAT model was used to numerically simulate the experiments and the model results were used to analyze the dynamics involved. Additional simulations were then performed for the specific objectives enumerated and the results from the different barrier settings were compared and analyzed.

3.2 Laboratory Approach

3.2.1 Experimental Setup

The experiments were conducted in a flow tank with internal dimensions 90 cm length, 60 cm height, and 8 cm width (Figure 3.1). To model an unconfined aquifer the middle section of the tank was packed with homogenous glass beads with a nominal diameter of 1.2 mm. To each side of the bead section were freshwater and saltwater reservoirs. The heads in the reservoirs were controlled by adjustable drainage pipes. Drainage pipe outflows were measured to estimate hydraulic conductivity and freshwater flux through the system. Freshwater and saltwater were supplied at constant flow rates to the respective reservoirs from large constant-head tanks positioned above the experimental setup. A slot for installing the cutoff wall of both the subsurface dam and the flow barrier is located in the main tank 20 cm from the saltwater reservoir. A slot for insertion of a shutoff wall between the main flow tank and the saltwater reservoir was constructed to separate the saltwater solution from the freshwater-filled porous tank at the start of each experiment. Perforated acrylic sheets and fine mesh screens separate the main tank from the wall slots and reservoirs. Because the cutoff wall slot effectively divided the flow tank volume, each section was packed with glass beads separately but successively between each section. Beads were packed in 5 cm layers under fully saturated conditions to prevent air entrapment. Each layer was homogenized with those below using a mixing rod to disrupt any possible layering. To ensure homogeneity of the porous medium, the glass beads were carefully compressed after each layer was filled. Clamps were used to prevent expansion of the tank sides during packing and ensured a fixed width for the flow tank.

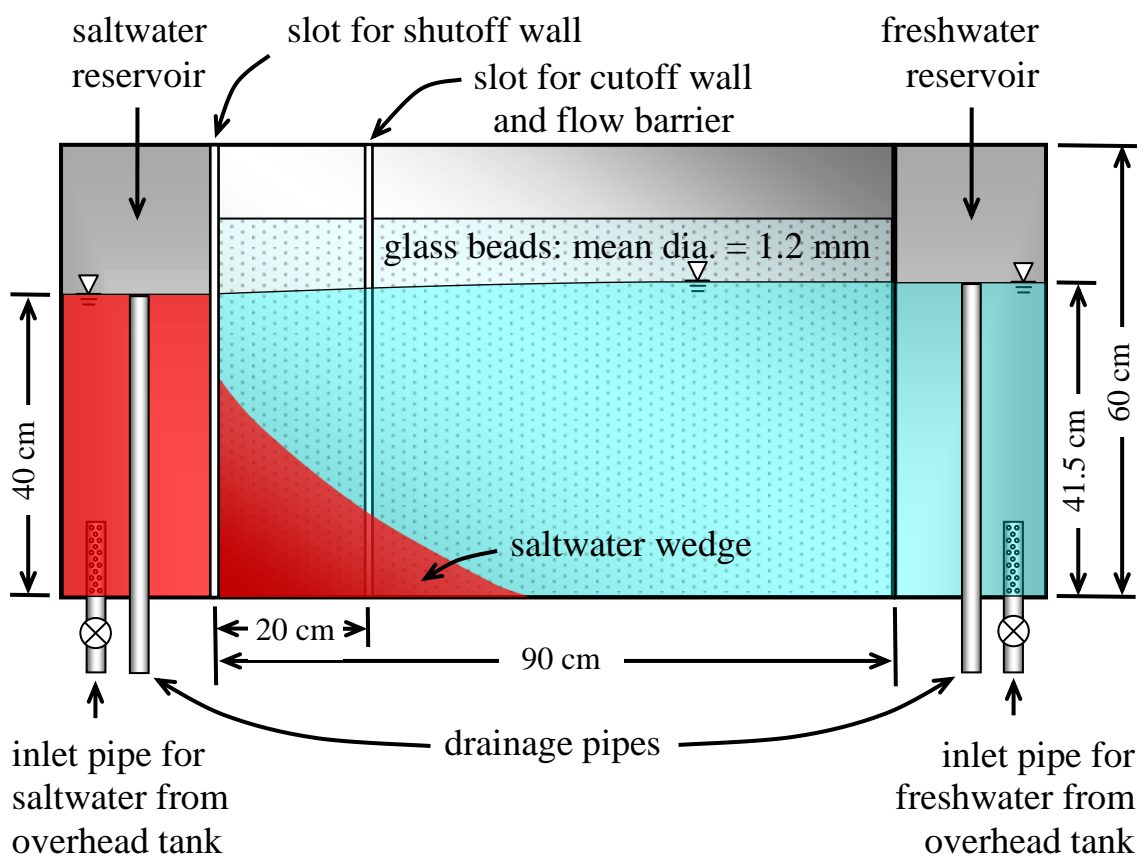


Figure 3.1 Schematic diagram of the experimental setup for the subsurface physical barrier experiments.

Saltwater was prepared in several 40 L barrels by dissolving commercial salt in tap water (Figure 3.2). To distinguish it from freshwater, the saltwater was dyed with a red food color [New Coccine Acid Red 18 (C.I. Number 16255), Kiriya Chemical Co., Ltd.] at a concentration of 20 g dye per 40 L saltwater solution (Figure 3.3). The suitability of the dye was demonstrated by consistently similar breakthrough curves of NaCl and dye in one-dimensional column tests. The saltwater solution density was maintained at 1.025 g/ml as measured with an Akanuma hydrometer (JIS certified, Yokota Keiki Mfg. Co. Ltd.) shown in Figure 3.4. The saltwater concentration was measured with a WTW-LF330 conductivity meter (Figure 3.5). A small pump and several siphon tubes were used to circulate and homogenize the saltwater solution in the overhead constant-head tank, the saltwater reservoir, and the barrels. The saltwater density and concentration at these locations were monitored. The pumps used to circulate the freshwater and saltwater from the barrels to the overhead tanks are shown in Figure 3.6. Tap water was used for freshwater source.

For the subsurface dam experiments, two cutoff walls with crest heights of 40 and 20 cm as measured from the bottom of the tank were used. For the flow barrier experiments, the wall was installed in such a way that it partially penetrates the porous medium leaving an opening at the bottom of the aquifer for freshwater flow towards the saltwater reservoir. The cutoff and shutoff walls were made of 4 mm thick acrylic sheets (Figure 3.7). Rubber seals attached to the sides of these walls prevented leakage. A grid of perpendicular lines at 10 cm spacing was etched on the flow tank and standard metallic rulers (cm and mm scales) were pasted along the bottom and sides of the flow tank to facilitate direct measurement of the saltwater wedge profile (particularly the saltwater toe) and the freshwater and saltwater levels.



Figure 3.2 Saltwater in 40 L barrels made from commercial salt dissolved in tap water.



Figure 3.3 Red food color used to dye the saltwater.

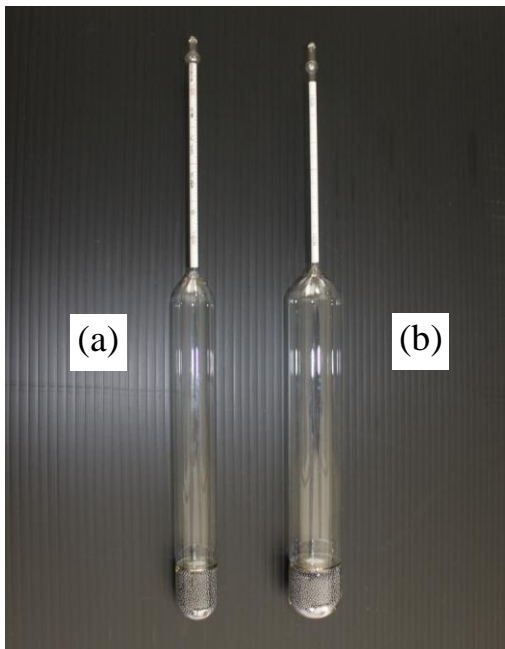


Figure 3.4 Akanuma hydrometers for (a) freshwater and (b) saltwater.



Figure 3.5 WTW-LF330 conductivity meter.

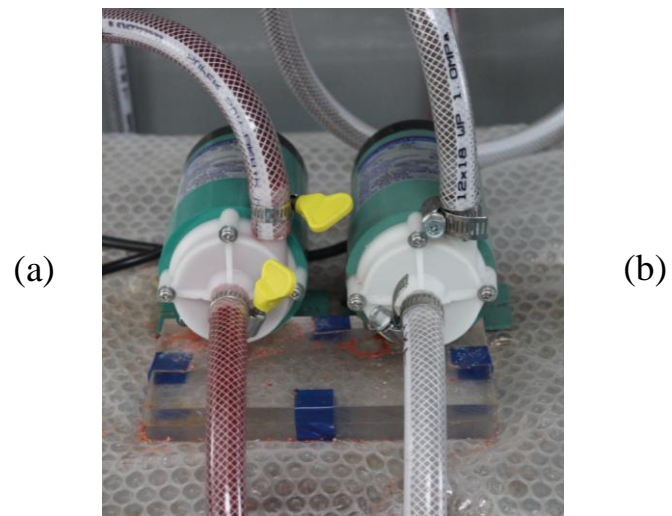


Figure 3.6 Small centrifugal pumps used to circulate the (a) saltwater and (b) freshwater.



Figure 3.7 Experimental subsurface barriers: (a) 20 cm cutoff wall, (b) 40 cm cutoff wall and (c) shutoff wall.

3.2.2 Experimental Procedure

For each experiment, the porous tank and reservoirs were initially filled with tap water from the overhead freshwater tank. The drainage pipes were adjusted to maintain a constant head 41.5 cm above the bottom of the tank on the freshwater side and 40.0 cm on the saltwater side. Estimated head fluctuations over the course of the experiment were on the order of ± 1.0 mm. This hydraulic gradient produced a flow of freshwater toward the saltwater reservoir. After the freshwater flow stabilized, hydraulic conductivity, K of the porous medium was estimated using Darcy's law, based on the preset hydraulic gradient and the measured discharge rate from the drainage pipes. The in situ approach applied by Oostrom et al. (1992) was used to estimate the average K of the flow tank.

The shutoff wall was then inserted separating the saltwater reservoir from the main tank. The freshwater in the saltwater reservoir was then replaced with red saltwater solution from the overhead saltwater tank and allowed to circulate until density and concentration measurements became stable. The saltwater intrusion process was initiated with the removal of the shutoff wall. As density driven flow progressed, the toe position of the intruding saltwater wedge was measured. Recorded data were cross-checked with photographs taken at various intervals with a high resolution digital camera. In the freshwater discharge zone at the saltwater boundary, the freshwater flowed vertically along the mesh screen and floated over the saltwater before draining out, indicating very little mixing between the freshwater and saltwater regions, similar to the condition described by Goswami and Clement (2007).

In each experiment, a steady state condition was established once changes were no longer observed in the toe position of the saltwater wedge and the drainage discharge from the system. After steady state was established in the subsurface dam experiments, the cutoff wall was inserted quickly but carefully into the slot, to avoid prolonged disruption of the existing flow condition during the installation process. A thin layer of grease is applied on the rubber seals of the cutoff wall for smoother and faster installation. Upon installation of the cutoff wall, the toe position and movement of the residual saltwater wedge were recorded. This process was performed for both 40 and 20 cm cutoff wall heights. The experiments were ended when there was no longer any observable change in the toe position of the residual saltwater or when the residual saltwater was completely flushed out.

For the subsurface flow barrier experiment, after obtaining the steady state saltwater intrusion wedge, the flow barrier was inserted into the slot at a specified depth of penetration measured from the saltwater level. This setup allows for an opening at the bottom of the aquifer for freshwater discharge. The subsequent movement of the toe of the saltwater wedge was observed and recorded until no movement was recorded signifying another steady state conditions. The flow barrier was then lowered at a new penetration depth, and the movement of the saltwater wedge toe was measured and recorded until steady state was again achieved. This procedure was followed with four different flow barrier depths of 11, 20, 30 and 35 cm. In all experiments, water levels in the flow tank were observed using piezometers connected from the bottom of the tank.

The effectiveness of subsurface flow barrier was measured in terms of the saltwater repulsion ratio R , which is calculated using Equation 3.1:

$$R = \frac{L_0 - L}{L_0} \quad (3.1)$$

where: L_0 is the initial toe position of the saltwater wedge [L] and

L is the final toe position after flow barrier installation [L].

3.3 Experimental Results and Discussion

3.3.1 Subsurface Dam Experiment

There was a long time lag between the conduct of the 40 and 20 cm experiments such that the porous medium was repacked for each experiment causing different flow field conditions and, consequently, different hydraulic conductivity values. The K values measured for the 40 and 20 cm cutoff wall height experiments were 1.18 and 1.27 cm/s, respectively. Average porosity, n of the porous medium was 0.4 as measured by both volumetric and gravimetric methods. Initial steady state condition was reached after about 2 h in both experiments.

The experimental results for the 40 and 20 cm high cutoff walls are shown in Figures 3.8 and 3.9, respectively. The toe of the saltwater wedge for the 40 and 20 cm case measured from the saltwater reservoir were 40.7 and 43.7 cm, respectively. The difference was probably caused by slightly different water temperatures and possibly different head gradients between the two experiments. There were irregularities in the smooth shape of the saltwater wedge at the cutoff wall slot due to the absence of glass beads inside the slot. Except in this region, the transition zone was estimated to be about

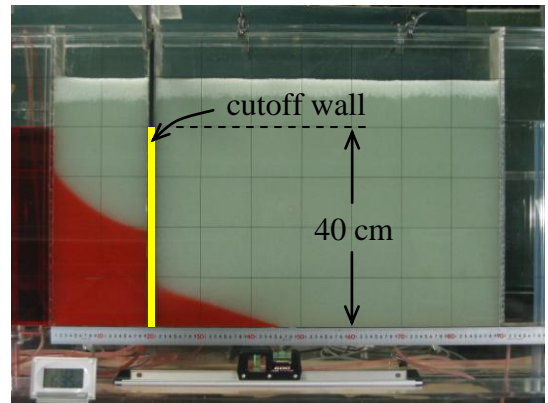
1.0 cm wide. Upon installation of the cutoff wall, the residual saltwater trapped in the storage area slowly flattened making it look like the toe of the residual saltwater advanced. This advance peaked at 45.8 cm in the 40 cm wall (Figure 3.8b) and at 44.4 cm in the 20 cm wall (Figure 3.9b).

The installation of the cutoff wall broke the freshwater-saltwater equilibrium and imposed a new flow field. The saltwater supply into the storage area of the cutoff wall was blocked and density differences caused the trapped residual saltwater to slide and tend to level beneath the freshwater. The freshwater flow gradually stopped this advance and pushed the residual saltwater against the cutoff wall. Dispersive and diffusive mixing between the freshwater and the residual saltwater continued along the interface and low concentration saltwater is slowly but continuously carried by the freshwater flow over the cutoff wall and toward the outlet. The residual saltwater gradually attenuated (Figures 3.8c and 3.9c) because the cutoff wall effectively blocked the supply of saltwater. Eventually all residual saltwater was completely removed from the storage area (Figures 3.8d and 3.9d). Oswald et al. (2002) showed the strong tendency for the saltwater to remain stagnant but stated that after a time much longer than the measurement period they used in their experiment, the salt water would be flushed completely by the incoming freshwater. These experiments have proven their statement to be correct.

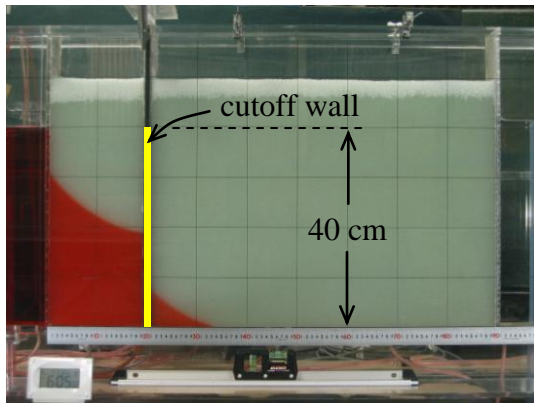
Note that the area occupied by the intruding saltwater on the “seaward” side of the 40 cm cutoff wall increased after installation. This is because the freshwater flow, which maintains the equilibrium condition, was blocked and forced to move upward over the cutoff wall. The size increase in the 40 cm case is clearly visible even with the



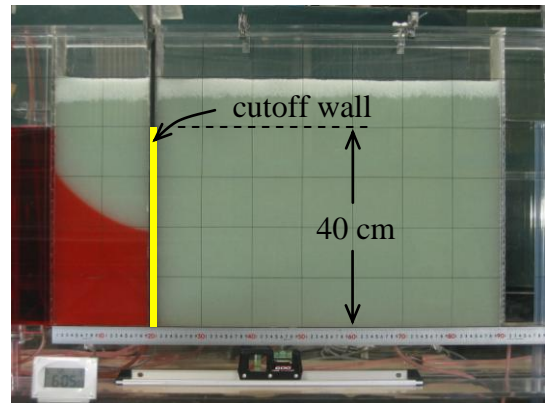
(a) Initial steady state condition



(b) Peak of advance of residual saltwater (30 min after cutoff wall installation)

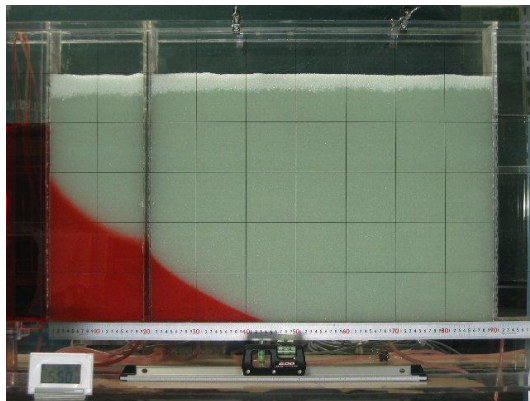


(c) Attenuation of residual saltwater (1 day after cutoff wall installation)

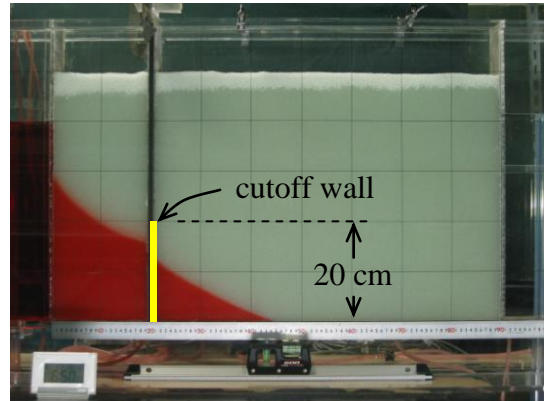


(d) Complete removal of residual saltwater (2 days after cutoff wall installation)

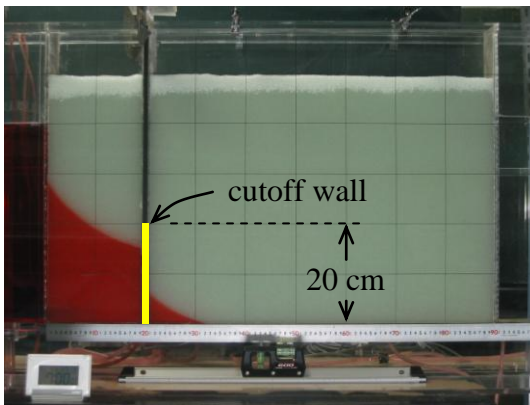
Figure 3.8 Behavior of the residual saltwater before and after installation of 40 cm cutoff wall.



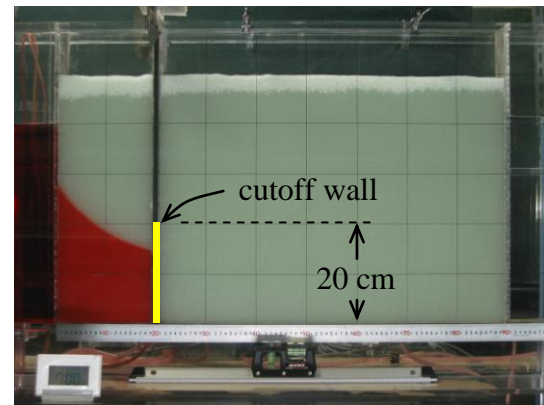
(a) Initial steady state condition



(b) Peak of advance of residual saltwater (20 min after cutoff wall installation)



(c) Attenuation of residual saltwater (12 h after cutoff wall installation)



(d) Complete removal of residual saltwater (1 day after cutoff wall installation)

Figure 3.9 Behavior of the residual saltwater before and after installation of 20 cm cutoff wall.

effect of the cutoff wall slot (Figures 3.8b, 3.8c, and 3.8d). A closer inspection of the 20 cm case (Figures 3.9b, 3.9c, and 3.9d) on the other hand, showed a slight decrease of the said area. It seems that wall height has an effect on the size of the intruding saltwater at the seaward side of the wall but this result remains inconclusive because of the problem at the cutoff wall slot. At any rate, any increase in the saltwater intrusion area at the seaward side of the wall has implications when determining the location of cutoff walls where the expected rise of saltwater and the reduction of freshwater volume in the coastal region of the cutoff wall should be taken into consideration.

Comparison of the transient saltwater wedge toe positions from the 40 cm and 20 cm cutoff wall experiments is shown in Figure 3.10. The residual saltwater wedge toe advanced farther after installation of the 40 cm cutoff wall than the 20 cm wall. The net advance of the residual saltwater is only 0.7 cm after about 20 min in the 20 cm wall experiment compared to the 5.1 cm advance after about 30 min in the 40 cm wall experiment. The higher wall produced a smaller opening for freshwater discharge and larger increased water levels, and required a longer flow path for the freshwater to travel. These circumstances resulted in more opportunity time for density difference to take effect before the new flow field was able to counterbalance and initiate residual saltwater removal. In relation to this, the removal of residual saltwater behind the shorter 20 cm cutoff was completed in 1 day, compared to 2 days behind the 40 cm cutoff wall. In each case, the rate of residual saltwater removal was constant, but slower for the 40 cm wall. Again this is due to the longer flow path the freshwater, carrying low concentration salt, had to flow before removal. The greater crest height and smaller size of the opening for the 40 cm wall increased the time for the freshwater discharge to flush the dispersed residual saltwater.

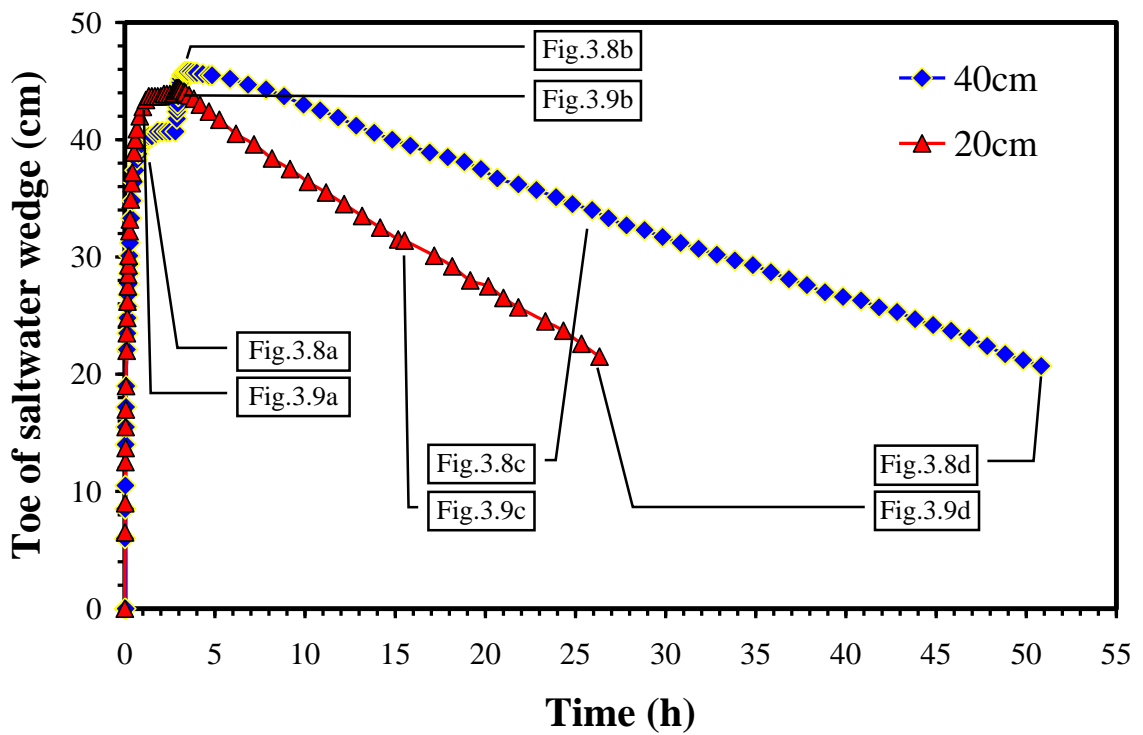
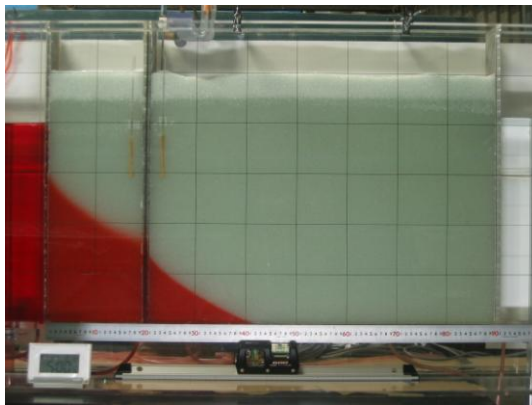


Figure 3.10 Comparison of the transient position of the saltwater wedge toe for the 40 and 20 cm cutoff wall experiments.

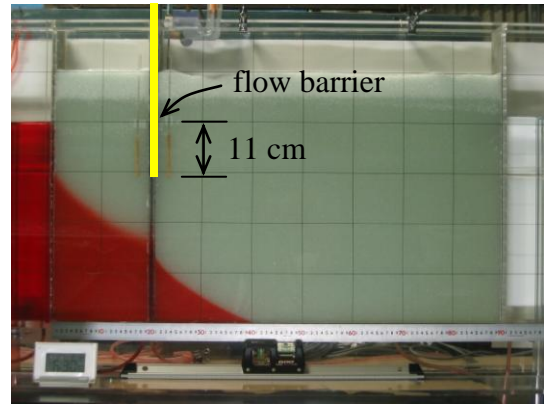
Note that in this study, it was assumed that the cutoff wall was installed completely at its designed height, trapping the residual saltwater as if being cut from the initial saltwater wedge. In actual subsurface dam construction using SMW and TRD methods, the wall is built in stages such that there is a possibility that saltwater interface may start retreating as soon as construction is initiated. Nevertheless, we assumed here that some residual saltwater were trapped in cutoff walls. One limitation of the experimental setup is that the absence of glass beads inside the cutoff wall slot created non-Darcy flows that distort the normal shape of the intruding saltwater wedge. Moreover, these analyses were performed under two-dimensional, homogeneous, isotropic conditions. Subsurface heterogeneity would, of course, result in different saltwater intrusion and attenuation behavior. Our results show that mechanical removal of residual saltwater may not be necessary. Depending on the sedimentary architecture, residual saltwater may not follow the same behavior observed in this experiment; it may become stagnant and require pumping out.

3.3.2 Subsurface Flow Barrier Experiment

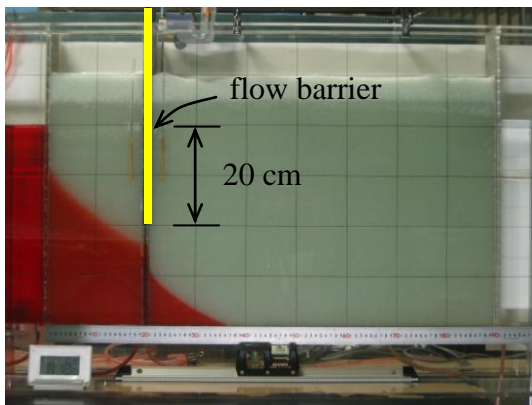
The steady state experimental results for the initial saltwater intrusion wedge and after installation of the 11, 20 and 35 cm deep flow barriers are shown in Figure 3.11. The average value of K and n in the flow barrier experiments were found to be 1.34 cm/s and 0.4, respectively. There were irregularities again in the smooth shape of the saltwater wedge at the barrier slot section due to the absence of glass beads inside the slot. Except in this region, the mixing zone was also estimated to be about 1 cm wide. The initial steady state condition prior to barrier installation is shown in Figure 3.11a. The initial toe position was measured at 41.7 cm from the saltwater reservoir. Upon



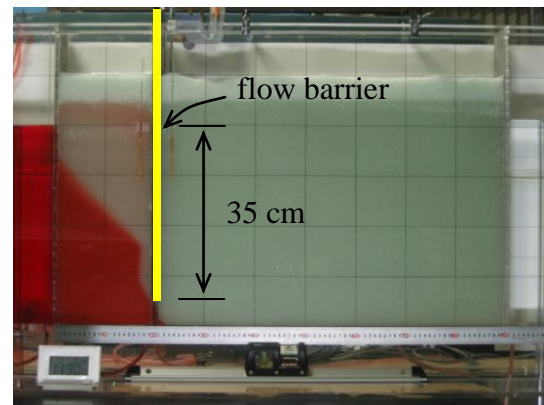
(a) Initial steady state condition



(b) 11 cm deep flow barrier



(c) 20 cm deep flow barrier



(d) 35 cm deep flow barrier

Figure 3.11 Steady state experimental results after installation of flow barriers at different penetration depths.

installation of the barrier to a depth of 11 cm, the saltwater wedge gradually attenuated and the steady state toe position retreated by 1.5 cm or about 4% repulsion of the saltwater wedge (Figure 3.11b). When the barrier penetration depth was increased to 20 cm, the retreat of the saltwater toe increased to 5.4 cm or about 13% repulsion (Figure 3.11c). Although not shown in Figure 3.11, the flow barrier was also lowered to a depth of 30 cm achieving a retreat of 14.7 cm or about 35% repulsion. Finally at 35 cm, the barrier forced a complete retreat of the saltwater wedge up to the barrier location achieving around 47% repulsion (Figure 3.11d). These scenarios showed that more effective repulsion of saltwater wedge is achieved with deeper flow barrier penetration.

Upon installation of the flow barrier, the initial freshwater–saltwater equilibrium was broken and a new flow field is imposed. The decrease in the opening for freshwater discharge towards the saltwater reservoir resulted in an increase in flow velocity at the opening and a corresponding increase in freshwater level in the landward side of the barrier. This new pressure condition forced the saltwater wedge to retreat. The deeper the barrier penetration, the smaller the opening and the greater the repulsion of saltwater intrusion wedge achieved. Looking into this relationship, we tried to apply an analytical method to calculate the freshwater–saltwater interface with a barrier, using our laboratory data. The analytical solution by Anwar (1983) for the interface profile with a barrier is presented in non-dimensional form as:

$$\left(\frac{K}{q} h_i\right)^2 = B \frac{2}{S_v \Delta (1 + \Delta)} \frac{K}{q} x + C_{ib} \quad (3.2)$$

where: h_i is vertical distance of the interface measured as depth from the mean sea level at any horizontal distance x [L],

S_v is the velocity shape factor [dimensionless],

$$\Delta = (\rho_s - \rho_f) / \rho_f$$

C_{ib} is an integration constant and

B is a non-dimensional barrier parameter in the form of:

$$B = 1 + \frac{\left(1 - \frac{x_b}{x}\right) \left(\frac{d_b}{h_s}\right)^2}{1 + \left(\frac{x - x_b}{h_s}\right)^2} \quad (3.3)$$

where: x_b is the horizontal location of the barrier from the coast [L] and

d_b is the barrier penetration depth [L].

The term d_b/h_s or the ratio of the penetration depth to the saltwater level is referred to as the penetration ratio. Equation 3.2 represents a linear relationship between $(K h_i / q)^2$ and $[(2BKx)/(q\Delta(1+\Delta))]$ with $1/S_v$ as the slope and C_{ib} as the y-intercept. Application of Anwar's method using the experimental data showed that a linear plot could not be achieved in the 30 and 35 cm deep barriers, cases where the d_b/h_s values are more than 0.5. It should be noted that Equation 4.2 was based on the assumption that the head gradient between the freshwater and saltwater levels, $h_f - h_s$, is very small compared to h_s , and that the flow profile being considered is well away from the barrier, which is not the case in the 30 and 35 cm barriers. In fact, Anwar used flow barriers with d_b/h_s ranging from 0.17 to only 0.52 in his experiments. At any rate, for the case of 11 and 20 cm deep barriers, S_v and C_{ib} were found to be 1.43 and 170.97, respectively, from a linear fit with an explained variance, $r^2 = 0.99$. Using these constants we derived the steady state toe position and computed the repulsion ratio achieved with each barrier

penetration in our experiments. The plots of R as a function of d_b/h_s from our experiment and those derived from Equation 3.2 are shown in Figure 3.12. The comparison, as expected, shows good agreement with the 11 and 20 cm barrier depths but deviate from the experimental results for the barriers with d_b/h_s of more than 0.5. Because of this limitation, numerical simulation was used to derive the relationship between the depth of penetration and location of flow barriers to seawater repulsion.

3.4 Numerical Approach

3.4.1 Subsurface Dam Numerical Parameters

In this study, the 20 cm cutoff wall experiment was simulated and used to verify the SEAWAT model code. Specific parameters other than the general boundary conditions described in Section 2.5 are enumerated here. The simulation area in the two-dimensional vertical cross section was 90 cm by 41.6 cm (Figure 3.13a). Two cases of block-centered finite-difference grid intervals were used for the discretization of the cross-sectional flow domain. Case 1 has a uniform grid of dimensions $\Delta x = \Delta z = 1$ cm except for the topmost layer occupied by the water table where $\Delta z = 2.6$ cm. Case 2 has a finer grid spacing with dimensions of $\Delta x = \Delta z = 0.5$ cm and a top layer of $\Delta z = 2.1$ cm.

Parameter values for the numerical simulations, measured during the experiments, are listed in Table 3.1. The saltwater level (h_s) was set at 40.0 cm while the freshwater level (h_f) was adjusted to 41.3 cm for a closer fit between numerical and experimental results. The adjusted freshwater head was outside the range of observed measurement error but produced model results that best matched the experimental results. In modeling the intrusion stage, the effect of the slot was initially represented by assuming

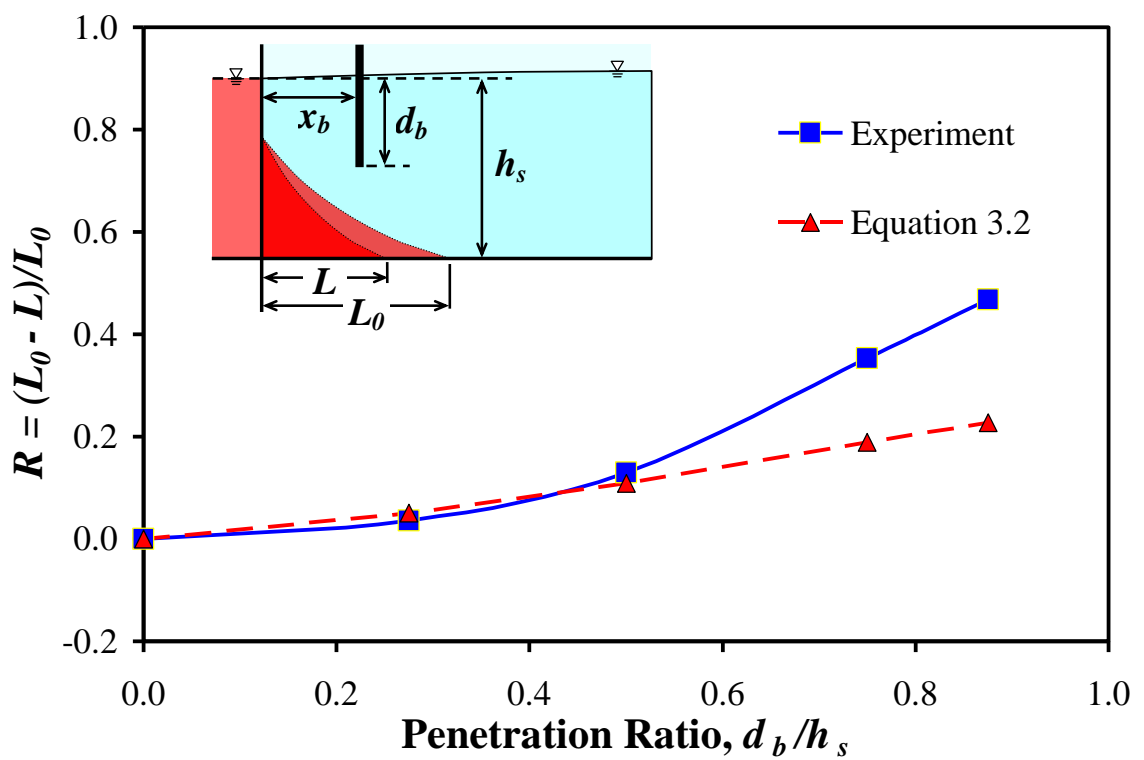
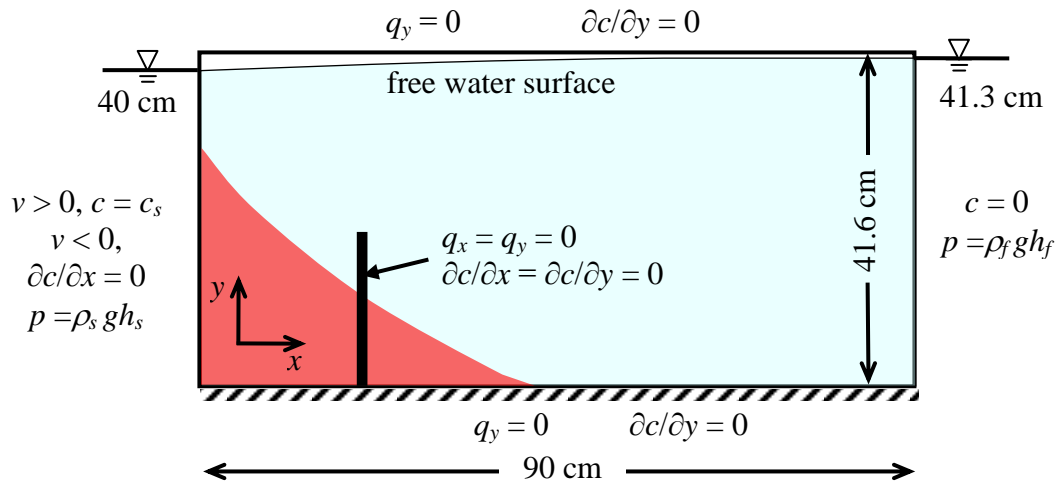
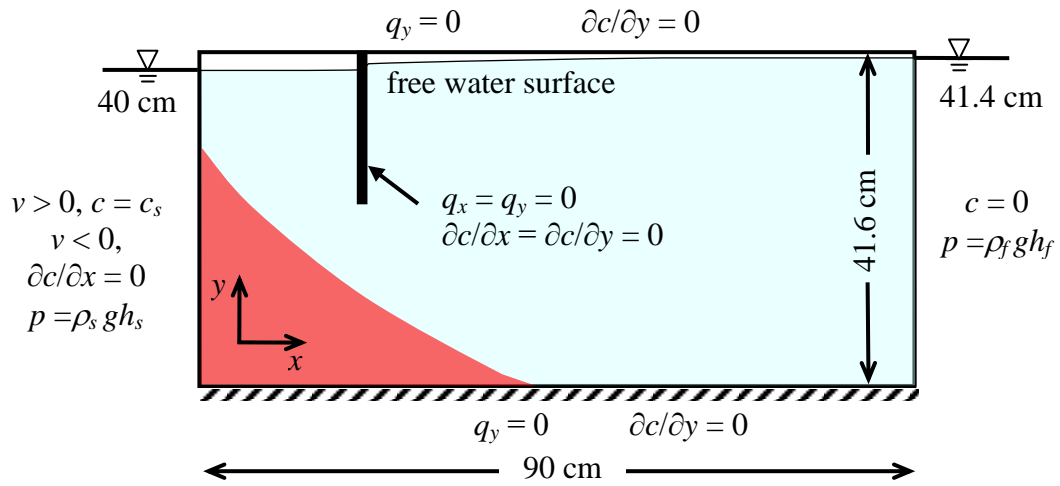


Figure 3.12 Comparison of repulsion ratio (R) values from experiment ($x_b = 20$ cm) and Equation 3.2 for different penetration ratio, d_b/h_s .



(a) subsurface dam simulation



(b) subsurface flow barrier simulation

Figure 3.13 Initial and boundary conditions for the subsurface physical barrier numerical simulations.

Table 3.1 Numerical simulation parameters for subsurface dam.

Input parameters	Values
Porosity	0.4
Freshwater level h_f (cm)	41.3
Saltwater level h_s (cm)	40.0
Freshwater density ρ_f (g/cm ³)	1.001
Saltwater density ρ_s (g/cm ³)	1.025
Saltwater concentration C (mg/L)	33600
Hydraulic conductivity k (cm/s)	1.27
Longitudinal dispersivity α_L (cm)	0.12
Transverse dispersivity α_T (cm)	0.012
Molecular diffusion coefficient (cm ² /s)	1×10^{-5}
Cell size	
Case 1: Layer 1; $\Delta x \times \Delta z$ (cm)	1.0×2.6
Layer 2 to 40; $\Delta x \times \Delta z$ (cm)	1.0×1.0
Case 2: Layer 1; $\Delta x \times \Delta z$ (cm)	0.5×2.1
Layer 2 to 80; $\Delta x \times \Delta z$ (cm)	0.5×0.5
Solution of flow equation	
Matrix solution technique	PCG
Head convergence value (m)	1×10^{-7}
Flow convergence value (kg/day)	1×10^{-7}
Solution of transport equation	
Advection term	MOC; TVD
Courant Number	0.1
MOC: NPMIN, NPMAX, NPLANE, NPL, NPH	4, 16, 2, 4, 8
Dispersion and source terms	GCG
Concentration convergence value	1×10^{-7}

a very high hydraulic conductivity at the slot section. The irregularity in the wedge shape was duplicated and the rate of advance of the toe has very good agreement with the experimental results. However, this exercise also produced unrealistically high velocity vectors which meant that to duplicate the limitations of the experiment will not serve the actual purpose of the study. As such the hydraulic conductivity of the porous medium was used for the slot section instead. Upon installation of the cutoff wall, the cells occupied by the wall were rendered inactive such that no flow and no flux conditions exist at the wall (Figure 3.13). The width of the cutoff wall section was 1.0 cm, equivalent to one column for the 1.0 cm grid simulation and two columns for the 0.5 cm grid.

Two transient stress periods were set for the simulations. The length of the first stress period was 12 h and involved the advancing front of the intruding saltwater wedge until it reach steady state. The head and concentration values obtained at each cell of the calculation domain after this initial simulation were used as the initial condition for the second stress period. This period started with the installation of the cutoff walls and was set at 26 h, enough to cover the time when the residual saltwater was completely removed in the experiments. The installation of the cutoff wall was assumed to be instantaneous, that is, the wall is already in place at the start of the second transient period. This also means that the portion of the saltwater wedge on the landward side (right side) of the wall is retained as residual saltwater. Both the MOC and TVD scheme were used to solve the advection term. Specifications for the different packages including the values for minimum (NPMIN) and maximum (NPMAX) number of particles allowed per cell, number of planes (NPLANE), number of particles

set when concentration \leq DCEPS (NPL) or when concentration $>$ DCEPS (NPH) for MOC are listed in Table 3.1.

In the additional simulations to investigate the effect of cutoff wall height on residual saltwater removal, only the TVD scheme was used for the advection term and all other parameters were the same as the 20 cm wall simulation.

3.4.2 Subsurface Flow Barrier Numerical Parameters

In this study, the 11 cm deep flow barrier experiment was simulated and used to verify the SEAWAT model code. Specific parameters other than the general boundary conditions described in Section 2.5 are enumerated here. The simulation area in the two-dimensional vertical cross section was the same as in the subsurface dam simulations (Figure 3.13b). The cross-sectional flow domain was discretized with the finer block-centered finite-difference grid interval with dimensions of $\Delta x = \Delta z = 0.5$ cm and a top layer of $\Delta z = 2.1$ cm. The freshwater level (h_f) was adjusted to 41.4 cm for a closer fit between numerical and experimental results. This is within the range of observed measurement error. The rest of the boundary conditions, longitudinal dispersivity and dispersivity ratio, freshwater and saltwater densities and concentrations used in the subsurface dam simulation were also used here. The n and K values were similar to the experiment values of 0.4 and 1.34 cm/s, respectively. The hydraulic conductivity of the porous medium was used for the barrier slot section to avoid the distortion in the normal saltwater wedge shape and the unrealistically high velocity vectors in the simulation results. Only the TVD scheme was used to solve the advection term. Parameter values for the simulations and specifications for the different packages are listed in Table 3.2.

Table 3.2 Numerical simulation parameters for subsurface flow barrier.

Input parameters	Values
Porosity	0.4
Freshwater level h_f (cm)	41.4
Saltwater level h_s (cm)	40.0
Freshwater density ρ_f (g/cm ³)	1.000
Saltwater density ρ_s (g/cm ³)	1.025
Saltwater concentration C (mg/L)	35000
Hydraulic conductivity k (cm/s)	1.34
Longitudinal dispersivity α_L (cm)	0.12
Transverse dispersivity α_T (cm)	0.012
Molecular diffusion coefficient (cm ² /s)	1×10^{-5}
Cell size	
Layer 1; $\Delta x \times \Delta z$ (cm)	0.5×2.1
Layer 2 to 80; $\Delta x \times \Delta z$ (cm)	0.5×0.5
Solution of flow equation	
Matrix solution technique	PCG
Head convergence value (m)	1×10^{-7}
Flow convergence value (kg/day)	1×10^{-7}
Solution of transport equation	
Advection term	TVD
Courant Number	0.1
Dispersion and source terms	GCG
Concentration convergence value	1×10^{-7}

3.5 Subsurface Dam Numerical Results and Discussion

To test the performance of the model, experimental transient positions of the advancing saltwater wedge prior to cutoff wall installation and the retreating residual saltwater after wall installation were compared with numerical predictions. Comparisons were based on the 0.1 and 0.5 isochlors. The simulation cases are defined as Case 1 ($\Delta x = \Delta z = 1.0$ cm) and Case 2 ($\Delta x = \Delta z = 0.5$ cm). To better explain the underlying processes observed in the experiments, steady state numerical results were compared to physical results at three times: (a) the initial steady state saltwater wedge; (b) the peak of advance of the residual saltwater after cutoff wall installation; and (c) 12 h after wall installation. We then examined numerical results for models of various cutoff wall heights.

3.5.1 Advancing Saltwater Intrusion Wedge

Simulations under MOC and TVD schemes for Cases 1 and 2 are shown in Figures 3.14 and 3.15, respectively. The points indicate the experimental results while the full lines and broken lines indicate the model predictions of the toe position at the 0.1 and 0.5 isochlors, respectively. Comparison was made up to 2 h only since steady state was already reached in both experiments and simulation results. Comparison showed that the invading front predicted by SEAWAT for both cases generally matched the experimental results. In both cases, model results temporally lagged the experimental data, particularly during the period before reaching steady state. This can be attributed to the absence of porous medium in the cutoff wall slot causing a faster rate of advance of the intruding saltwater in the experimental results. The Case 1 MOC result (Figure 3.14a) underestimated the steady state position of the intruding saltwater wedge but it

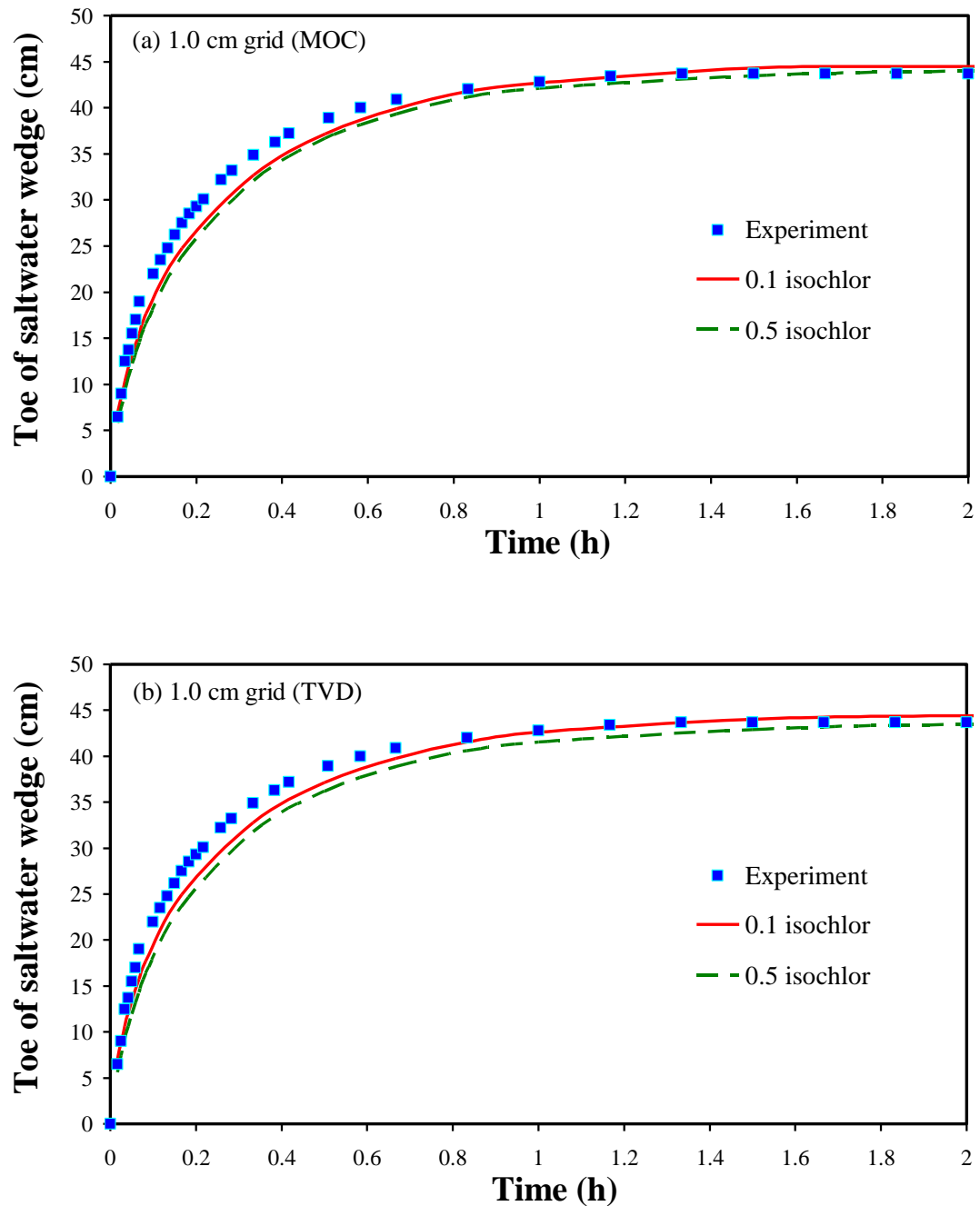


Figure 3.14 Comparison of model-predicted transient positions of the intruding saltwater wedge with experimental data for Case 1 (1.0 cm grid).

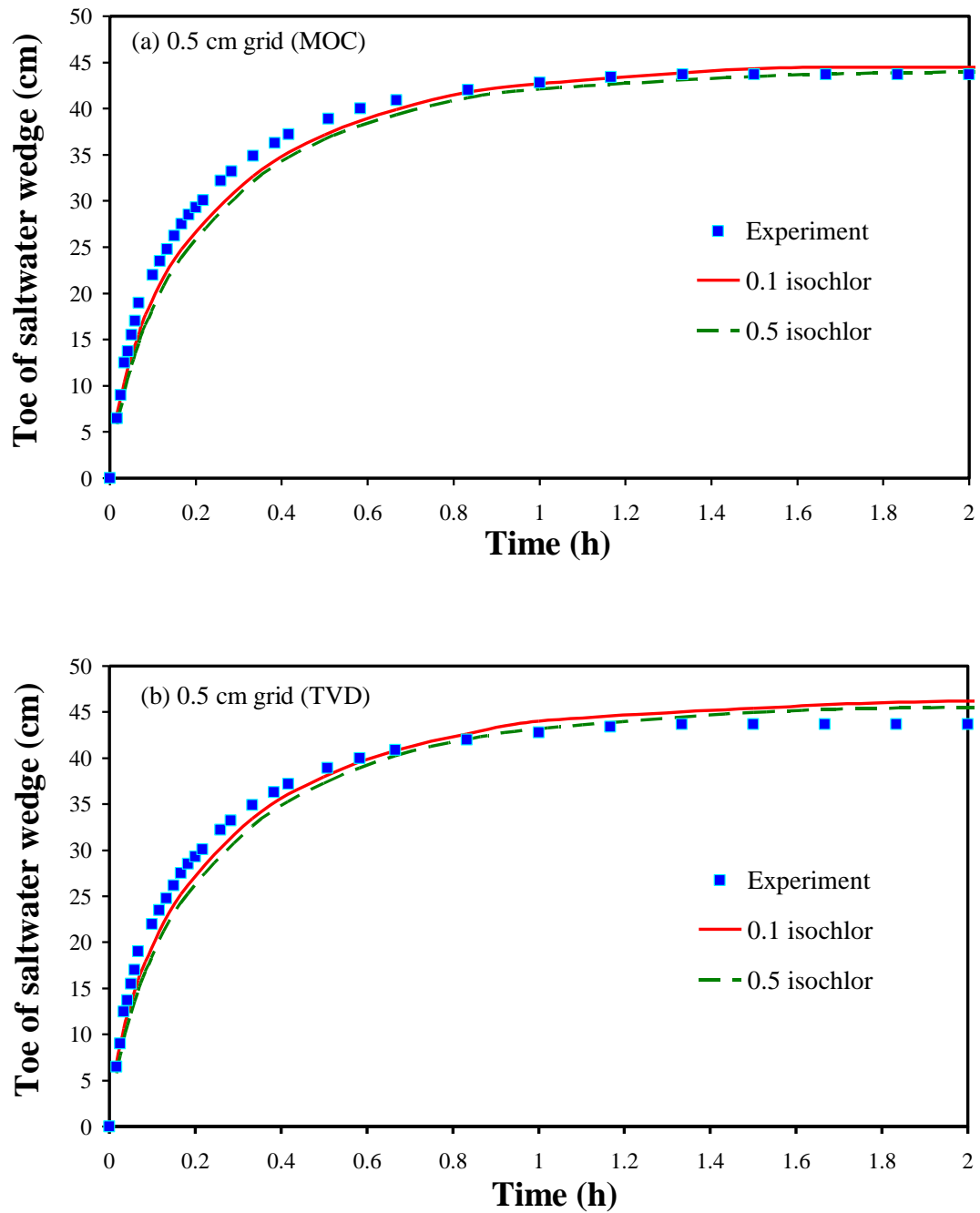


Figure 3.15 Comparison of model-predicted transient positions of the intruding saltwater wedge with experimental data for Case 2 (0.5 cm grid).

was accurately predicted in Case1 TVD (Figure 3.14b). The toe position was also accurately predicted in Case 2 MOC (Figure 3.15a) while the TVD result slightly overestimated its position (Figure 3.15b). The effect of the two grid sizes is not clearly apparent in the advancing saltwater intrusion stage as SEAWAT was able to closely predict the experimental results in both cases.

3.5.2 Retreating Residual Saltwater

Model results for retreating residual saltwater using MOC and TVD schemes for Cases 1 and 2 are shown in Figures 3.16 and 3.17, respectively. Case 1 with MOC (Figure 3.16a) predicted the initial advance of the saltwater wedge but since the steady state toe position had been underestimated previously, the overall simulation was a poor match. This case also exhibited a faster attenuation, completing removal of residual saltwater in only 15 h. The Case 1 TVD result (Figure 3.16b) accurately predicted the initial wedge advance but also exhibited a faster removal of the saltwater than experimentally achieved, completing the process in 18 h. For Case 2, the MOC result (Figure 3.17a) closely predicted the initial advance of the residual saltwater then exhibited a sudden increase in rate of saltwater removal before stabilizing at the same rate as the experiment, and finally completing saltwater removal in 21 hours. The Case 2 TVD result (Figure 3.17b) overshot the experimental initial advance since it also overestimated the initial steady state toe position, but then showed a rate of saltwater removal that was consistent with the experiment completing the removal in 26 h. This Case 2 TVD result showed the best simulation match to the experimental result.

In each case, the 0.5 isochlor lines eventually disappear, indicating significant dispersion of the residual saltwater. The effects of grid resolution are clearly apparent

by comparison. The coarser 1.0 cm grid spacing resulted in faster attenuation and earlier complete removal of residual saltwater, while with the 0.5 cm grid, the simulated transition zones and rate of removal are more consistent with the experimental results.

The grid Peclet number (Pe_{grid}) measures the sharpness of the concentration front or the degree to which the transport problem is dominated by advection. A common criterion used to ensure accurate results is $Pe_{\text{grid}} < 4$ or the more severe condition $Pe_{\text{grid}} < 2$ (Huyakorn and Pinder, 1983; Voss and Souza, 1987). Although the above inequality was proposed for finite-element and finite-difference based simulations of variable density flow and transport, it is a commonly accepted constraint regardless of the method used to solve the advection-dispersion equation (Brovelli et al., 2007). In this study, both the 1.0 cm and 0.5 cm grid simulations are advection dominated with Pe_{grid} values of about 8 and 4, respectively. More accurate solutions were not achieved because of the relatively high Pe_{grid} values. Although the Case 2 simulation is within the upper criterion of $Pe_{\text{grid}} < 4$, a grid spacing of 0.25 cm would yield a more accurate solution with $Pe_{\text{grid}} \approx 2$. However, this would require additional computer memory and longer run times. The grid resolution used in the modeling exercise was deemed adequate for the defined objectives.

3.5.3 Discussion of Model Results

Consider the 20 cm cutoff wall experimental results (Figure 3.9) and the numerical results for Case 2 using the TVD method shown in Figure 3.18. The simulation results display the saltwater intrusion wedge, velocity vector distribution, groundwater level, and relative concentration profile. The relative concentration (C_{rs}) is defined as $C_{rs} = (\rho - \rho_f) / (\rho_s - \rho_f)$ where ρ is the density of the fluid, ρ_s is the saltwater

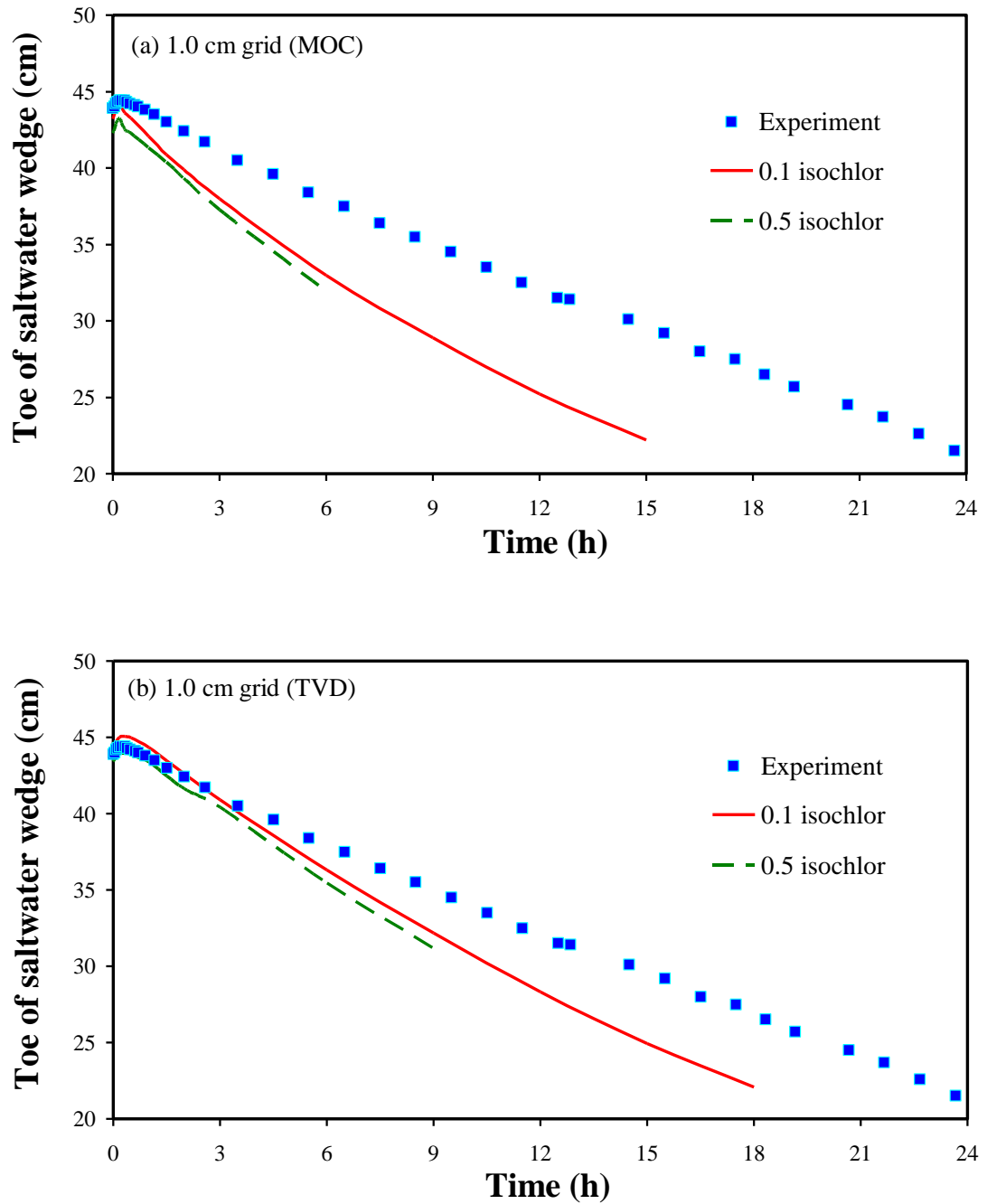


Figure 3.16 Comparison of model-predicted transient positions of the residual saltwater with experimental data for Case 1 (1.0 cm grid).

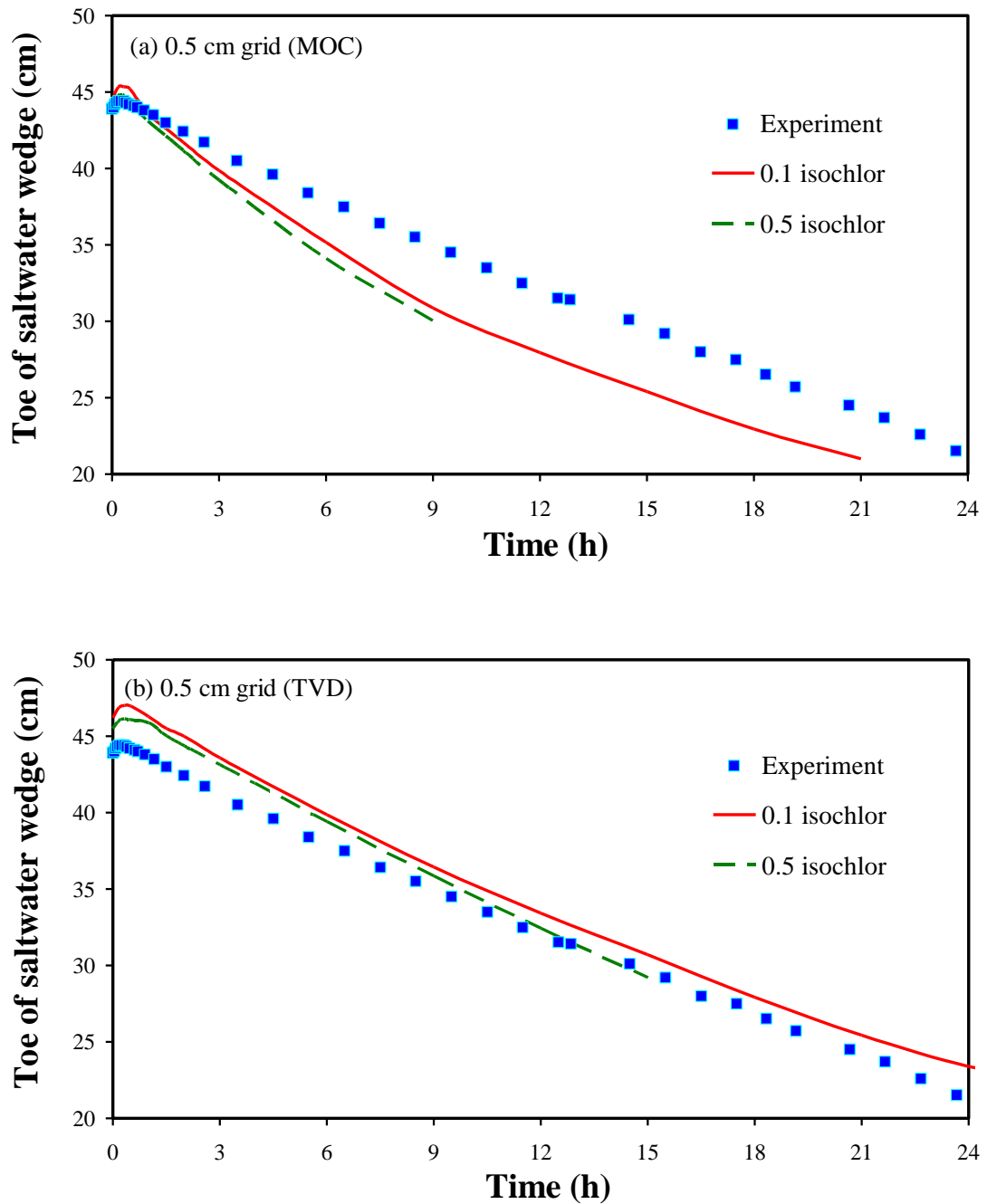
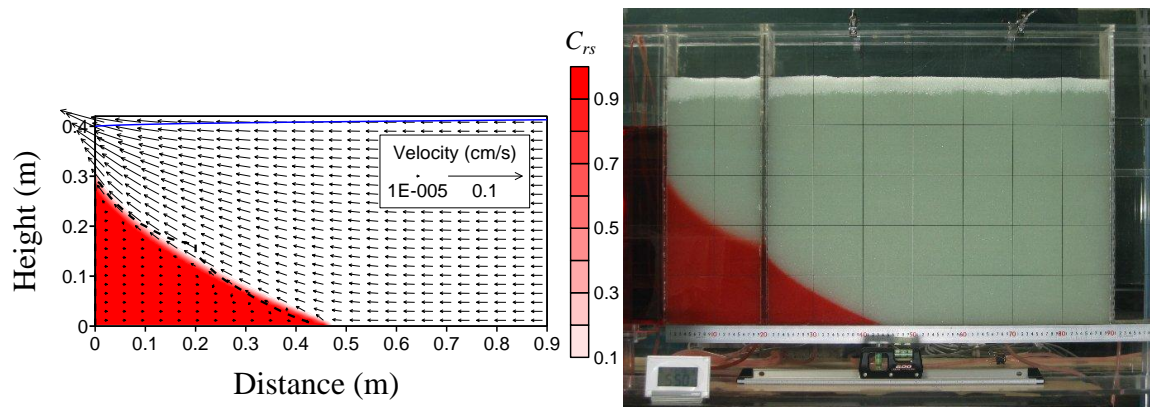


Figure 3.17 Comparison of model-predicted transient positions of the residual saltwater with experimental data for Case 2 (0.5 cm grid).

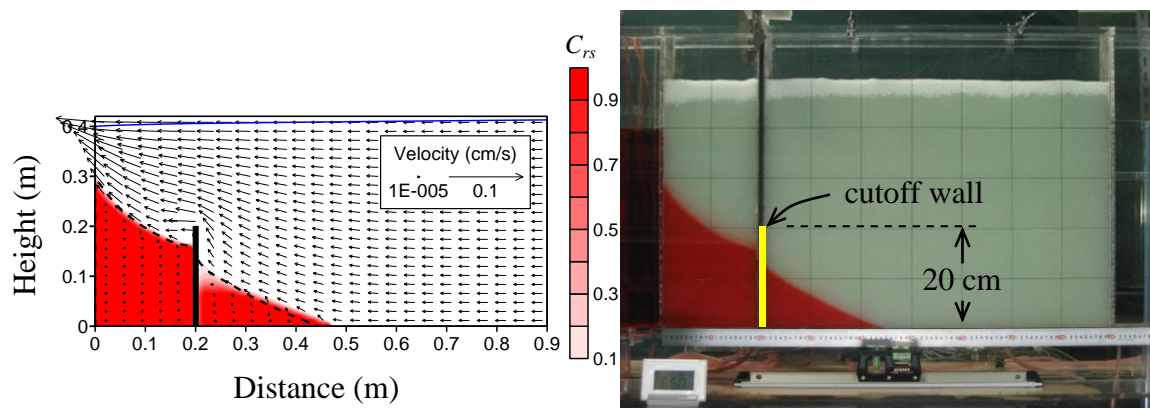
density and ρ_f is the freshwater density. A C_{rs} value of 0 corresponds to freshwater and a C_{rs} of 1 to the saltwater concentration. The relative concentration profile is in 0.1 isochlor intervals. The dashed lines mark the saltwater plume shape from the experiment for the same time periods.

The initial steady state toe position predicted by the model for TVD was 46.2 cm at the 0.1 isochlor and 45.5 cm at the 0.5 isochlor, both numbers are high compared to the 43.7 cm measured in the experiment (Figure 3.15b and 3.18a). The MOC result (Figure 3.15a) showed a better fit with the experiment, at 44.5 cm and 44.0 cm for the 0.1 and 0.5 isochlors, respectively. This equilibrium state was achieved after about 2 h in both the experimental and numerical results. The effect of the cutoff wall slot is clearly apparent in the bulge of the experimental result as compared to the smooth shape of the saltwater wedge in the model result. The transition or mixing zone between the 0.1 and 0.9 isochlors is about 1 cm, similar to that observed in the experiment. Careful observation of the modeled flow patterns and relative concentration contours provided a clearer understanding of the residual saltwater behavior. The intruding saltwater velocity vectors are quite small compared to the freshwater flow velocities (Figure 3.18a). Dispersion and diffusion take place at the saltwater and freshwater mixing zone and the freshwater flow transported low concentration salt towards the outlet. The equilibrium freshwater-saltwater wedge is maintained by the continuous saltwater intrusion and density gradient is balanced by the freshwater flow.

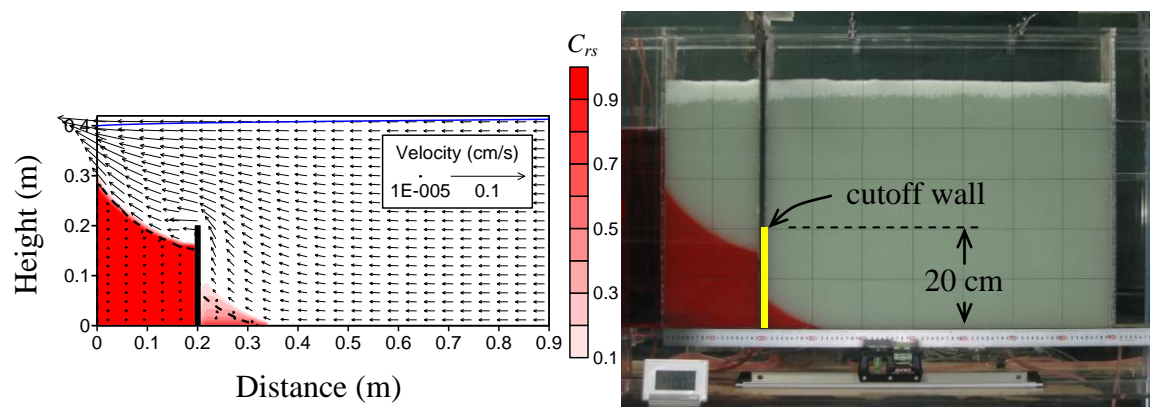
The experimental and numerical results at 20 min after cutoff wall installation showed a slight advance of the residual saltwater (Figure 3.17b and 3.18b). The MOC result (Figure 3.17a) predicted the peak at 45.3 and 44.8 cm for the 0.1 and 0.5 isochlors,



(a) Steady state condition.



(b) Peak of advance of the residual saltwater (20 min after wall installation).



(c) Attenuation of residual saltwater (12 h after wall installation).

Figure 3.18 Comparison of experimental and numerical results for the 20 cm cutoff wall (the dashed lines in the model results indicate the saltwater profile from the experiment).

respectively. This is close to the 44.4 cm in the experiment. The TVD results are relatively high at 47.0 and 46.1 cm for the 0.1 and 0.5 isochlors, respectively. The general shape of the wedge however, matched well with that in the experiment. Upon installation of the cutoff wall, density gradient and the increase in freshwater level forced the residual saltwater plume to flatten out and appear to advance. The direction of the velocity vectors in the residual saltwater confirms this behavior (Figure 3.18b). In time, the freshwater flow balanced the density effect and stopped the advance of the residual saltwater. Dispersion developing at the upper part of the residual saltwater wedge can also be observed indicating the start of low concentration salt removal by the freshwater. The flow patterns indicate increased freshwater velocity over the cutoff wall.

Attenuation and complete removal of residual saltwater was accurately predicted by the numerical model. Comparison of experimental and numerical results at 12 h after cutoff wall installation is shown in Figure 3.18c. Consider also the steady state numerical result for the 20 cm cutoff wall after complete removal of the residual saltwater (Figure 3.19a). In the model, significant dispersion was observed in the upper portion of the residual saltwater although this was not much apparent in the experimental observations. The 0.5 isochlor disappeared after 9 h in the MOC result (Figure 3.17a) and after 15 h in the TVD result (Figure 3.17b). Similar to the saltpool experiments (Johannsen et al., 2002; Oswald and Kinzelbach, 2004) dispersive flux of salt is carried with the freshwater as it flows along the mixing zone and over the cutoff wall. Salt is transported into the freshwater flow by diffusion and lateral dispersion and then carried to the outlet. The decreasing size of the residual saltwater plume and the weakening color concentration confirm this (Figure 3.18c). Since the cutoff wall prevented additional supply of saltwater, there is a net flux of salt flowing out over the

wall and the residual saltwater plume in the storage area of the cutoff wall slowly but continuously decreased. All the residual saltwater was eventually flushed out by the freshwater discharge (Figure 3.19a).

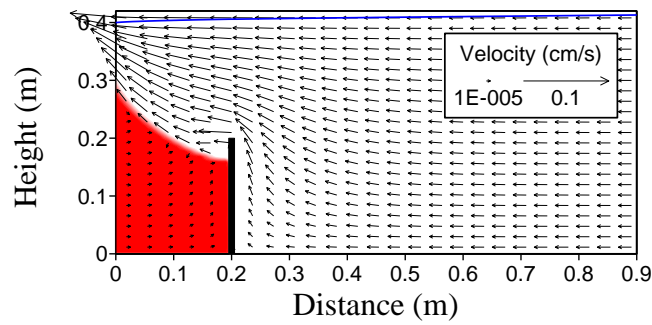
3.5.4 Effect of Cutoff Wall Height

Additional numerical simulations of shorter cutoff walls were performed to examine the effect of wall height on residual saltwater removal, using the same parameters as in the 20 cm simulation. There were marked differences in the final steady state condition modeled for 20, 10, 9, and 5 cm height cutoff walls (Figures 3.19a to 3.19d). The 10 cm cutoff wall achieved a faster complete removal of residual saltwater than the 20 cm cutoff wall taking only 21 h. This confirms the experimental results which showed that a shorter cutoff wall exhibited faster attenuation and earlier complete removal of the residual saltwater than a higher wall. Residual saltwater was not completely removed in the case of the 9 and 5 cm walls. Both the 9 cm and 5 cm wall case exhibited minimal retreat of residual saltwater (Figures 3.19c and 3.19d).

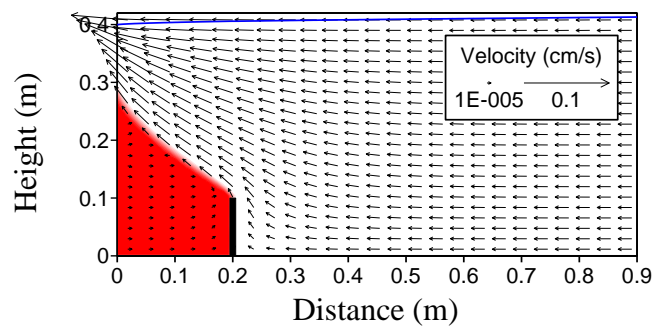
These results revealed a minimum height requirement for cutoff walls below which residual saltwater will not be completely flushed out. Flow patterns indicated a continuous flow of saltwater over these shorter cutoff walls into the storage area such that low concentration saltwater flushed out by the freshwater discharge was replaced with new saltwater. The crests of the 10 cm, 9 cm and 5 cm cutoff walls were further discovered to be all below the mixing zone. The crest of the 10 cm wall however lies just below the mixing zone and the force of the freshwater discharge was able to prevent inflow of saltwater into the storage area behind the wall. With the 9 and 5 cm walls, there are enough clearance between the wall crests and the mixing zone that freshwater

discharge cannot prevent saltwater to flow into the storage area on the landward side of the wall.

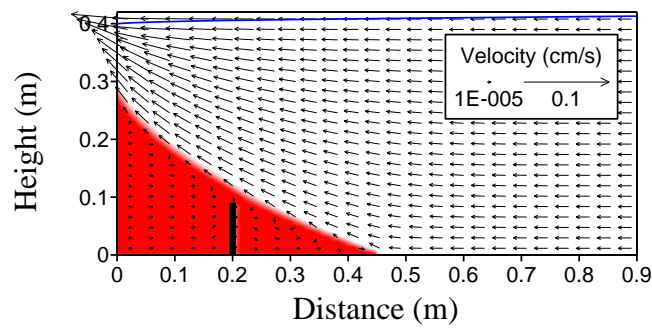
Consider again the area of intruding saltwater on the seaward side of the cutoff wall. In the experimental results in section 4.3, it was discussed that this area increased upon installation of the cutoff wall in the 40 cm case. This effect cannot be confirmed however, in the case of the 20 cm wall because of the irregularity in the saltwater wedge shape in the experiment. Using the model results, it can be clearly seen that the area of intruding saltwater on the seaward side of the cutoff wall also increased in the 20 cm wall (Figure 3.19a) compared to the initial steady state saltwater wedge (Figure 3.18a). The size increase is not that much compared to the 40 cm experiment case because the increased freshwater velocity at the crest (as shown in the flow pattern in Figure 3.19a) is pushing the wedge downward. This flow condition established a new equilibrium and prevented further intrusion. The wall crest of the 40 cm wall is high such that any increased velocity at the crest has negligible effect on the saltwater wedge. In the 10 cm high wall (Figure 3.19b) on the other hand, the intruding saltwater area actually decreased up to the tip of the crest. These results show that reducing the cutoff wall height also reduces the expected rise of the intruding saltwater at the seaward side of the wall. Of course, if the residual saltwater is not removed as in the 9 and 5 cm wall cases (Figures 3.19c and 3.19d), the intruding saltwater area will be about the same as when the cutoff wall was not installed.



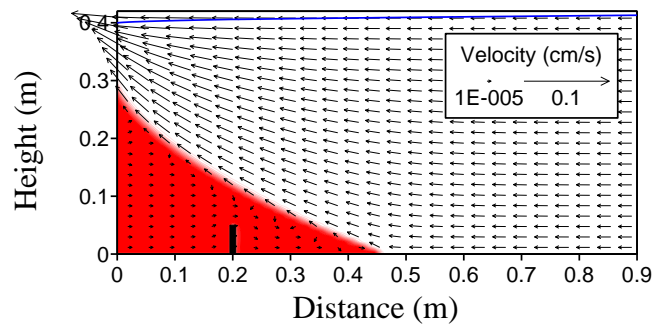
(a) 20 cm cutoff wall (after 26 h)



(b) 10 cm cutoff wall (after 21 h)



(c) 9 cm cutoff wall



(d) 5 cm cutoff wall

Figure 3.19 Steady state model results for 20, 10, 9 and 5 cm cutoff walls.

3.6 Subsurface Flow Barrier Numerical Results and Discussion

The steady state numerical result for the subsurface flow barrier with $d_b = 11$ cm and $x_b = 20$ cm (Figure 3.20) was first compared with the experimental result (Figure 3.11b) to test the performance of the model. The bold line indicates the initial steady state saltwater wedge profile where the toe position was calculated to be 43.1 cm at the 0.5 isochlor. This is higher than the 41.7 cm measured in the experiment. The model result also exhibited a higher retreat than that measured in the experiment and computed from Equation 3.2, achieving 3.6 cm or about 8% repulsion of the residual saltwater. However, considering that the simulations did not incorporate the barrier slot (no porous medium inside the slot), the model results adequately agree with the experiments. A more sophisticated test of the model's performance was performed in the subsurface dam section (4.5.1 and 4.5.2). The steady state simulation results for the different combinations of barrier penetration depths and locations are shown in Appendix A.

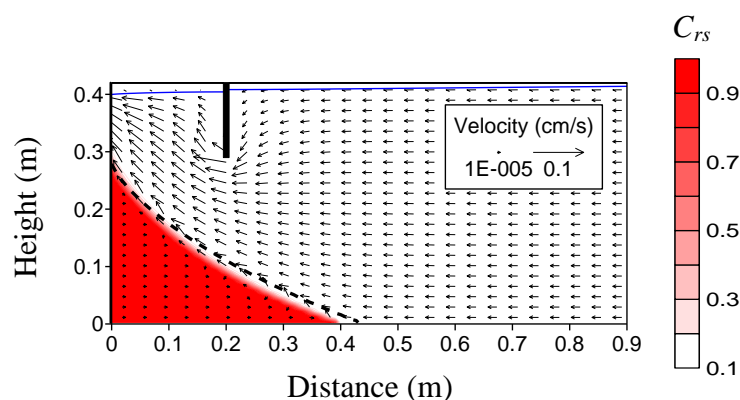


Figure 3.20 Numerical simulation of experimental flow barrier with penetration depth of 11 cm (dashed line indicates initial steady state saltwater wedge)

The saltwater repulsion ratios computed from simulation results for the different flow barrier penetration depths and locations were then evaluated. The penetration depth was expressed in the non-dimensional penetration ratio d_b/h_s , while the barrier location was expressed in non-dimensional form as $1 - x_b/L_0$. The repulsion ratio R was plotted against d_b/h_s as shown in Figure 3.21. Each horizontal barrier location is represented by the same symbol. At $d_b/h_s = 0$, that is without any flow barrier, there is of course no change in the initial steady state toe position so no saltwater repulsion or $R = 0$. As d_b/h_s increases or as the barrier penetrates deeper into the aquifer, the saltwater repulsion R rapidly increases. The exception is when the barrier location is greater than the initial saltwater toe position L_0 , as in the case of $x_b = 50$ cm ($1 - x_b/L_0 = -0.15$). In this case, as the penetration depth increases the barrier is essentially preventing the freshwater flow from repulsing the saltwater intrusion. Intrusion is thus induced beyond the original toe position as shown by the negative values of repulsion ratio. As penetration ratio approaches 1, the maximum repulsion ratio is achieved with the saltwater wedge toe being pushed seaward beyond the barrier location. In the extreme case of $d_b/h_s = 1$, that is, the barrier fully penetrates up to the impermeable layer, saltwater will then intrude up to the barrier location and R values will be the same as the values for $1 - x_b/L_0$. Figure 3.21 also showed that the closer the barrier is to the saltwater reservoir, the greater is the saltwater repulsion.

This is better explained in Figure 3.22 where computed R values were plotted against $1 - x_b/L_0$. The symbols now are the same for each penetration ratio. When $1 - x_b/L_0 = 0$, that is when $x_b = L_0$ or when the barrier is horizontally located at the saltwater wedge toe position, the repulsion is minimal to almost zero regardless of the penetration

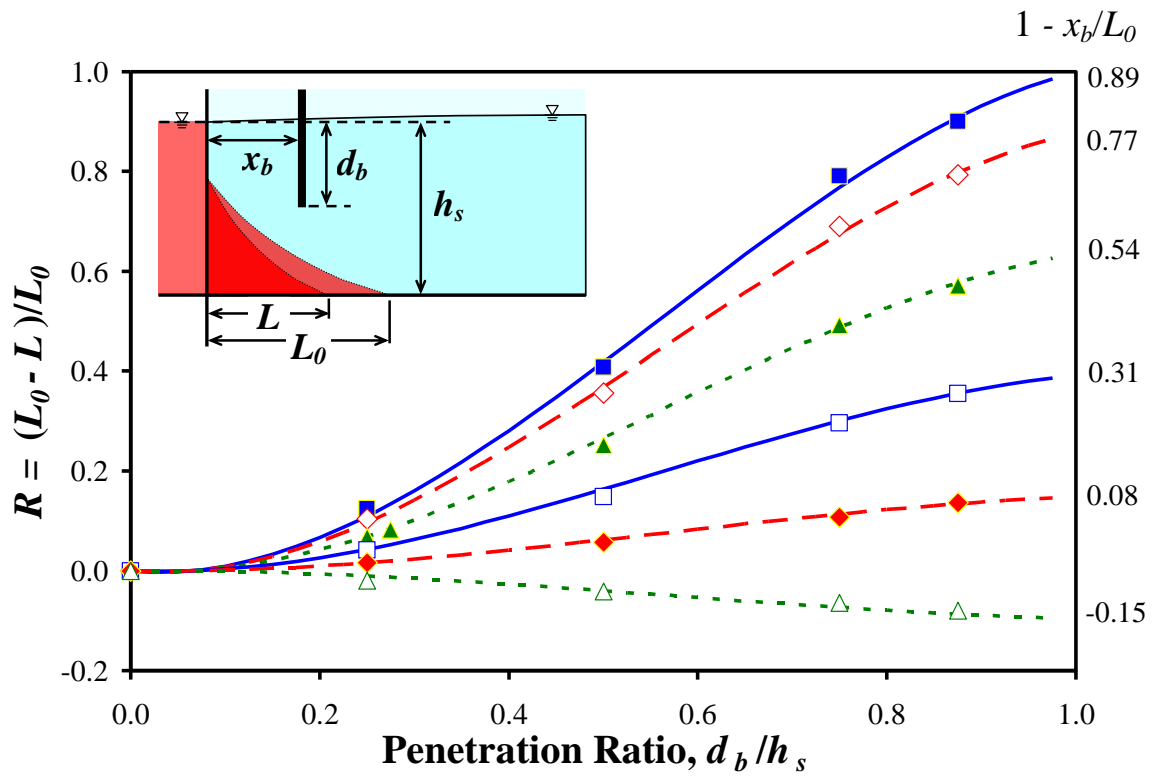


Figure 3.21 Repulsion ratio ($R = (L-L_0)/L_0$) with respect to barrier penetration ratio (d_b/h_s): Model results (symbols); Equation 3.4 (lines).

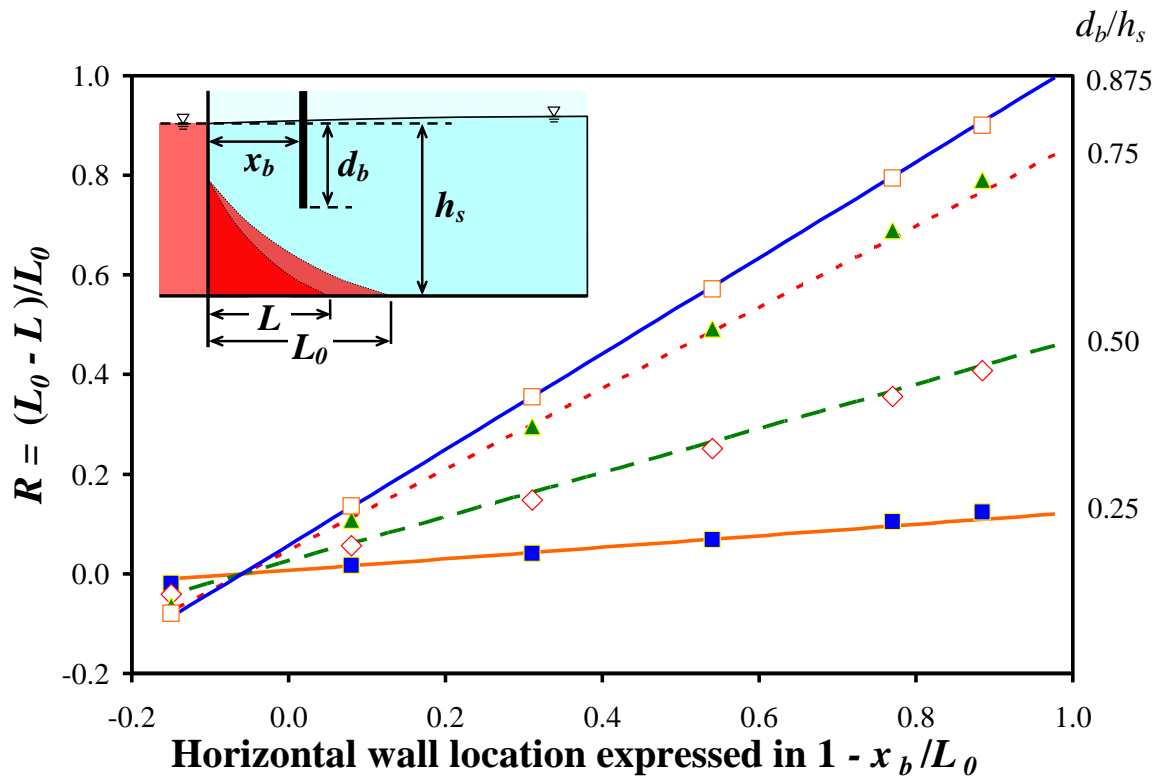


Figure 3.22 Repulsion ratio ($R = (L-L_0)/L_0$) with respect to barrier horizontal location ($1 - x_b/L_0$): Model results (symbols); Eq. 3.4 (lines)

depth. As $1 - x_b/L_0$ increases, that is, when the barrier is located closer to the saltwater reservoir, saltwater repulsion increases. The maximum R values are computed when $1 - x_b/L_0 = 1$, that is at $x_b = 0$ or when the barrier is located at the saltwater reservoir. Again when $x_b > L_0$ as in the case of $x_b = 50$ cm, R values are negative indicating that saltwater intrusion increased beyond the original toe position.

Figure 3.21 show that repulsion ratio is a polynomial function of penetration ratio. Figure 3.22, on the other hand, shows that repulsion ratio is linearly related to $1 - x_b/L_0$. The effects of the two functions were combined to form this generalized equation:

$$R = \frac{L_0 - L}{L_0} = \left[a \left(1 - \frac{x_b}{L_0} \right) + 1 \right] \times \left[b \left(\frac{d_b}{h_s} \right)^3 + c \left(\frac{d_b}{h_s} \right)^2 + d \left(\frac{d_b}{h_s} \right) \right] \quad (3.4)$$

where the first term on the right hand side of the equation refers to the linear relation between repulsion ratio and barrier location, and the second term on the right refers to the 3rd degree polynomial function of repulsion ratio with penetration ratio. The constants a , b , c and d were then derived using a nonlinear optimization method and their values were found to be: $a = 16.85$; $b = -0.1065$; $c = 0.1083$; and $d = -0.01096$. Substituting these constants into Equation 3.4 and using the model values for $1 - x_b/L_0$, R values were computed using several assumed values of d_b/h_s . The generated curves of R versus d_b/h_s were then compared with the model results as also shown in Figure 3.21. The same was done in Figure 3.22 where Equation 3.4 was used to solve for R values assuming several values $1 - x_b/L_0$ for each of the values of d_b/h_s . The generated curves from Equation 3.4 in both Figure 3.21 and 3.22 are perfect fit to the model generated points proving that the derived constants were accurate. The generated curves in Figure

3.21 continue to rise as d_b/h_s approaches 1, which is not the case in the simulation results. This behavior suggests a 4th degree polynomial function but for all practical purposes this case can be neglected and the 3rd degree polynomial would suffice.

The combined effect of barrier location and penetration depth on saltwater repulsion is shown in Figure 3.23; where $1 - x_b/L_0$ is on the x -axis, d_b/h_s on the y -axis and $R = (L-L_0)/L_0$ on the z -axis. The linear relationship of R with $1 - x_b/L_0$ and the polynomial function of R with d_b/h_s are clearly apparent. It should be noted however that the constants derived in these results are true for the given boundary condition, specifically the freshwater discharge as a function of the specified hydraulic gradient in the experiment. Results from preliminary studies with different hydraulic gradient indicates that for a given barrier location and depth of penetration, the repulsion ratio increases with increasing hydraulic gradient. Further studies are required to verify this and to determine their general relationships.

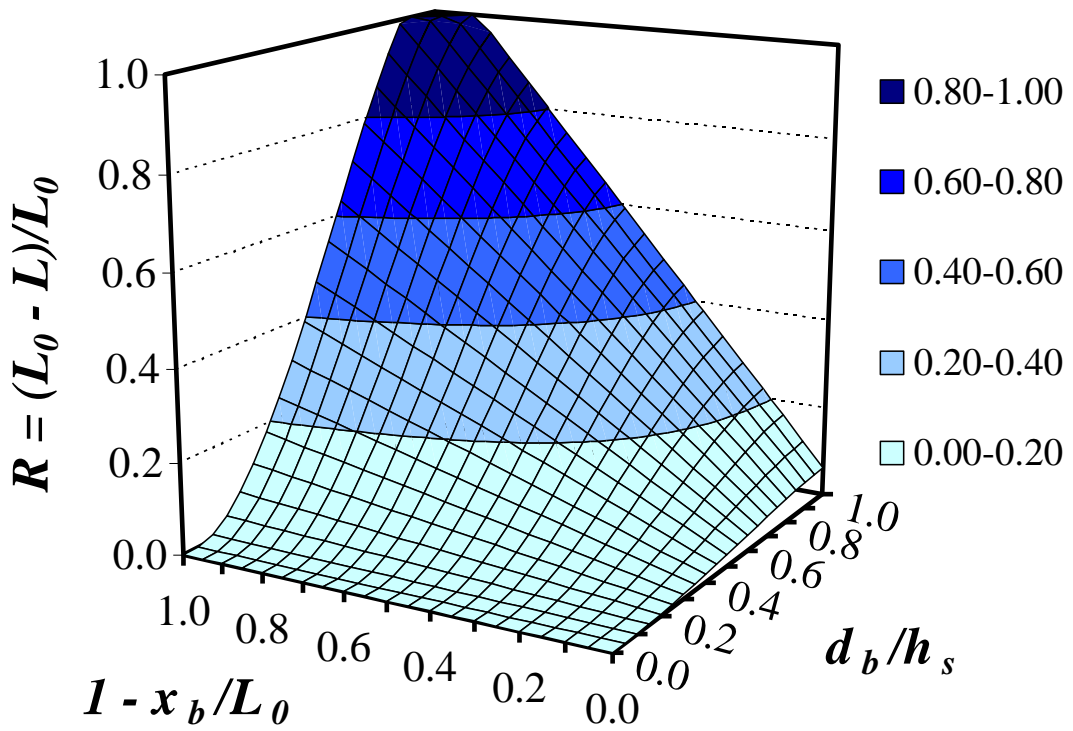


Figure 3.23 Repulsion ratio ($R = (L_0 - L)/L_0$) with respect to horizontal barrier location ($1 - x_b/L_0$) and penetration ratio (d_b/h_s) as computed from Equation 3.4.

3.7 Conclusion

Experiments and numerical studies were conducted to examine the dynamics of residual saltwater after installation of cutoff walls with the objective of determining the effects of subsurface dams on seawater intrusion. Experimental results showed that after installation of a cutoff wall, the residual saltwater wedge first flattens, causing the toe to advance, then gradually attenuates and eventually is completely removed from the storage area on the landward side of the wall. The SEAWAT model adequately predicts the behavior of the advancing saltwater intrusion wedge and the retreating residual saltwater after cutoff wall installation using the transient toe position of the saltwater wedge as point of comparison. Careful analyses of the flow patterns and relative concentration contours from the model helped explain the residual saltwater behavior due to cutoff wall installation. Flow patterns indicated that as freshwater flows along the mixing zone and over the cutoff wall, it transported dispersive flux of salt gradually removing the residual saltwater. Since the inflow of saltwater is prevented, all the residual saltwater was eventually removed from the storage area of the cutoff wall. This study have proven that saltwater trapped in an enclosing wall would be completely flushed out by the freshwater flow from inland. This phenomenon proves that subsurface dams are effective not only in preventing saltwater intrusion, but also in reclaiming previously saline-intruded coastal aquifers for freshwater storage and supply.

The experimental and numerical results show that a shorter cutoff wall achieves a faster residual saltwater removal rate than a higher cutoff wall. Shorter cutoff wall heights also reduce the expected rise in the intruding saltwater area at the seaward side of the wall. It was shown that residual saltwater will be completely flushed out when

wall height exceeds the thickness of the saltwater wedge at the cutoff wall location under steady state condition. These results imply that there is a potential for construction cost savings by installing shorter subsurface dams. Tidal fluctuations were not considered in this study but the effect of tides may be easily accounted for by increasing the height of the dam to cover for the highest expected sea level rise. The cutoff wall to be installed only need to exceed the thickness of the saltwater wedge at the desired location plus allowances to account for the tides and expected rise in seawater levels to ensure complete removal of residual saltwater.

Experimental and numerical studies were also conducted to determine the effects of penetration depth and location of subsurface flow barrier on saltwater repulsion. Experimental results for a flow barrier partially imbedded in an unconfined aquifer show that saltwater repulsion increases as barrier penetration depth increases. An analytical solution agrees well with the experimental results at penetration depths about half the aquifer thickness. The model results adequately predicted the experimental results. Additional simulations with flow barriers at different locations show that saltwater repulsion also increases as horizontal distance from the coast decreases. This means that more effective saltwater repulsion is achieved with deeper barrier penetration and at locations closer to the coast. Conversely, when the barrier is installed upstream of the original toe position, saltwater intrusion increases as barrier depth increases. For barrier installations, saltwater repulsion was found to be linearly related to horizontal barrier location and a third-order polynomial function of penetration depth. For a particular freshwater discharge, this relationship can be used to determine the theoretical saltwater repulsion achieved by subsurface flow barriers of specific depth and location relative to the toe of the intruding saltwater wedge.

Chapter

4

**Effects of Artificial
Recharge on
Seawater Intrusion**

4.1 Introduction

Artificial recharge of groundwater from spreading basins and recharge ponds can be applied to eliminate overdrafts and maintain ground water levels and gradients. Freeze and Cherry (1979) cited the works of G.E. Seaburn describing hydrologic studies carried out at two recharge basins (out of more than 2000) in Long Island, New York, to provide artificial recharge of storm runoff from residential and industrial areas. Mahesha and Nagaraja (1996) performed parametric studies to investigate the effect of uniform recharge on seawater intrusion. They established relationships between the interface motion and the intensity and duration of uniform recharge. While rainfall was their recharge source, these relationships can be used for artificial recharges.

The object of freshwater injection through recharge wells is to produce a hydraulic barrier by raising the piezometric head of the aquifer and prevent the saltwater from moving inland. A battery of recharge wells is usually installed paralleling the coast to create and maintain a “freshwater ridge” to control seawater intrusion. Bruington and Seares (1965) reported the effectiveness of a well recharge facility in Los Angeles County, California (USA). Harpaz (1971) described the use of recharge wells to control seawater intrusion in Israel. The United States Environmental Protection Agency (USEPA) classifies saltwater intrusion barrier wells as Class V underground injection control (UIC) wells and reported that there were more than 609 (315 were properly documented) saltwater intrusion barrier wells in the USA (USEPA 1987).

Hunt (1985) obtained closed-form solutions for the steady-state location of the freshwater–saltwater interface and stagnation points when either single or multiple

recharge wells are used to inject freshwater into both unconfined and confined aquifers. These closed-form solutions were derived from solutions for abstraction wells by Strack (1976) and are based on a sharp interface approach. The solutions of Hunt (1985) are only applicable for recharge wells located on the landward side of the interface and not for those located at the toe or within the saltwater wedge itself. Mahesha (1996a, 1996b) also obtained solutions for the steady-state and transient effects of a series of injection wells on the freshwater–saltwater interface using a sharp interface finite element model. His solutions however are for confined aquifers with fully penetrating recharge wells. His parametric studies showed that as much as 60–90% repulsion of seawater intrusion could be achieved through the proper selection of the injection rate and spacing between wells.

The design and management of artificial recharge facilities for coastal unconfined groundwater systems also requires the prediction of the location and movement of the saltwater–freshwater interface. In both studies, the objectives were to examine the behavior of the recharge plumes in order to determine the effect of application and recharge rate on saltwater repulsion. For the study on recharge wells, another objective is to determine the effects of location and mode of application in achieving the most effective repulsion of saltwater intrusion. Flow-tank experiments were first performed to model recharge ponds and recharge wells in an unconfined coastal aquifer. The saltwater repulsions achieved for each setting were determined and compared. The SEAWAT model was then used to numerically simulate the recharge well experiments to test the model code. The recharge pond experiment was not simulated due to the complicated mechanisms of unsaturated flow. Instead recharge well simulation with the injection point located just below the recharge zone was performed in its place.

Additional numerical simulations were then performed to model recharge wells at different locations and with different modes of applications. Finally, saltwater repulsions achieved from the different recharge well settings were compared and analyzed.

4.2 Laboratory Approach

4.2.1 Experimental Setup

The flow tank used for the artificial recharge experiments has internal dimensions of 60 cm length, 40 cm height and 4 cm width (Figure 4.1). The main flow tank was also packed with homogenous glass beads with a nominal diameter of 1.2 mm to model an unconfined aquifer. The main tank is bounded on each side by the freshwater and saltwater reservoirs, where the heads are controlled by adjustable drainage pipes. For the recharge pond experiments, freshwater recharge was applied through 8 nozzles distributed evenly within a $4 \times 4 \text{ cm}^2$ recharge zone located 10 cm from the freshwater reservoir. The nozzles are connected by rubber tubes to two small pumps, which distribute equal recharge rate to each nozzle. For the recharge well experiments, freshwater recharge was applied through a 5 mm diameter stainless steel tube spanning the entire width of the flow tank perpendicular to the walls. The tube is located 10 cm from the freshwater reservoir and 5 cm from the bottom. Small holes are strategically located around the tube to ensure even flow on all angles and the tube is wrapped in wire mesh so that no glass beads will block the flow.

Saltwater was prepared with the same red color, density and concentration as in the previous experiments. The saltwater concentration in these experiments was

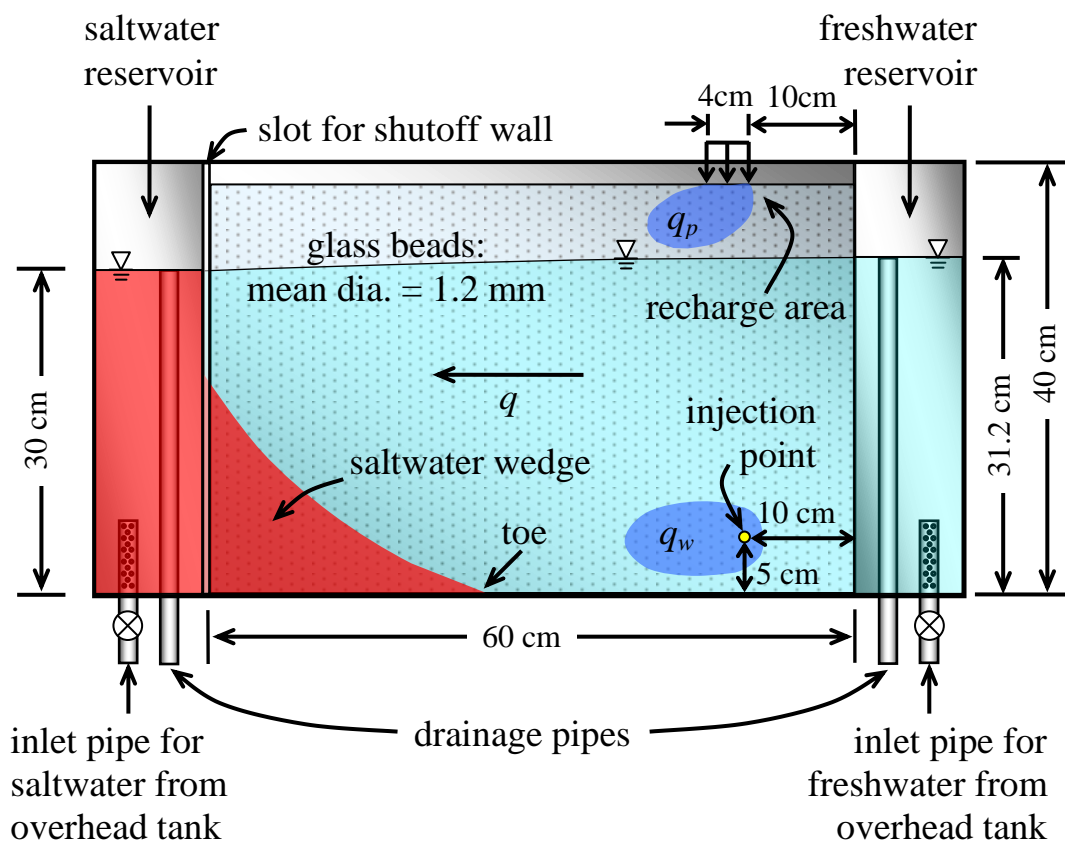


Figure 4.1 Schematic diagram of the experimental setup for the artificial recharge experiments.

measured with a Horiba ES-51 conductivity meter (Figure 4.2). Several buckets of freshwater recharge, which was dyed with a blue food color [Brilliant Blue 2 (C.I. Number 42090), Kiriya Chemical Co., Ltd.], were also prepared to act as a tracer and distinguish it from the actual freshwater discharge (Figure 4.3). With a concentration of 0.2 g dye per 12 L solution, the recharge water retained the same density as the freshwater. Filtered tap water was used for freshwater source. Recorded data were also cross-checked with photographs taken at various intervals with a high resolution digital camera.

4.2.2 Experimental Procedure

The porous section and reservoirs were initially filled with freshwater. The drainage pipes on the freshwater and saltwater reservoirs were then adjusted to maintain constant heads of 31.1 cm and 30.0 cm, respectively. Estimated head fluctuations over the course of each experiment were on the order of ± 1.0 mm. This hydraulic gradient allowed for flow from the freshwater reservoir to the saltwater reservoir. After the freshwater flow had stabilized, the hydraulic conductivity of the porous medium was determined. The average value of K and n in the flow barrier experiments were found to be 1.31 cm/s and 0.4, respectively. The shutoff wall was then inserted and tap water on the left tank was replaced with the red saltwater. The saltwater intrusion process was initiated with the removal of this shutoff wall. Density driven flow progressed until an equilibrium condition was achieved forming the characteristic saltwater wedge.

Two types of experiments were performed after the equilibrium saltwater wedge position was reached. The first set of experiments involves the application of freshwater recharge from the surface to simulate a recharge pond. The second set of experiments



Figure 4.2 Horiba ES-51 conductivity meter.



Figure 4.3 Blue food color used to dye the freshwater recharge.

involves the application of freshwater recharge by continuous point injection simulating a recharge well with a small perforated portion at the bottom end of the pipe. This is different from fully penetrating recharge well usually applied in confined aquifers (e.g. Mahesha 1996a, 1996b). The initial freshwater flux (q) resulting from the head gradient was measured from the drainage discharge through the system and the corresponding recharge rates from the recharge pond (q_p) and recharge well (q_w) were computed from this value. As in the case reported by Goswami and Clement (2007), the freshwater flux transmitted in the presence of the saltwater wedge was expectedly less than the flow values without the wedge or during the estimation of the hydraulic conductivity value. Both the recharge pond and recharge well experiments include two cases. Case 1 has recharge rates q_p and q_w of about 20% of the initial freshwater flux while Case 2 has q_p and q_w values of about 40% of the initial freshwater flux. Specific recharge values for each experimental case are listed in Table 4.1.

Upon application of freshwater recharge in both the recharge pond and recharge well experiments, the toe position and movement of the saltwater intrusion wedge were observed and recorded. The recharge plume development and its effect on the salt wedge were observed and analyzed. Freshwater levels in the flow tank were also observed using piezometers connected from the bottom of the tank. The experiments were ended once a steady state condition was established, that is, changes were no longer observed in the toe position of the saltwater wedge and the drainage discharge from the system. The saltwater repulsion ratio R achieved in each experiment was again calculated using Equation 3.1, where L in this case is the final toe position after recharge application.

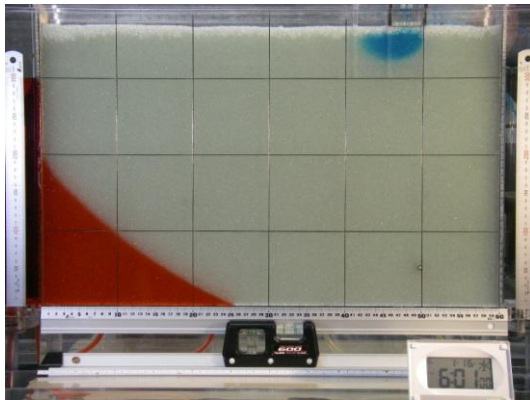
Table 4.1 Experimental parameters for artificial recharge.

Experiment and Case Number		q (cm ² /s)	$q_{recharge}$ (cm ² /s)	$q_{recharge}/q$ (%)
1. Recharge pond	Case 1	0.598	0.120	20.1
	Case 2	0.568	0.238	41.9
2. Recharge well	Case 1	0.589	0.114	19.4
	Case 2	0.620	0.250	40.3

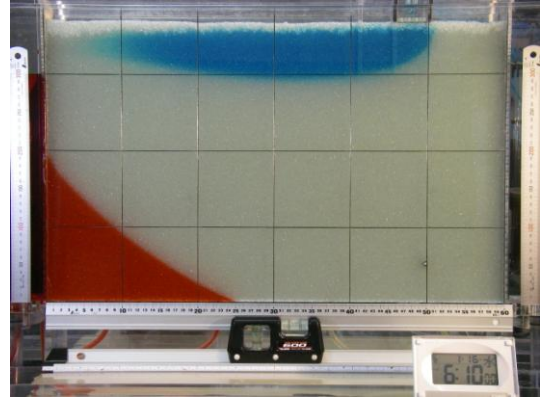
4.3 Experimental Results and Discussion

4.3.1 Recharge Pond Experiment

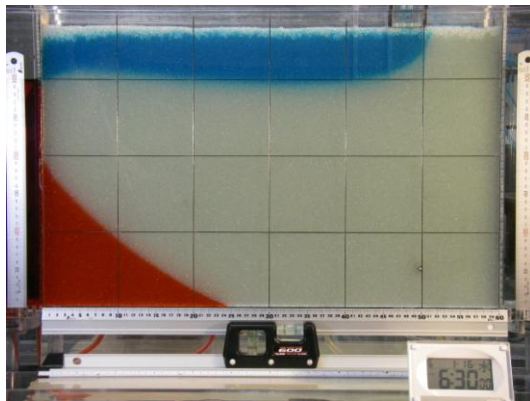
The initial steady state saltwater intrusion and the resulting saltwater wedge after surface recharge application at time intervals of 1, 10, 30 min for Cases 1 and 2 are shown in Figures 4.4 and 4.5, respectively. The original saltwater wedge pattern is indicated by the dashed line. The red segment is the saltwater intrusion wedge while the blue plume represents the freshwater recharge flow. The blue freshwater plume acts as a tracer showing the actual recharge flow. Because they have the same density as the freshwater discharge, the blue recharge plume stayed at or near the surface as it flowed towards the saltwater reservoir. This indicated that the effect of surface recharge lies on increasing the hydraulic head to counteract the density effect of the intruding saltwater wedge.



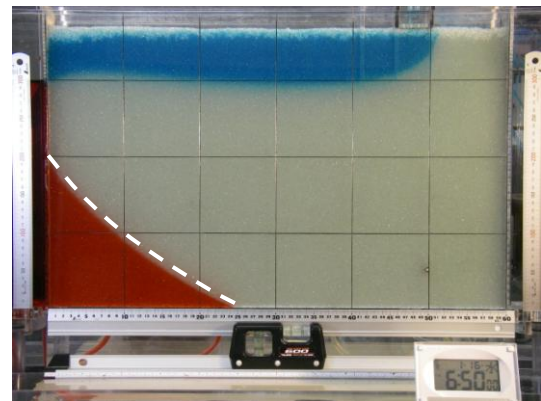
(a) After 1 min



(b) After 10 min

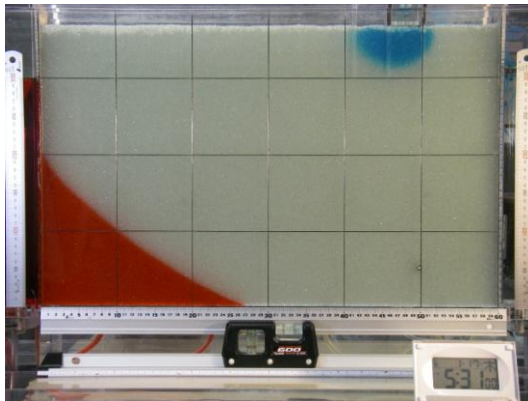


(c) After 30 min

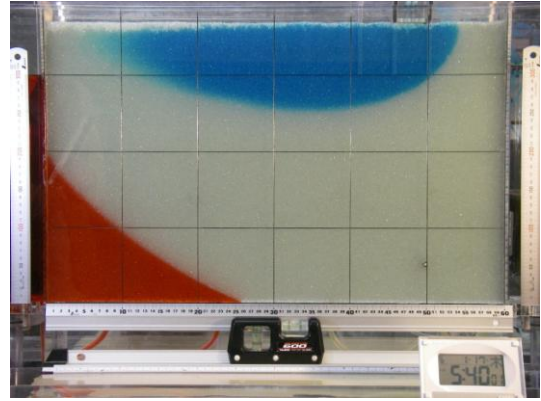


(d) Steady state condition (dashed line indicates original saltwater profile)

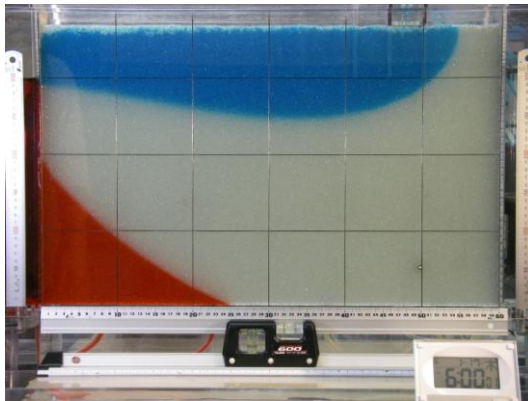
Figure 4.4 Behavior of the saltwater wedge after application of 20% surface recharge (Case 1).



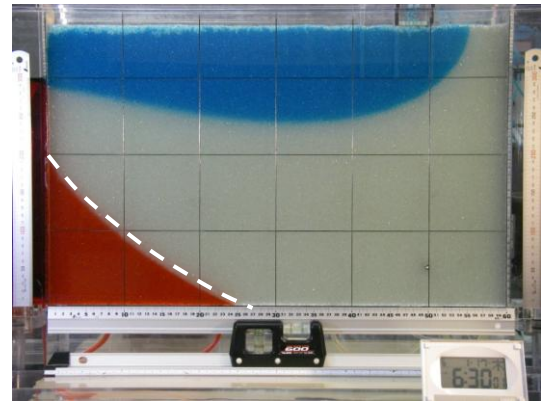
(a) After 1 min



(b) After 10 min



(c) After 30 min



(d) Steady state condition (dashed line indicates original saltwater profile)

Figure 4.5 Behavior of the saltwater wedge after application of 40% surface recharge (Case 2).

The initial steady state saltwater toe position was measured at 25.5 cm from the saltwater reservoir. The application of about 20% surface recharge (Case 1) attained a saltwater toe retreat of only 1.2 cm from the original toe position for a little less than 5% repulsion. Increasing the surface recharge to around 40% (Case 2) also increased the retreat of the toe position to 2.3 cm or about 8% repulsion. The retreat or reduction in the saltwater wedge toe position after recharge application and the corresponding saltwater repulsion R for the two cases are shown in Figure 4.6. Equilibrium conditions after surface recharge application was usually achieved in less than 1 h. For the given initial and boundary conditions, these results showed that the application of about 20% recharge could achieve percentage repulsions equivalent to the annual reduction achieved in coastal unconfined aquifers under high annual rainfall condition (Mahesha and Nagaraja, 1996). The results also showed that the application of recharge from surface resulted only in minor attenuation of the saltwater wedge. Increasing the recharge resulted in a slight increase in the attenuation of the saltwater wedge. But this increase in surface recharge rate is impractical considering that a larger pond area would be required for a small percentage increase in saltwater repulsion.

4.3.2 Recharge Well Experiment

The initial steady state saltwater intrusion and the resulting saltwater wedge after recharge application by point injection at time intervals of 1, 10, 30 min for Cases 1 and 2 are shown in Figures 4.7 and 4.8, respectively. The original saltwater wedge pattern is again indicated by the dashed line. As the recharge plume flows towards the saltwater wedge and over the transition zone, we observed the reduction in the toe length of the saltwater intrusion. The recharge plume for Case 2 reached into the bottom of the flow

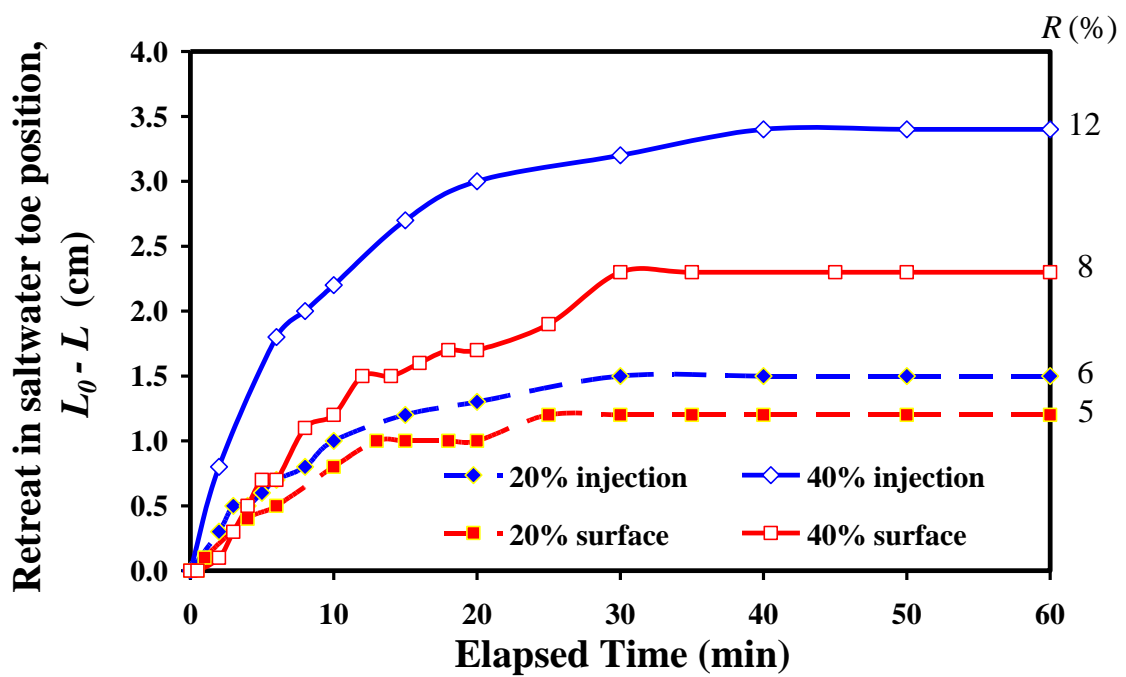
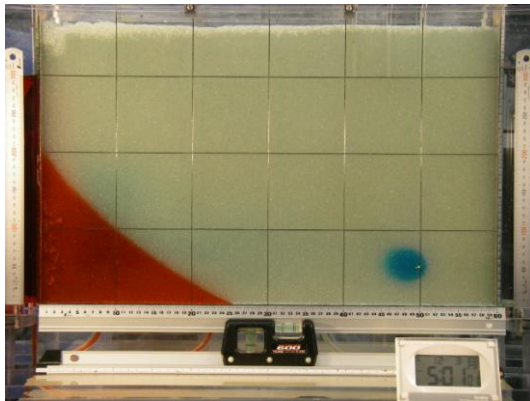
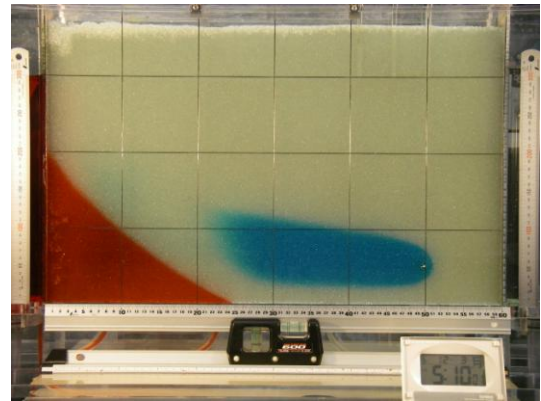


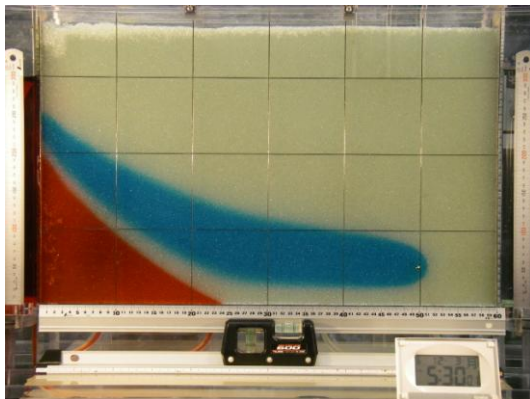
Figure 4.6 Retreat in saltwater wedge toe position with time after recharge application and the corresponding saltwater repulsion R .



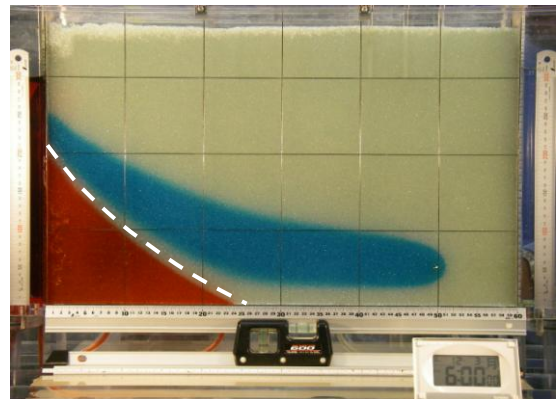
(a) After 1 min



(b) After 10 min

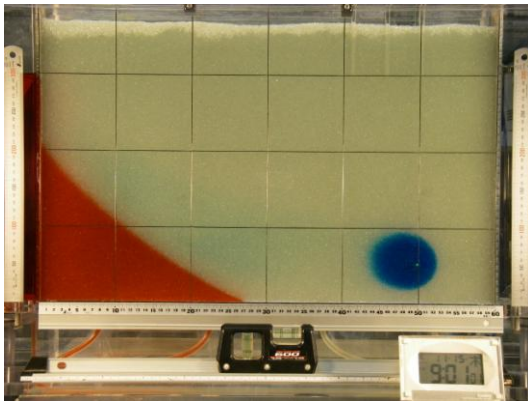


(c) After 30 min

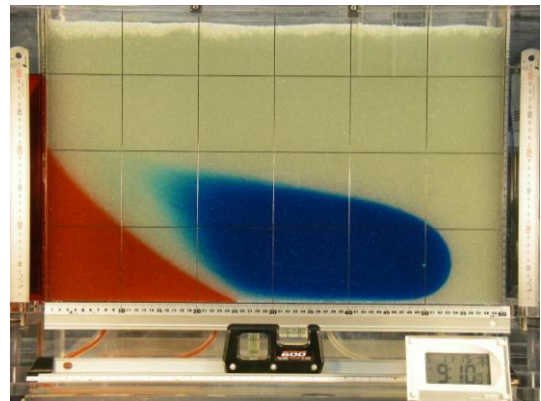


(d) Steady state condition (dashed line indicates original saltwater profile)

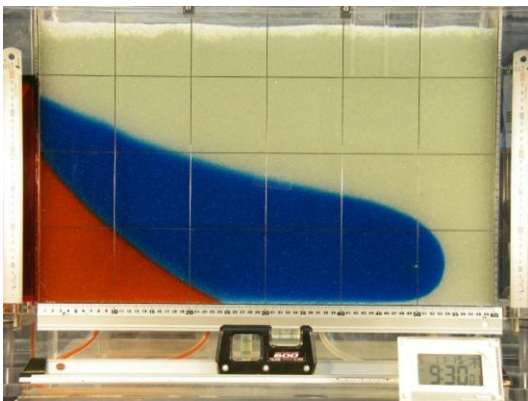
Figure 4.7 Behavior of the saltwater wedge after application of 20% injection recharge (Case 1).



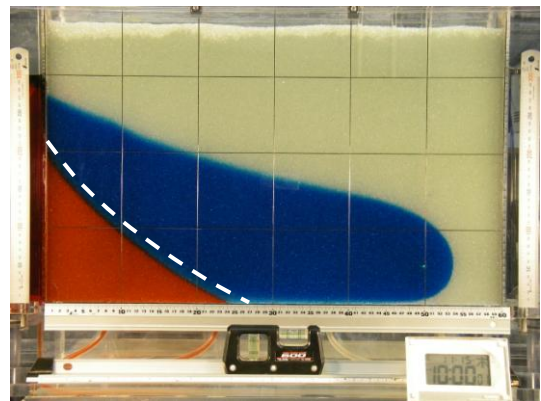
(a) After 1 min



(b) After 10 min



(c) After 30 min



(d) Steady state condition (dashed line indicates original saltwater profile)

Figure 4.8 Behavior of the saltwater wedge after application of 40% injection recharge (Case 2).

tank and flowed over the saltwater wedge forming the transition zone. This transition zone between the blue recharge plume and the saltwater wedge is more distinct and was estimated to be about 1 cm wide confirming the results from the previous experiments.

The initial toe position was also measured at 25.5 cm from the saltwater reservoir. The reduction in the saltwater wedge toe position after recharge by point injection and the corresponding repulsion R for the two cases well are also shown in Figure 4.6. Application of about 20% recharge by point injection (Case 1) achieved a reduction of only 1.5 cm from the original toe position or about 6% saltwater repulsion. The toe position retreated further to 3.4 cm, or about 12% repulsion, when the injected recharge was increased to about 40% (Case 2) of the initial freshwater discharge. Increasing the recharge rate resulted in further increase in the reduction of the saltwater wedge, hence more effective saltwater repulsion. A recharge rate that is 40% of the actual seaward freshwater flow may be quite impractical in reality, but in this experiment it gives emphasis to the importance of increased freshwater discharge in repulsing saltwater intrusion. The most practicable recharge rate possible should be applied to achieve maximum repulsion.

The analytical solution by Hunt (1985) was applied to calculate the saltwater wedge toe position resulting from the injection recharge applied in our experiment. Hunt's solution for the interface toe is given as:

$$\frac{K h_s^2}{2} \Delta(1 + \Delta) = Lq + \frac{Q_w}{2\pi} \ln\left(\frac{x_w + L}{x_w - L}\right) \quad (4.1)$$

where: L is the final toe position after injection recharge [L],

h_s is the saltwater level at the reservoir measured from the bottom of the aquifer [L] and,

Q_w is the volumetric recharge rate [L^3T^{-1}] at the well located x_w [L] from the coast.

Applying the laboratory data into Equation 4.1, the repulsions were computed to be about 4% and 11% for the conditions of Case 1 and 2, respectively. These are in good agreement with the recharge well experimental results. Hunt's steady state equation is valid only for x_w greater than the expected saltwater wedge toe L . Moreover, the cases treated here are for point injection of recharge because a two-dimensional representation of a recharge well with a screened portion (line injection) is difficult to perform in the existing laboratory setup. Observation of the recharge plume also showed that a hydraulic barrier is not achieved even after the recharge rate was doubled. As such, numerical simulations were used to try to duplicate the experiments and then determine the location of injection points that would achieve effective saltwater repulsion. Recharge application by point and line injection were also compared.

4.4 Numerical Approach

The recharge well experiment Case 1 was numerically simulated to test the SEAWAT model code. The surface recharge experiment was not simulated due to the complexity brought about by flow through the unsaturated zone. Instead simulation of injection recharge located just below the recharge zone was performed in its place. The simulation area in the two-dimensional vertical cross section was 60 by 32 cm in the x and z directions, respectively (Figure 4.9). The block-centered finite-difference grid interval was set at $\Delta x = \Delta z = 0.5$ cm. The boundary conditions, longitudinal dispersivity and dispersivity ratio, freshwater and saltwater densities and concentrations used in the subsurface dam simulation were also used here. Values of n and K were similar to the experiment at 0.4 and 1.31 cm/s, respectively. The injected recharge flux (q_w) of 0.114 cm²/s was also the same as in the experiment but was given a minimal concentration of 1.0 mg/L to distinguish it from the freshwater inflow and act as a conservative tracer. The injection points were set at different locations outside of the saltwater wedge. Numerical simulations with line injections having 5 and 10 cm screens from the bottom of the aquifer were also performed and the results were compared with those from point injections. The same recharge flux was used for the point and line injection simulations.

Two transient stress periods were also set for the simulations. The first stress period for the intruding saltwater wedge was set to only 3 h, enough to cover the time until steady state is reached. The second stress period started with the recharge application and was set to 6 h. Only the TVD scheme was used to solve the advection term. Parameter values for the simulations are listed in Table 4.2. Simulation of the recharge well was repeated at different injection points outside of the saltwater wedge to

determine at which location the maximum repulsion will be achieved. The percentage repulsion R values achieved at each point were then computed using Equation 3.1.

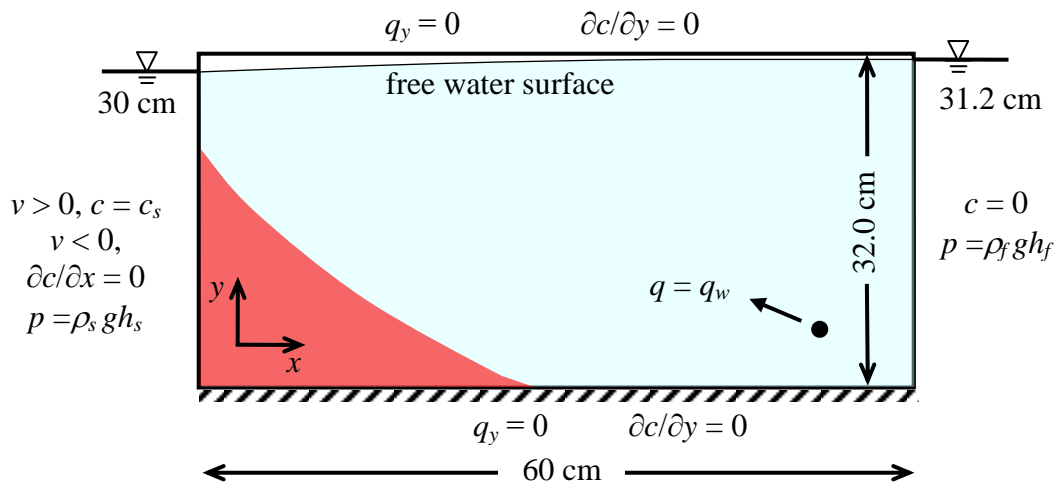


Figure 4.9 Initial and boundary conditions for the artificial recharge numerical simulations.

Table 4.2 Numerical simulation parameters for recharge wells.

Input parameters	Values
Porosity	0.4
Freshwater level h_f (cm)	31.2
Saltwater level h_s (cm)	30.0
Freshwater density ρ_f (g/cm ³)	1.000
Saltwater density ρ_s (g/cm ³)	1.025
Saltwater concentration C (mg/L)	35000
Recharge concentration C_f (mg/L)	1.0
Recharge flux q_w (cm ² /s)	0.114
Hydraulic conductivity k (cm/s)	1.31
Longitudinal dispersivity α_L (cm)	0.12
Transverse dispersivity α_T (cm)	0.012
Molecular diffusion coefficient (cm ² /s)	1×10^{-5}
Cell size	
Layer 1 to 80; $\Delta x \times \Delta z$ (cm)	0.5×0.5
Solution of flow equation	
Matrix solution technique	PCG
Head convergence value (m)	1×10^{-7}
Flow convergence value (kg/day)	1×10^{-7}
Solution of transport equation	
Advection term	TVD
Courant Number	0.1
Dispersion and source terms	GCG
Concentration convergence value	1×10^{-7}

4.5 Numerical Results and Discussion

The simulation results displaying the saltwater intrusion wedge, velocity vector distribution and concentration profile are shown in Figure 4.10. The relative saltwater concentrations (C_{rs}) are fractions of the 35 g/L salt concentration (Figure 4.10a) while the relative recharge concentrations (C_{rf}) are fractions of the 0.001 g/L recharge concentration. The modeling results in Figures 4.10a to 4.10d may be compared to the experimental results for recharge well Case 1 shown in Figures 4.7a to 4.7d. The initial toe position in the simulation result is 25.2 cm at $C_{rs} = 0.5$ or at the 0.5 isochlor line. This agrees well with the 25.5 cm measured in the experiment. This initial equilibrium state was achieved after about 2 h in both the experimental and numerical results. The freshwater–saltwater mixing zone between the 0.1 and 0.9 isochlors is about 1 cm thick, similar to that observed in the experiment. The simulation results for the point injection of about 20% recharge achieved a reduction of 1.3 cm from the original toe position for a little over 5% saltwater repulsion. This agrees well with the 1.5 cm or about 6% repulsion achieved in the experiment and the 1.1 cm and 4% repulsion using Equation 4.1. This shows that the SEAWAT model can accurately duplicate the experimental results.

Figure 4.11 shows the location of injection points with reference to the initial saltwater wedge at the 0.5 isochlor. The experimental injection point is at the bottom extreme right while the injection point representing the experimental recharge pond is at the topmost extreme right. The rest of the points are separated by 10 cm in both x and z directions. More points were added in the vicinity of saltwater toe, including one point at the actual toe position and one immediately to its right, bringing the total to 17

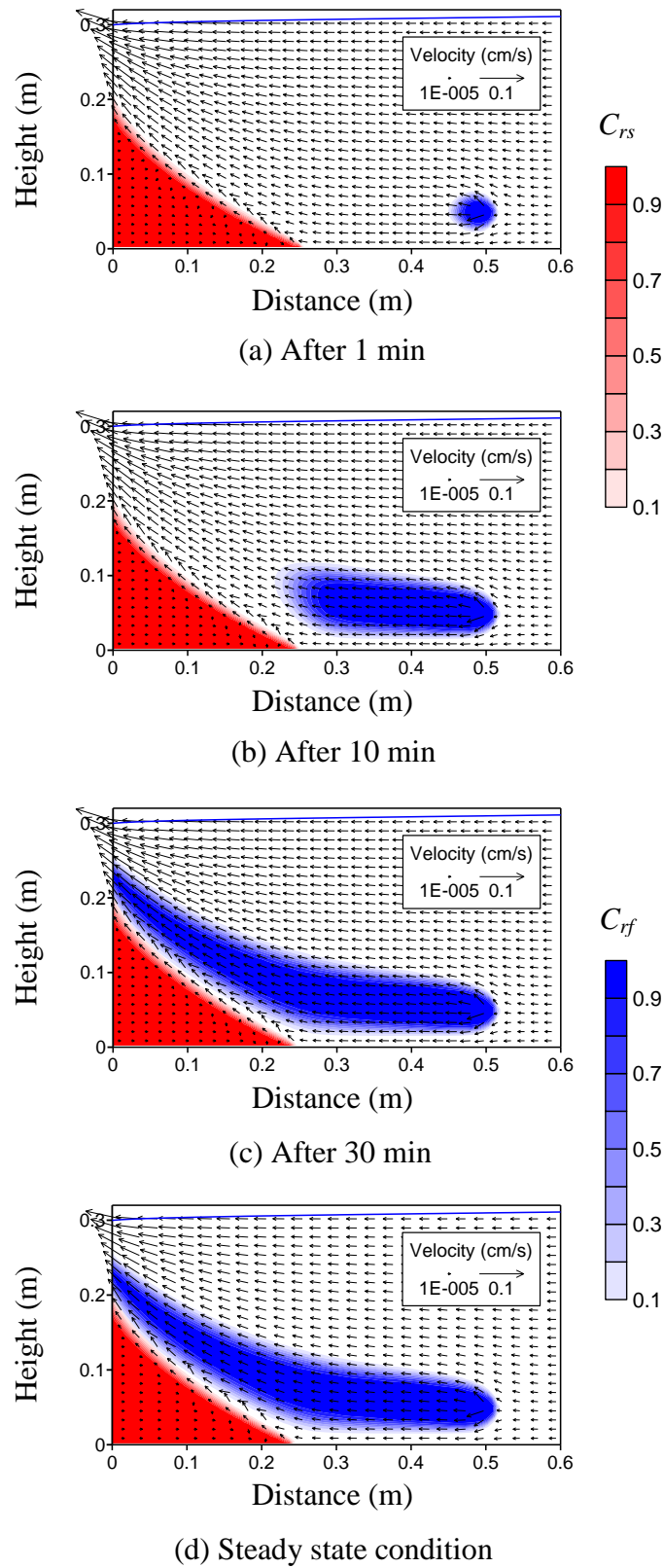


Figure 4.10 Steady state model results for recharge well (Case 1).

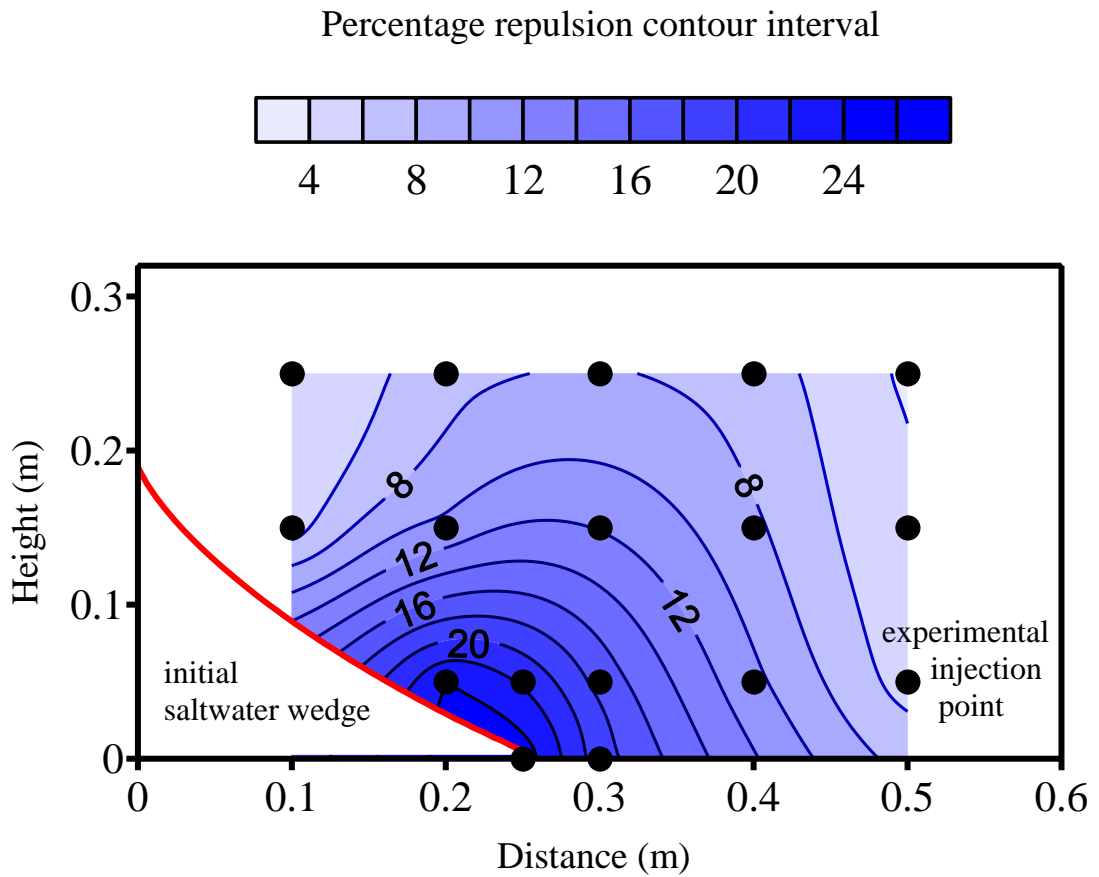


Figure 4.11 Percentage repulsion of seawater intrusion based on location of recharge well injection points (●).

injection points. The steady state simulation results for the different recharge injection points are not shown in this section but can be reviewed in Appendix B.1. Instead, the computed repulsion ratio R from the simulation result at each injection point was interpolated to generate contour lines of equal repulsion rates as shown in Figure 4.11. The maximum repulsion of about 25% was achieved by the injection point at the toe itself. At this point, the recharge water created a hydraulic barrier emanating from the aquifer bottom that directly repels the intruding saltwater [Appendix B.1 (q)]. The point just above and to the left of the toe ($x = 20$ cm, $z = 5$ cm) attained a 24% repulsion. The hydraulic pressure created at this point was still effective but did not reach the aquifer bottom allowing the saltwater to intrude from below [Appendix B.1 (e)]. The injection point on top of the toe 5 cm from the bottom achieved about 22% repulsion while the point just right of the toe ($x = 30$ cm) achieved about 19% repulsion. The computed saltwater repulsion then decreases as the injection point becomes farther from or higher than the toe position. The results in Figure 4.11 indicate that the most effective location for recharge application by injection is near the saltwater toe. The created hydraulic pressure is very effective if directly applied near the saltwater toe and diminishes when applied farther away from the toe. These results also suggest that surface recharge would be less effective than injection wells in controlling saltwater intrusion for the same recharge rate. The simulation result for the injection point representing the experimental recharge pond achieved a saltwater repulsion of about 4%, close to the 5% achieved in the experiment. For surface recharge, the most effective location would be above the toe because of the increased pressure head created by the recharge water, as shown by the 8% repulsion attained at this location for the same recharge rate.

Recharge wells with 5 and 10 cm screened lengths (line injection) from the bottom of the aquifer were also simulated. They were installed at horizontal distances of $x = 25, 30, 40$ and 50 cm. The same recharge rate, q_w as in the point injection was also applied. The steady state simulation results for the screened recharge wells are shown in Appendix B.2. The results show that at the saltwater toe ($x = 25$ cm), the 5 cm screened well achieved about 24% repulsion, which is not much different from that attained by the point injection well at the toe, while the 10 cm well achieved about 22% repulsion, which is the same as that achieved by point injection at $z = 5$ cm. Moreover, results from both the 5 and 10 cm screened wells at $x = 30, 40$ and 50 cm are not much different from the point application results at $z = 5$ cm. At locations outside the saltwater wedge, line injection merely spreads the applied recharge vertically such that for the same recharge rate, point application of recharge achieves the same repulsing effect as line application. A more concentrated hydraulic pressure is exerted on the salt front by point injection than line injection for the same recharge rate. A shorter well screen length can therefore be used as long as the recharge water is directly applied near the saltwater toe.

Note that this study is for a two-dimensional analysis of a single recharging well. A series of closely spaced well is usually installed paralleling the coast where the formation of the hydraulic barrier is also dependent on the spacing of the wells. It is assumed here that the well spacing is close enough to create a uniform barrier paralleling the coast. Moreover, the recharge wells used in this study are set outside the initial saltwater wedge. Recharge water may be applied directly within the intruding saltwater wedge. With enough recharge flux to overcome the density effect, the

recharge water can cause increased dispersion and create a hydraulic barrier that can effectively repel the intruding saltwater.

4.6 Conclusion

Laboratory-scale experiments and numerical simulations were performed to examine the behavior of the saltwater intrusion wedge upon application of artificial recharge from recharge ponds and recharge wells. Specifically, the effects of recharge rate, as well as, the effects of location and mode of application in recharge wells were determined. The recharge wells presented here are located outside the intruding saltwater wedge. The experimental results show that saltwater repulsion increases with recharge rate in both recharge pond and recharge well experiments. The model results for injection recharge agree well with both the experimental results and a closed-form analytical solution. Numerical simulations with different injection locations show that more effective saltwater repulsion can be achieved if recharge is applied near the toe of the saltwater wedge. Recharge application becomes less effective if applied farther and higher from the saltwater wedge toe. Recharge application works by creating a hydraulic barrier against the density effect of the intruding seawater and is more effective when applied directly at the saltwater wedge toe. These results also suggest that for the same recharge rate, recharge ponds would be less effective than recharge wells in controlling saltwater intrusion. For surface recharge, the most effective location would be above the toe because of the increased pressure head created by the recharge water. Model results also show that there is not much difference between point and line applications, particularly at distances farther away from the saltwater toe.

Chapter

5

**General Conclusion and
Recommendations**

This research presented two methods to control seawater intrusion into unconfined coastal aquifers. The first countermeasure involves the construction of subsurface physical barriers, through subsurface dams and subsurface flow barriers. The second control method is the application of artificial recharge from both recharge ponds and recharge wells. A series of laboratory-scale experiments and numerical simulations were performed to determine the effectiveness of each method. The summary of the important findings from each of the studies in this research are discussed below.

The main contribution of this research is that it showed that the residual saltwater trapped in the storage area of cutoff walls will be gradually but completely flushed out by the freshwater flow from inland. Although this phenomenon was predicted by Oswald et al. (2002), they did not actually present the complete removal of saltwater from a closed system. This study has proven the effectiveness of subsurface dams in controlling saltwater intrusion and in increasing groundwater storage capacity. And while residual saltwater removal in real-world scenarios may involve a much longer time than are shown in the experimental and numerical results in these studies, the analyses of the flow dynamics involved show that complete removal will eventually occur. Moreover, this study has shown that at the desired installation site, the crest of the subsurface dam to be constructed need only exceed the thickness of the saltwater wedge in order to induce complete saltwater removal. This shows that shorter subsurface dams could be installed to save on costs. This also implies that a higher crest is needed if the dam is to be installed closer to the coast. Height allowances for the tides and expected rise in seawater levels should also be incorporated in the design.

For subsurface flow barriers, a general equation was developed relating barrier penetration depth and horizontal location with saltwater repulsion. This study showed that saltwater repulsion is linearly related to horizontal barrier location and a third-order polynomial function of barrier penetration depth. More effective saltwater repulsion can be achieved with deeper barrier penetration and at locations closer to the coast. Conversely, when the barrier is installed upstream of the original toe position, freshwater flow towards the sea is impeded and saltwater intrusion will be exacerbated. There are, of course, site and depth limitations to be considered in actual cases. For the given hydraulic gradient, the generalized equation could prove useful in determining the theoretical saltwater repulsion expected from a subsurface flow barrier of specific depth and location relative to the toe of the intruding saltwater wedge. When confronted with site, depth and cost limitations, the optimal barrier location and depth of penetration that would result to more effective saltwater repulsion can be determined. The derived equation, however, is applicable for the given boundary conditions only. Future studies would include the effect of varying groundwater flow as a function of changing hydraulic gradient. Although results from preliminary studies have shown that repulsion ratio increases with hydraulic gradient, the exact relationship should still be determined to generate a more generalized equation than previously derived in this study. The validity of these results could also be tested under varying factors such as hydraulic conductivity, dispersivity, etc.

Artificial recharge was more effective in saltwater repulsion if applied near the toe of the saltwater wedge and less effective if applied farther and higher from the saltwater wedge toe. Artificial recharge works by creating a hydraulic barrier that exerts pressure on the salt front. This effect diminishes when recharge is applied farther away from the

saltwater toe. Thus for the same recharge rate, recharge wells are more effective than recharge ponds in controlling saltwater intrusion. Recharge ponds or spreading basins should be located directly above the toe for more effective saltwater repulsion because of the increased pressure head created by the recharge water. This is not easy to implement in actual cases because the critical sites are more often located in urban areas where available lands are limited and costly. In terms of application, for the same recharge rate, the hydraulic pressure exerted on the salt front by point injection is about the same as that by line application. Considering the high costs of perforated pipes and gravel packing for wells, a smaller well screen length may be more advantageous than fully penetrating wells, as long as the pipe screened section is set near the saltwater toe.

The study was conducted under two-dimensional, homogeneous, isotropic conditions, and tidal fluctuation was neglected. While a three-dimensional experimental setup require sophisticated instrumentation for non-intrusive salt concentration measurement and the actual experimentation is difficult to perform, a three-dimensional simulation having different boundary settings could be easily performed using the SEAWAT model. Prior to actual field investigations, field scale numerical analyses using actual field scenarios could be considered. This may or may not include tidal fluctuations but parameter sensitivity analysis should be included. Subsurface heterogeneity would result in different saltwater intrusion and repulsion than presented in this research, and should also be considered in future studies. In the numerical simulation, the longitudinal dispersivity (α_L) was set equal to the mean diameter of the glass beads while the horizontal dispersivity (α_T) was set to 1/10 that of α_L . While these values are within generally accepted ranges and have been used in many previous

researches, accurate values can be derived for the given porous medium using either one-dimensional cylindrical tests or flow tank experiments.

This research has shown the value of numerical simulation in helping explain the phenomena observed from the experiments. Careful analyses of the flow patterns and relative concentration contours from the model helped explain the dynamics of saltwater upon introduction of a new set of boundary conditions such as the installation of physical barriers and the application of artificial recharge. These would not have been possible or would have proven difficult using only experimental observation from laboratory-scale flow tanks or actual field monitoring. As long as the parameters, assumptions and boundary conditions used represents, or are close to actual conditions, and that proper model tests are performed, numerical simulations can provide fairly accurate and convenient solutions to many groundwater problems. With regards to model testing, this research presented the worthiness of the SEAWAT code in simulating the variable-density groundwater flow problems. The model was able to accurately predict the transient positions of the advancing saltwater wedge and the retreating residual saltwater after cutoff wall installation. This transient behavior provides a more robust test for other density-coupled groundwater flow models than the steady state Henry problem.

The applicability of all these findings to actual scenarios lies on accurate prediction of the extent of saltwater intrusion and toe location, thus, the importance of onsite investigation and monitoring should be emphasized. It is my fervent hope that the findings from this research will help in future planning and design of subsurface barriers and artificial recharge facilities for seawater intrusion control.

References

- Abarca, E., Vazquez-Suñe, E., Carrera, J., Capino, B., Gamez, D., Batlle, F., 2006. Optimal design of measures to correct seawater intrusion. *Water Resources Research* 42, W09415, doi:10.1029/2005WR004524.
- Ackerer, P., Younes, A., Mose, R., 1999. Modeling variable density flow and solute transport in porous medium: I. Numerical model and verification. *Transport in Porous Media* 35, 345-373.
- Anwar, H.O., 1983. The effect of a subsurface barrier on the conservation of freshwater in coastal aquifers. *Water Research* 17 (10), 1257-1265.
- Ataie-Ashtiani, B., Volker, R.E., Lockington, D.A., 1999. Tidal effects on sea water intrusion in unconfined aquifers. *Journal of Hydrology* 216, 17-31.
- Bakker, M., Oude Essink, G.H.P., Langevin, C.D., 2004. The rotating movement of the three immiscible fluids – a benchmark problem. *Journal of Hydrology* 287, 270-278.
- Bauer, P., Held, R.J., Zimmermann, S., Linn, F., Kinzelbach, W., 2006. Coupled flow and salinity transport modelling in semi-arid environments: The Sahshe River Valley, Botswana. *Journal of Hydrology* 316, 163-183.
- Bear, J., 1961. On the tensor form of dispersion in porous media. *Journal of Geophysical Research* 66 (4), 1185-1197.
- Bear, J., 1972. *Dynamics of fluid in porous media*. Elsevier, New York.

- Bear, J., 1979. *Hydraulics of Groundwater*. McGraw-Hill Book Co., Inc., New York.
- Bear, J., Cheng, A.H.-D., 1999. Introduction. In: *Seawater intrusion in coastal aquifers – concepts, methods and practices*. Bear, J., Cheng, A.H.-D., Sorek, S., Ouazar, D., Herrera, I. (Eds.). Kluwer Academic Publishers. Dordrecht, The Netherlands, pp.1-8.
- Brovelli, A., Mao, X., Barry, D.A., 2007. Numerical modeling of tidal influence on density-dependent contaminant transport. *Water Resources Research* 43, W10426, doi:10.1029/2006WR005173.
- Bruington, A.E., Seares, F.D., 1965. Operating a seawater barrier project. *Journal of Irrigation and Drainage Engineering* 91 (1), 117-140.
- Bues, M.A., Oltean, C., 2000. Numerical simulations for saltwater intrusion by the mixed hybrid finite element method and discontinuous finite element method. *Transport in Porous Media* 40 (2), 171–200.
- Croucher, A.E., O’Sullivan, M.J., 1995. The Henry problem for saltwater intrusion. *Water Resources Research* 31 (7), 1809–1814.
- Dagan, G., Bear, J., 1968. Solving the problem of local interface upconing in a coastal aquifer by the method of small perturbation. *Journal of Hydraulic Research* 6, 15-44.
- Diersch, H-J.G., Kolditz, O., 1998. Coupled groundwater flow and transport: 2. Thermohaline and 3D convection systems. *Advances in Water Resources* 21 (5), 401–425.

- Diersch, H-J.G., Kolditz, O., 2002. Variable-density flow and transport in porous media: Approaches and challenges. *Advances in Water Resources* 25, 899–944.
- Freeze, R.A., Cherry, J.A., 1979. *Groundwater*. Prentice-Hall, Inc., New Jersey.
- Gambolati, G., Putti, M., Paniconi, C., 1999. Three-dimensional model of coupled density-dependent flow and miscible salt transport in groundwater. . In: *Seawater intrusion in coastal aquifers – concepts, methods and practices*. Bear, J., Cheng, A.H.–D., Sorek, S., Ouazar, D., Herrera, I. (Eds.). Kluwer Academic Publishers. Dordrecht, The Netherlands, pp. 315-362.
- Goswami, R.R., Clement, T.P., 2007. Laboratory-scale investigation of saltwater intrusion dynamics. *Water Resources Research* 43, W04418, doi:10.1029/2006WR005151.
- Guo, H., Jiao, J.J., 2007. Impact of coastal land reclamation on ground water level and the sea water interface. *Ground Water* 45 (3), 362-367.
- Guo, W., Langevin, C.D., 2002. User's guide to SEAWAT: a computer program for simulation of three-dimensional variable-density groundwater flow. US Geological Survey Techniques of Water Resources Investigations 6-A7. Tallahassee, Florida.
- Hanson, G., Nilsson, A., 1986. Ground-water dams for rural-water supplies in developing countries. *Ground Water* 24 (4), 497-506.
- Harbaugh, A.W., Banta, E.R., Hill, M.C., McDonald, M.G., 2000. MODFLOW-2000, The U.S. Geological Survey modular ground-water model – User guide to

- modularization concepts and the ground-water flow process. USGS Open File Report 00-92. Reston, Virginia.
- Harleman, D.R.F., Rumer, R.R., 1963. Longitudinal and lateral dispersion in an isotropic porous medium. *Journal of Fluid Mechanics* 16 (3), 385-394.
- Harpaz, Y., 1971. Artificial groundwater recharge by means of wells in Israel. *Journal of Hydraulic Engineering* 97 (12), 1947-1964.
- Henry, H.R., 1964. Effects of dispersion on salt encroachment in coastal aquifers. US Geological Survey Water-Supply Paper 1613-C, C71-C84.
- Herbert, A.W., Jackson, C.P., Lever, D.A., 1988. Coupled groundwater flow and solute transport with fluid density strongly dependent upon concentration. *Water Resources Research* 24 (10), 1781–1795.
- Hill, M.C., 1990. Preconditioned Conjugate-Gradient 2 (PCG2), a computer program for solving groundwater flow equations. USGS Water-Resources Investigation Report 90-4048, Denver.
- Holzbecher, E.O., 1998. Modeling density-driven flow in porous media: principles, numerics, software. Springer, Berlin.
- Hubbert, M.K., 1940. The theory of ground-water motion. *Journal of Geology* 48 (8), 785-944.
- Hunt, B., 1985. Some analytical solutions for seawater intrusion control with recharge wells. *Journal of Hydrology* 80, 9-18.

- Huyakorn, P.S., Andersen, P.F., Mercer, J., White, H., 1987. Saltwater intrusion in aquifers: development and testing of a three-dimensional finite element model. *Water Resources Research* 2 (23), 293–312.
- Huyakorn, P.S., Pinder, G.F., 1983. *Computational methods in subsurface flow*. Academic Press, New York.
- Illangasekare, T., et al., 2006. Impacts of the 2004 tsunami on groundwater resources in Sri Lanka. *Water Resources Research* 42, W05201, doi:10.1029/2006 WR004876.
- Intergovernmental Panel on Climate Change (IPCC), 2001a. *Climate change 2001: The scientific basis. Contribution of Working Group I to the Third Assessment Report of the IPCC*. <http://www.grida.no/publications/other/ipcc_tar>
- Intergovernmental Panel on Climate Change (IPCC), 2001b. *The regional impacts of climate change: An assessment of vulnerability. Contribution of Working Group II to the Second Assessment Report of the IPCC*. <http://www.grida.no/publications/other/ipcc_sr>
- Japan Green Resources Agency, 2004. *Technical reference for effective groundwater development*. Kanagawa, Japan.
- Johannsen, K., Kinzelbach, W., Oswald, S., Wittum, G., 2002. The salt-pool benchmark problem – Numerical simulation of saltwater upconing in a porous medium. *Advances in Water Resources* 25 (3), 335-348.
- Kim, K.-Y., Seong, H., Kim, T., Park, K.-H., Woo, N.-C., Park, Y.-S., Koh, G.-W., Park, W.-B., 2006. Tidal effects on variations of fresh–saltwater interface and

- groundwater flow in a multi-layered coastal aquifer on a volcanic island (Jeju Island, Korea). *Journal of Hydrology* 330, 525-542.
- Kipp, K.L., 1997. Guide to the revised heat and solute transport simulator: HST3D – Version 2. USGS Water-Resources Investigation Report 97-4157.
- Kolditz, O., Habbar, A., Kaiser, R., Schulze-Ruhfus, M., Thorenz, C., 1998. ROCKFLOW – Theory and Users Manual. Release 3.2. Institut für Stömungsmechanik und Elektronisches Rechnen im Bauwesen, Universität Hannover.
- Kolditz, O., Ratke, R., Diersch, H-J.G., Zielke, W., 1998. Coupled groundwater flow and transport: 1. Verification of variable density flow and transport models. *Advances in Water Resources* 21 (1), 21-46.
- Konikow, L.F. Bredehoeft, J.D., 1978. Computer model of two-dimensional solute transport and dispersion in ground water. U.S. Geological Survey Water Resources Investigation Book 7, Chapter C2, 90 pp.
- Konikow, L.F., Reilly, T.E., 1999. Seawater intrusion in the United States. In: Seawater intrusion in coastal aquifers – concepts, methods and practices. Bear, J., Cheng, A.H.–D., Sorek, S., Ouazar, D., Herrera, I. (Eds.). Kluwer Academic Publishers. Dordrecht, The Netherlands, pp. 463-506.
- Konikow, L.F., Sanford, W.E., Campbell, P.J., 1997. Constant-concentration boundary condition: Lessons from the HYDROCOIN variable-density groundwater benchmark problem. *Water Resources Research* 33 (10), 2253-2261.

- Langevin, C.D., 2003. Simulation of submarine ground water discharge to a marine estuary: Biscayne Bay, Florida. *Ground Water* 41 (6), 758-771.
- Langevin, C.D., Guo, W., 2006. MODFLOW/MT3DMS-based simulation of variable-density ground water flow and transport. *Ground Water* 44 (3), 339 – 351.
- Langevin, C.D., Shoemaker, W.B., Guo, W., 2003. MODFLOW-2000, the U.S. Geological Survey modular ground-water model – Documentation of the SEAWAT-2000 version with the variable-density flow process (VDF) and the integrated MT3DMS transport process (IMT). USGS Open-File Report 03-426. Tallahassee, Florida.
- Mahesha, A., 1996a. Transient effect of battery of injection wells on seawater intrusion. *Journal of Hydraulic Engineering* 122 (5), 266-271.
- Mahesha, A., 1996b. Steady-state effect of freshwater injection wells on seawater intrusion in coastal aquifers. *Journal of Irrigation and Drainage Engineering* 122 (3), 149-154.
- Mahesha A., Nagaraja, S.H., 1996. Effect of natural recharge on sea water intrusion in coastal aquifers. *Journal of Hydrology* 174, 211-220.
- Melloul, A.J., Zeitoun, D.G., 1999. A semi-empirical approach to intrusion monitoring in Israeli coastal aquifer. In: *Seawater intrusion in coastal aquifers – concepts, methods and practices*. Bear, J., Cheng, A.H.–D., Sorek, S., Ouazar, D., Herrera, I. (Eds.). Kluwer Academic Publishers. Dordrecht, The Netherlands, pp.543-558.

- Momii, K., Shoji, J., Nakagawa, K., 2005. Observations and modeling of seawater intrusion for a small limestone island aquifer. *Hydrological Processes* 19, 3897-3909.
- Nagata, S., Azuma, K., Asano, M., Nishijima, T., Shiiba, H., Yang, D.S., Nakata, R., 1994. Nakajima subsurface dam, Water policy and management: solving the problems. Proceeding of the 21st Annual Conference, Water Resources Planning and Management Division, ASCE. Denver, Colorado. <http://www.danielsandhouse.com/subsurface_dam.shtm>
- Nakagawa, K., Momii, K., Berndtsson, R., 2005. Saltwater intrusion in coastal aquifer – comparison between the CIP and MOC simulation technique. *Environmental Modeling and Assessment* 10, 323-329.
- Nishigaki, M., Kankam-Yeboah, K., Komatsu, M., 2004. Underground dam technology in some parts of the world. *Journal of Groundwater Hydrology* 46 (2), 113-130.
- Ogata, A., 1970. Theory of dispersion in a granular medium. US Geological Survey Professional Paper 411-I.
- Oldenburg, C.M., Pruess, K., 1995. Dispersive transport dynamics in a strongly coupled groundwater-brine flow system. *Water Resources Research* 31 (2), 289-302.
- Oostrom, M., Hayworth, J.S., Dane, J.H., Guven, O., 1992. Behavior of dense aqueous phase leachate plumes in homogeneous porous media. *Water Resources Research* 28 (8), 2123-2134.

- Organisation for Economic Co-operation and Development (OECD), 1988. The International HYDROCOIN project – level 1: Code verification. Rep. 71617, Paris.
- Osuga, K., 1997. The development of groundwater resources on the Miyakojima Islands, Freshwater Resources in Arid lands. Uitto, J.I., Schneider, J. (Eds.). United Nations University Press, Tokyo. <<http://www.unu.edu/unupress/unupbooks/uu02fe/uu02fe0c.htm> >
- Oswald, S.E., Kinzelbach, W., 2004. Three-dimensional physical benchmark experiments to test variable-density flow models. *Journal of Hydrology* 290, 22-42.
- Oswald, S.E., Scheidegger, M.B., Kinzelbach, W., 2002. Time-dependent measurement of strongly density-dependent flow in a porous medium via nuclear magnetic resonance imaging. *Transport in Porous Media* 47, 169-193.
- Oude Essink, G.H.P., 2001. Improving fresh groundwater supply – problems and solutions. *Ocean and Coastal Management* 44, 429-449.
- Pinder, G.F., Cooper, H.H., 1970. A numerical technique for calculating the transient position of the saltwater front. *Water Resources Research* 6 (3), 885-892.
- Sanford, W.E., Konikow, L.F., 1985. A two-constituent solute-transport model for ground-water having variable density. USGS Open-File Report 91-536.
- Sauter, F., Leijnse, A., Beusen, A., 1993. METROPOL. User's Guide. Technical Report 725205.003, National Institute of Public Health and Environmental Protection, Bilthoven, the Netherlands.

- Segol, G., 1994. Classic groundwater simulations – proving and improving numerical models. PTR Prentice-Hall, Englewood Cliffs.
- Segol, G., Pinder, G.F., 1976. Transient simulation of saltwater intrusion in southeastern Florida. *Water Resources Research* 12 (1), 65-70.
- Segol, G., Pinder, G.F., Gray, W.G., 1975. A Galerkin-finite element technique for calculating the transient position of the saltwater front. *Water Resources Research* 11 (2), 343-347.
- Sherif, M., 1999. Nile delta aquifer in Egypt. In: *Seawater intrusion in coastal aquifers – concepts, methods and practices*. Bear, J., Cheng, A.H.-D., Sorek, S., Ouazar, D., Herrera, I. (Eds.). Kluwer Academic Publishers. Dordrecht, The Netherlands, pp.559-590.
- Shibasaki, T. and Research Group for Water Balance, 1995. *Environmental management of groundwater basins*. Tokai University Press. Tokyo, Japan.
- Shoemaker, W.B., 2004. Important observations and parameters for a salt water intrusion model. *Ground Water* 42 (6), 829-840.
- Simmons, C.T., 2005. Variable density groundwater flow: from current challenges to future possibilities. *Journal of Hydrogeology* 13, 116-119.
- Simmons, C.T., Fenstemaker, T.R., Sharp, J.M.Jr., 2001. Variable-density groundwater flow and solute transport in heterogeneous porous media: approaches, resolutions and future challenges. *Journal of Contaminant Hydrology* 52 (1-4), 245-275.

- Simpson, M.J., Clement, T.P., 2004. Improving the worthiness of the Henry problem as a benchmark for density-dependent groundwater flow models. *Water Resources Research* 40, W01501.
- Stakelbeek, A., 1999. Movement of brackish groundwater near a deep-well infiltration system in the Netherlands. In: *Seawater intrusion in coastal aquifers – concepts, methods and practices*. Bear, J., Cheng, A.H.–D., Sorek, S., Ouazar, D., Herrera, I. (Eds.). Kluwer Academic Publishers. Dordrecht, The Netherlands, pp.531-541.
- Strack, O.D.L., 1976. A single-potential solution for regional interface problems in coastal aquifers. *Water Resources Research* 12 (6), 1165-1174.
- Strack, O.D.L., 1995. A Dupuit–Forcheimer model for three-dimensional flow with variable density. *Water Resources Research* 31 (12), 3007-3017.
- Thorenz, C., Kosakowski, G., Kolditz, O., Berkowitz, B., 2002. An experimental and numerical investigation of saltwater movement in coupled saturated-partially saturated systems. *Water Resources Research* 38 (6), 10.1029/2001WR000364.
- Todd, D.K., 1959. *Ground water hydrology*. John Wiley & Sons, New York.
- USEPA, 1987. *Report to Congress: Class V Injection Wells, Office of Groundwater and Drinking Water*. Washington D.C., EPA/ 816-R-99-014t.
- van Dam, J.C., 1999. Exploitation, restoration and management. In: *Seawater intrusion in coastal aquifers – concepts, methods and practices*. Bear, J., Cheng, A.H.–D., Sorek, S., Ouazar, D., Herrera, I. (Eds.). Kluwer Academic Publishers. Dordrecht, The Netherlands, pp. 73-125.

- Voss, C.I., 1984. SUTRA—Saturated Unsaturated Transport—A finite-element simulation model for saturated-unsaturated, fluid-density-dependent ground-water flow with energy transport or chemically-reactive single-species solute transport. USGS Water-Resources Investigation Report 84-4369.
- Voss, C.I., Souza, W.R., 1987. Variable density flow and solute transport simulation of regional aquifers containing a narrow freshwater-saltwater transition zone. *Water Resources Research* 23 (10), 1851-1866.
- Ward, D., 1991. Data input for SWIFT/386, version 2.50. Technical Report, GeoTrans, Sterling, Virginia.
- Youness, A., Ackerer, P.H., Mose, R., 1999. Modeling variable density flow and solute transport in porous medium: 2. Re-evaluation of the salt dome flow problem. *Transport in Porous Media* 35, 375–394.
- Zhang, Q., Volker, R.E., Lockington, D.A., 2001. Influence of seaward boundary condition on contaminant transport in unconfined coastal aquifers. *Journal of Contaminant Hydrology* 49, 201-215.
- Zheng, C., Bennett, G.D., 2002. Applied contaminant transport modeling. 2nd ed. John Wiley and Sons, Inc., New York.
- Zheng, C., Wang, P.P., 1999. MT3DMS: A modular three-dimensional multispecies transport model for simulation of advection, dispersion and chemical reactions of contaminants in groundwater systems. Vicksburg, Miss. Waterways Experiment Station, U.S. Army Corps of Engineers.

Acknowledgement

I wish to express my sincerest gratitude and appreciation to the following persons and institutions that have helped make this academic endeavor possible. Special thanks to my primary supervisor, Professor Kazuro Momii for his kindness, patience and understanding; and for his guidance and supervision in my experiments, simulations, scientific paper preparations and oral presentations. I also like to thank the members of my advisory committee: Dr. Kei Nakagawa, for his support and all his help especially in the modeling aspect of my research; and Dr. Masahiro Seguchi of Saga University for his encouragement and continued support. I also appreciate the valuable reviews and comments from Dr. Akira Tanaka of Saga University and Dr. Anshun Yoshinaga from University of the Ryukyus.

The Water Use Engineering Laboratory, with its students especially Dr. Yuji Ito and Yuka Yoshimitsu, provided a friendly and stimulating environment for conducting my research. I acknowledge the assistance of my lab mates Fujiyama, Kai, Funahashi, Imahase, Fujimoto, Mitsuzono and Kozono in conducting the different experiments, and to Mr. Masahiro Takahashi of Nippon Koei Co., Ltd. in the modeling exercises. I also like to thank Dr. Azuma Takagi, Dr. Hiroki Hiyama, Dr. Mizuki Hira and the students of the Land Conservation Engineering Laboratory, for the support and encouragement.

I am indebted to my parent institution, the Land and Water Resources Division, University of the Philippines Los Baños, for allowing me to go on study leave to pursue my studies here in Japan. I am grateful to Japan Ministry of Education, Culture, Sports,

Acknowledgement

Science and Technology (Monbukagakusho) for the scholarship. Special thanks also to my Nihongo teachers, and the International Students Center and United Graduate School of Agricultural Sciences staff, for their help and kindness. To my Kaikan friends Daisuke, Ben, Gia, Imran, Keiichi and Nathan, thanks for the fun and adventures.

To the Filipino students and Filipino community in Kagoshima; Christian, Lota, Shirley, Audi, Elena, Nats, Che, Mario, Hannah, Menchie, Paul, Rex, Brian, Jasmin, Harold, Erwin, Roger, Eugene, Sheila, Janice, Ma'am Da, Kuya Rod, Rande, Reyna, Billy, Necie, Mary, Joy, Ma'am Chim, Father Dino, Erica, Evelyn, Marie, Rico and all the others: thank you for the friendship and support, for the parties and travels, and for making me feel that I'm never alone even in a foreign country. I am especially indebted to Engr. Kunio Serigano, his wife Mileth, Nanay Esther (†) and kids Yumi, Kento and Kenshi, for adopting me and my wife as part of their family. Their friendship and generosity made our stay in Japan a beautiful and unforgettable experience.

To my parents, brothers and sisters, and in-laws, thank you for the encouragement and prayers and for watching over my family during my absence. To Mommy and Daddy, who instilled in me the value of education, of patience and self-sacrifice, this is the culmination of your dreams for me. I especially dedicate this work to my beautiful and loving wife, Lov, and our adoring children, Patricia Marie, Elisa Marie, John Matthew and Johanna Marie, who are my eternal source of love, joy and inspiration. Thank you for your love, prayers, patience, sacrifices and understanding.

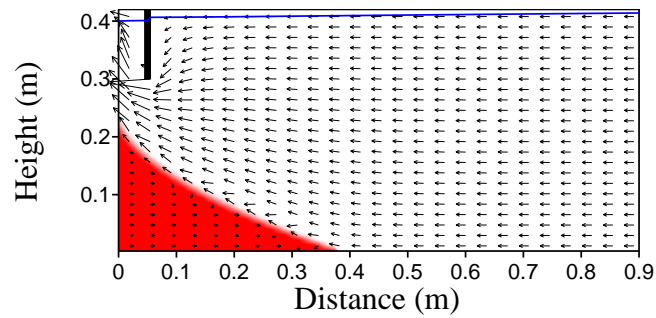
Above all, honor and glory to our Lord God Almighty. Praise you and thank you for all the blessings you have bestowed on me and my family. All my dreams and aspirations have come to fruition because of you. I offer all of these to Thee.

Appendix A

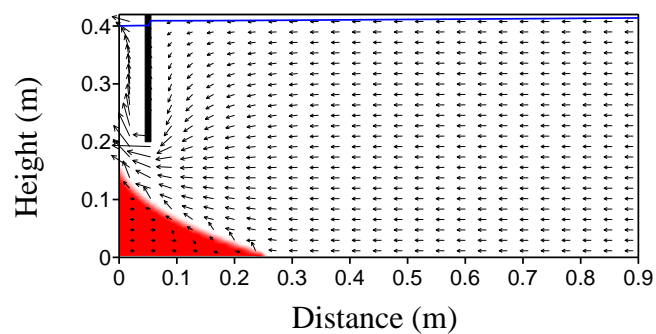
Steady State Simulation Results for the Study of

Subsurface Flow Barriers

A.1 Horizontal Barrier Location $x_b = 5$ cm

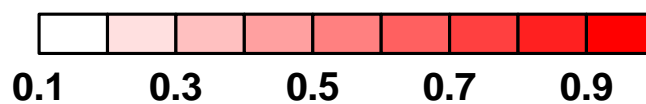


(a) Penetration Depth $d_b = 10$ cm



(b) Penetration Depth $d_b = 20$ cm

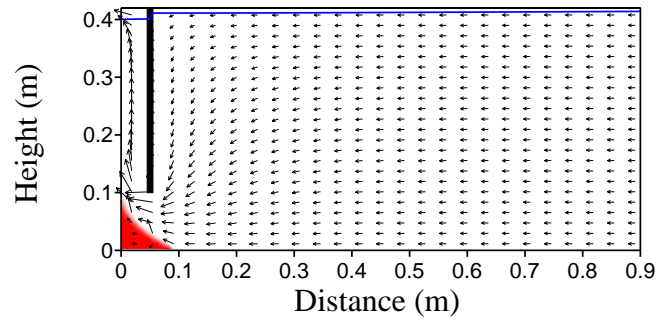
Relative Saltwater Concentration (C_{rs})



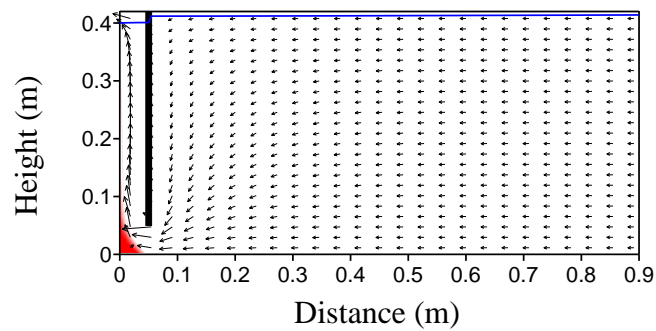
A.1 Horizontal Barrier Location $x_b = 5$ cm (continuation)

Velocity (cm/s)

1.0E-005 1.0E-001

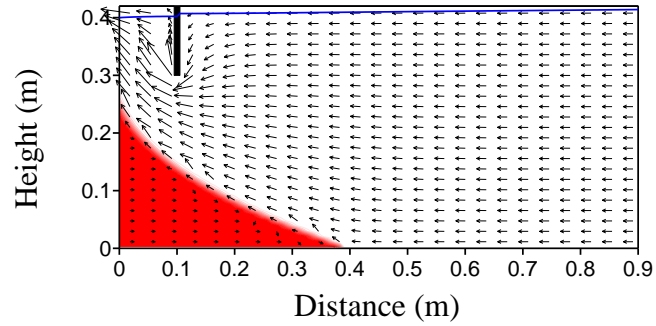


(c) Penetration Depth $d_b = 30$ cm

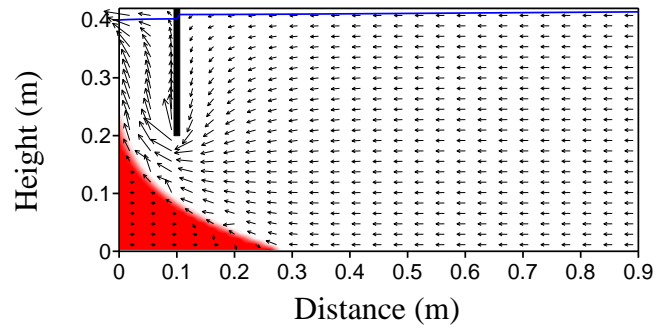


(d) Penetration Depth $d_b = 35$ cm

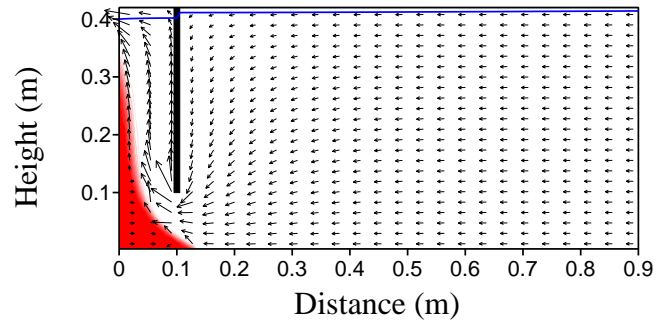
A.2 Horizontal Barrier Location $x_b = 10$ cm



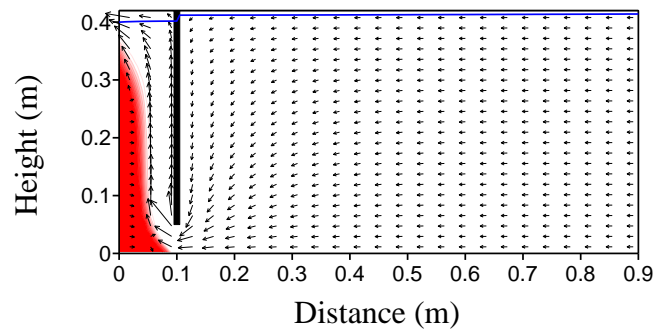
(a) Penetration Depth $d_b = 10$ cm



(b) Penetration Depth $d_b = 20$ cm

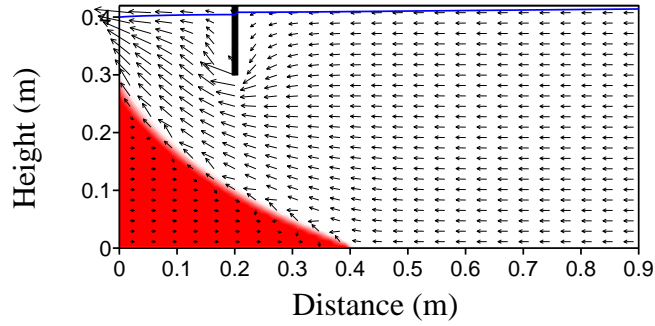


(c) Penetration Depth $d_b = 30$ cm

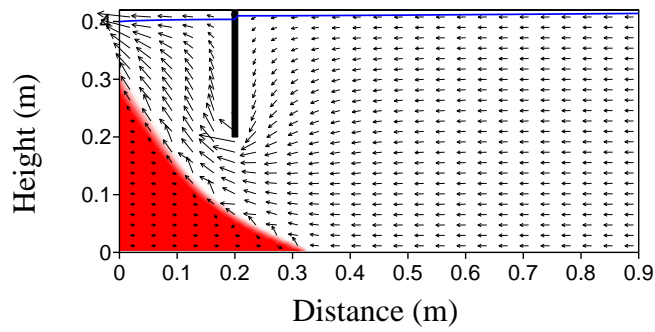


(d) Penetration Depth $d_b = 35$ cm

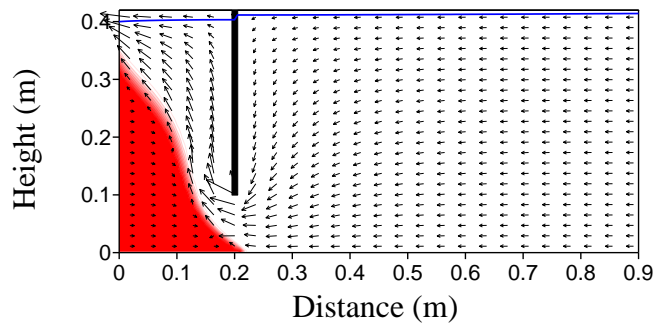
A.3 Horizontal Barrier Location $x_b = 20$ cm



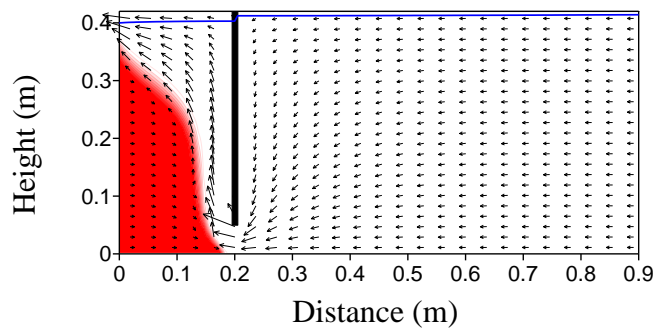
(a) Penetration Depth $d_b = 10$ cm



(b) Penetration Depth $d_b = 20$ cm

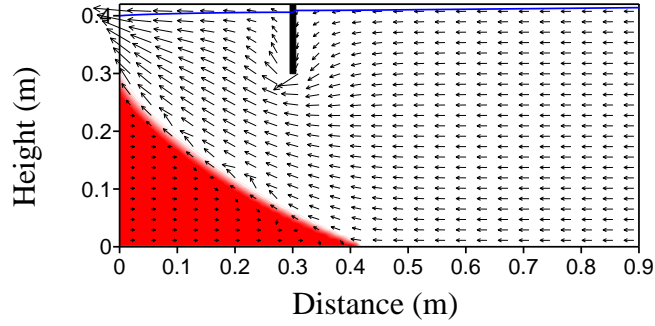


(c) Penetration Depth $d_b = 30$ cm

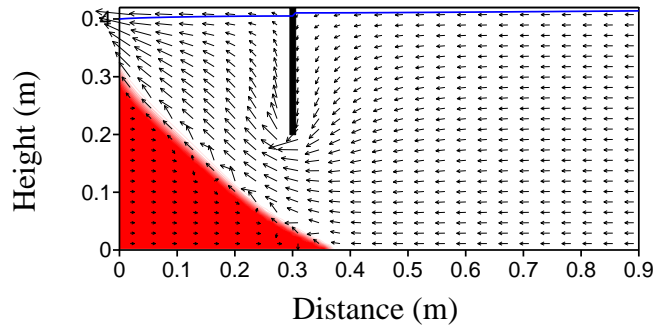


(d) Penetration Depth $d_b = 35$ cm

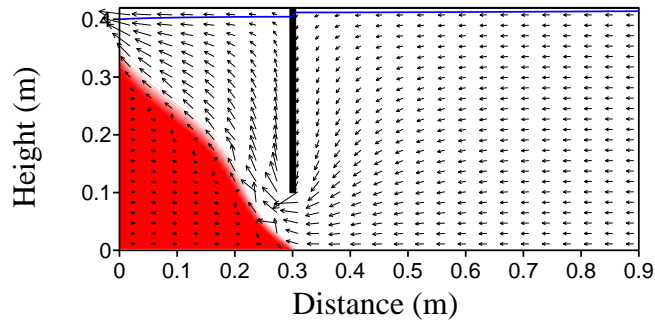
A.4 Horizontal Barrier Location $x_b = 30$ cm



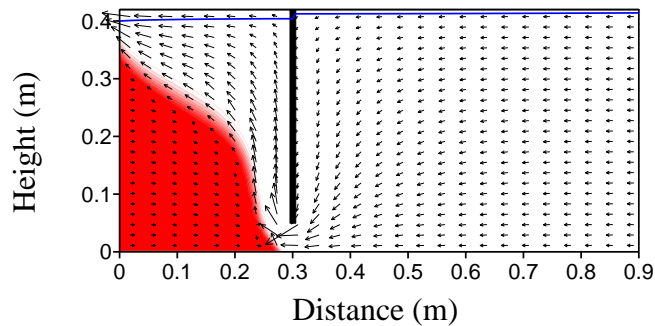
(a) Penetration Depth $d_b = 10$ cm



(b) Penetration Depth $d_b = 20$ cm

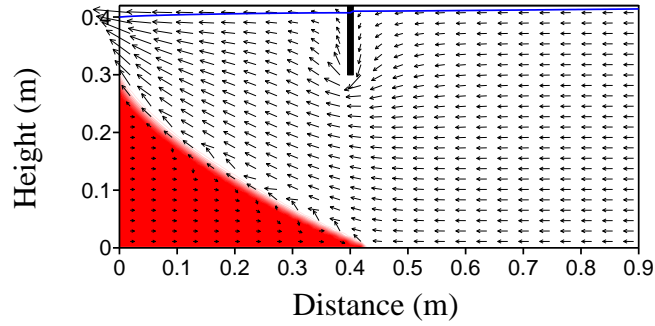


(c) Penetration Depth $d_b = 30$ cm

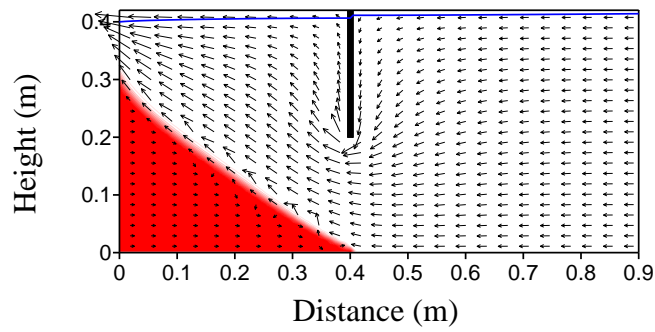


(d) Penetration Depth $d_b = 35$ cm

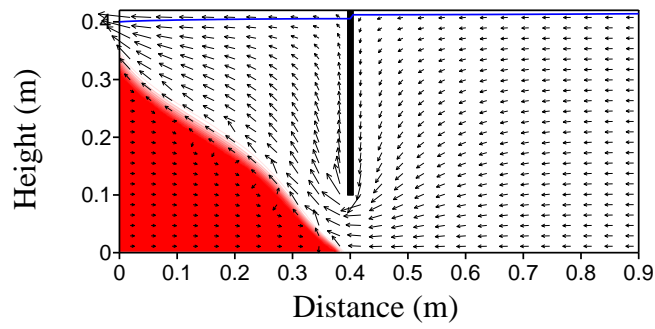
A.5 Horizontal Barrier Location $x_b = 40$ cm



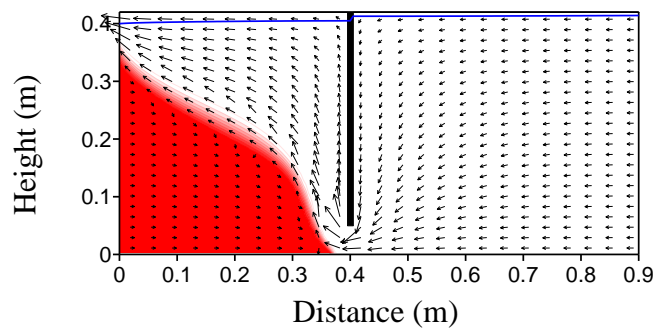
(a) Penetration Depth $d_b = 10$ cm



(b) Penetration Depth $d_b = 20$ cm

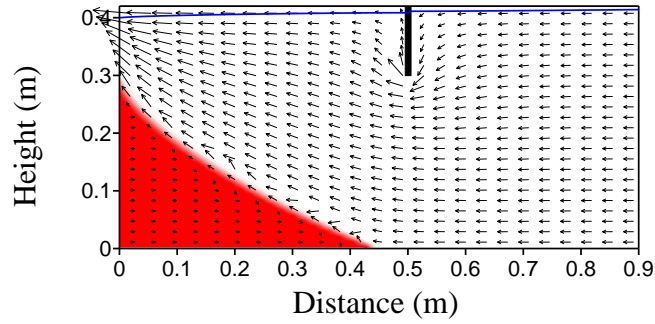


(c) Penetration Depth $d_b = 30$ cm

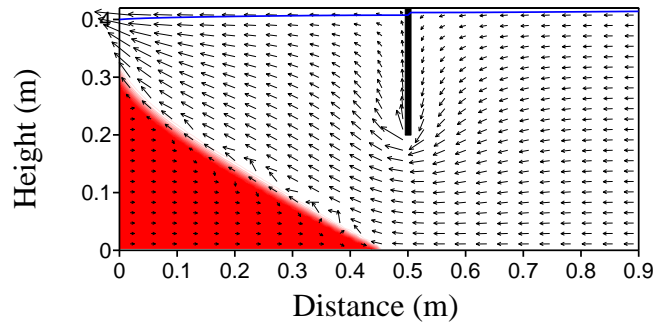


(d) Penetration Depth $d_b = 35$ cm

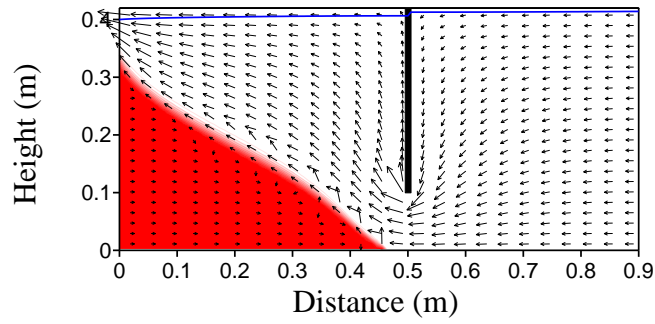
A.6 Horizontal Barrier Location $x_b = 50$ cm



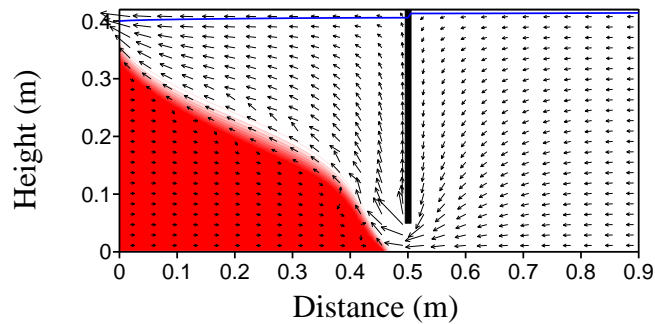
(a) Penetration Depth $d_b = 10$ cm



(b) Penetration Depth $d_b = 20$ cm



(c) Penetration Depth $d_b = 30$ cm



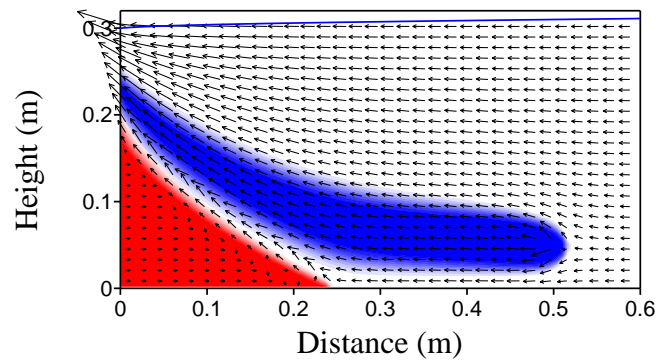
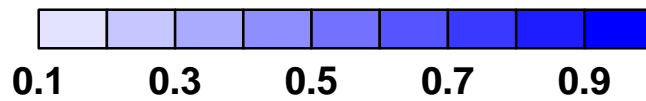
(d) Penetration Depth $d_b = 35$ cm

Appendix B

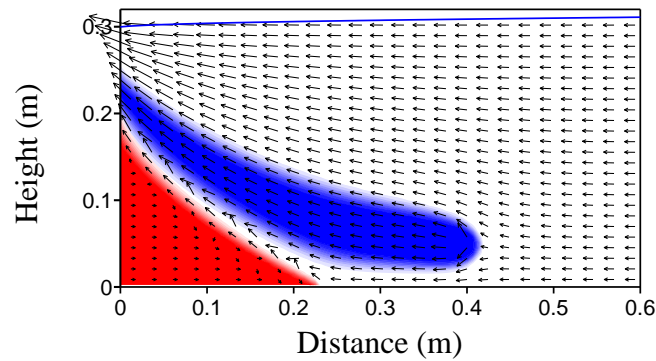
Steady State Simulation Results for the Study of Recharge Wells

B.1 Point Injection at Different Locations

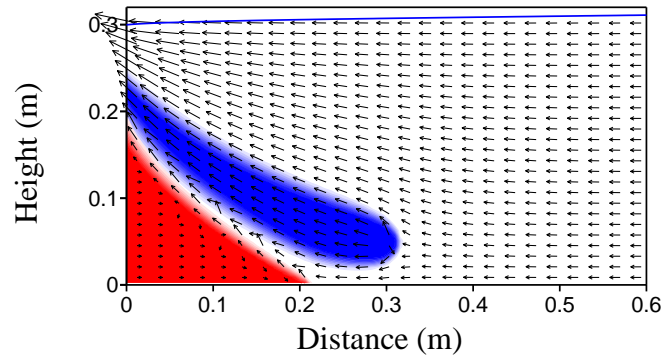
Relative Freshwater Recharge Concentration (C_{rs})



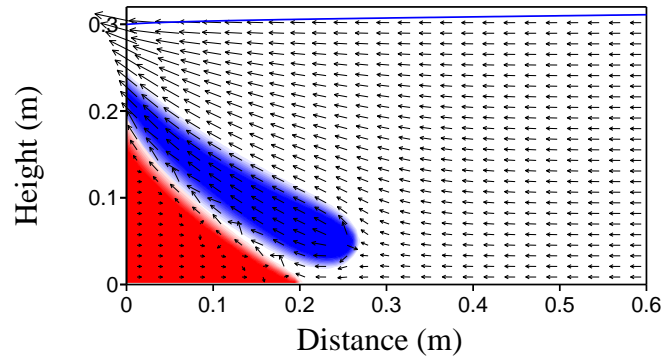
(a) $x = 50$ cm; $z = 5$ cm (Experimental Injection Point)



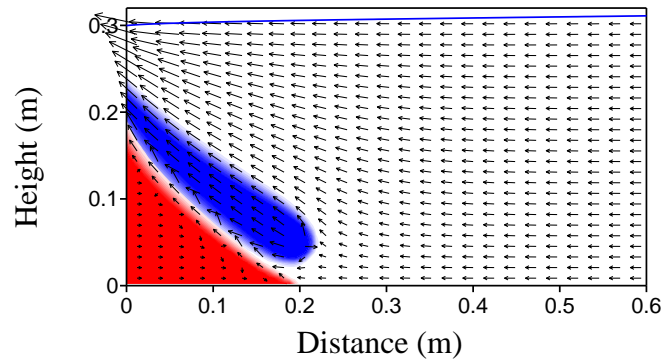
(b) $x = 40$ cm; $z = 5$ cm



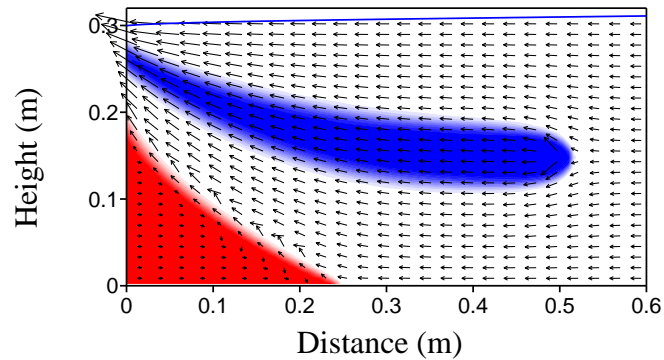
(c) $x = 30$ cm; $z = 5$ cm



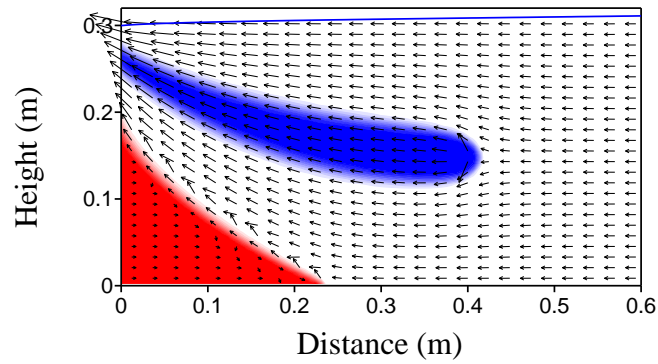
(d) $x = 25$ cm; $z = 5$ cm



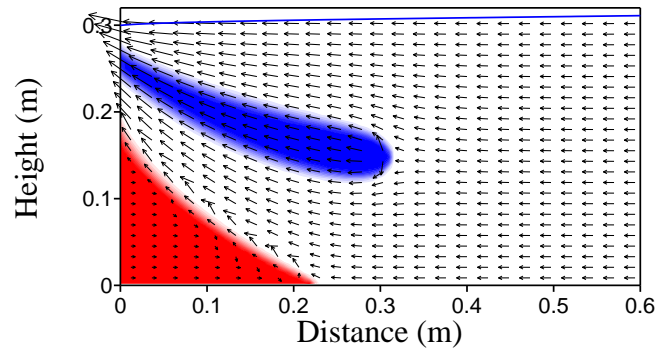
(e) $x = 20$ cm; $z = 5$ cm



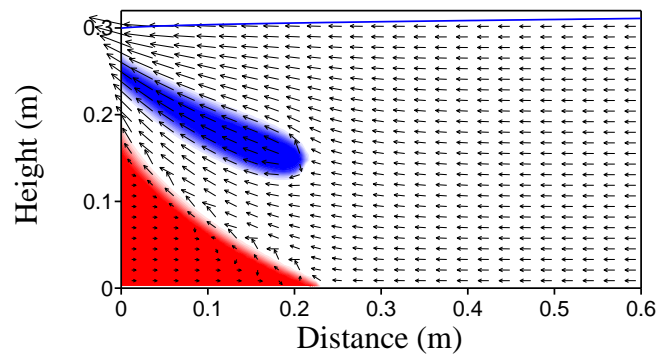
(f) $x = 50$ cm; $z = 15$ cm



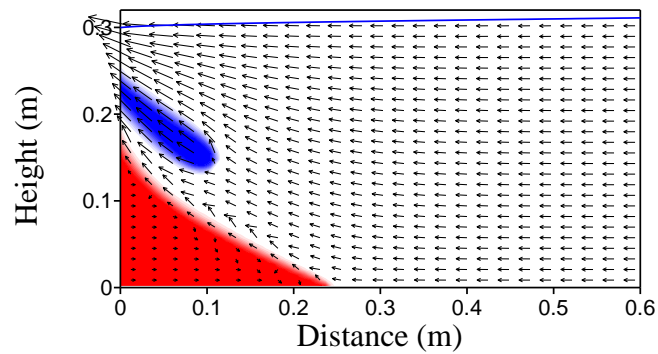
(g) $x = 40$ cm; $z = 15$ cm



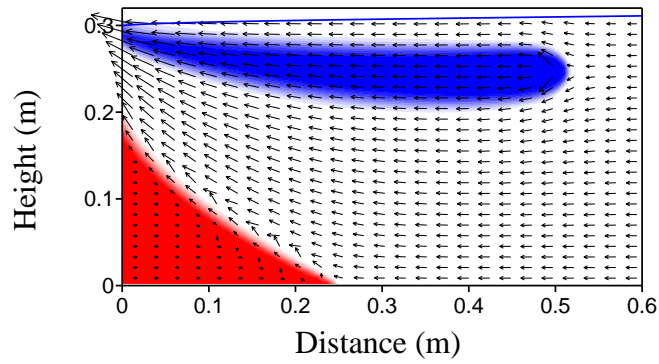
(h) $x = 30$ cm; $z = 15$ cm



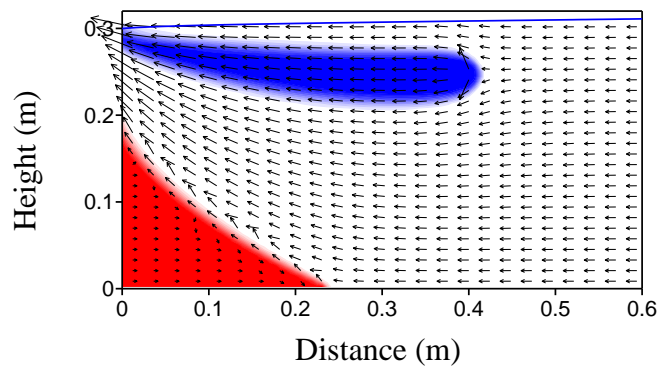
(i) $x = 20$ cm; $z = 15$ cm



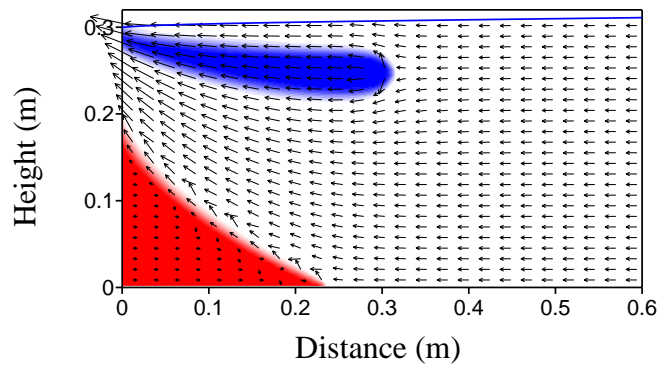
(j) $x = 10$ cm; $z = 15$ cm



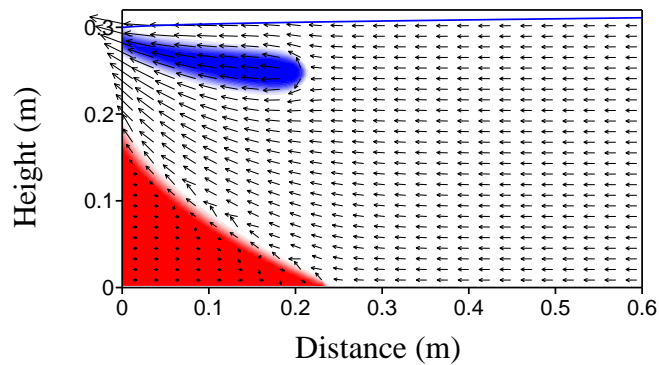
(k) $x = 50$ cm; $z = 25$ cm (represents experimental recharge pond)



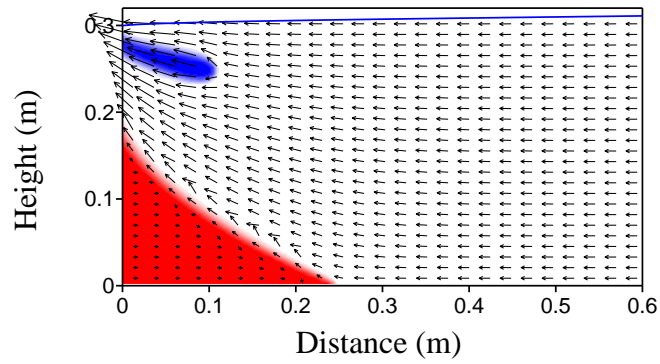
(l) $x = 40$ cm; $z = 25$ cm



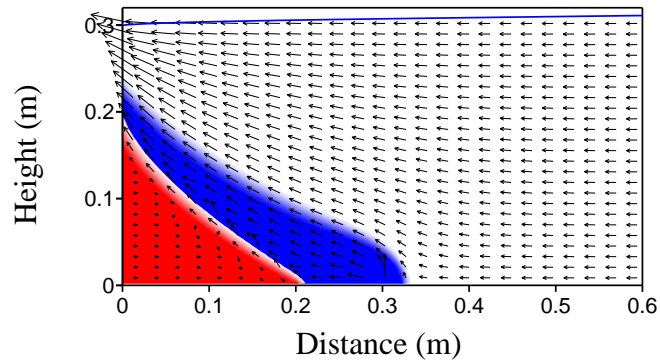
(m) $x = 30$ cm; $z = 25$ cm



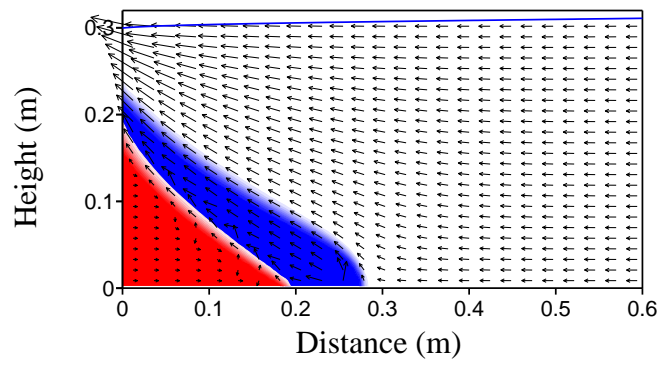
(n) $x = 20$ cm; $z = 25$ cm



(o) $x = 10$ cm; $z = 25$ cm

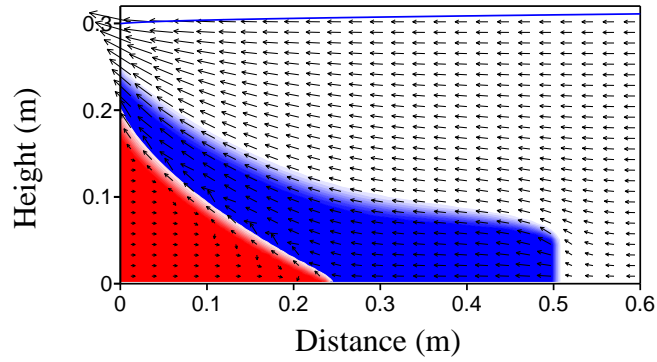


(p) $x = 30$ cm; $z = 0$ cm

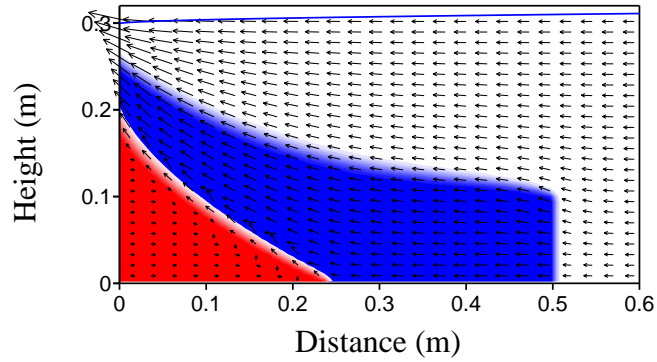


(q) $x = 25$ cm; $z = 0$ cm

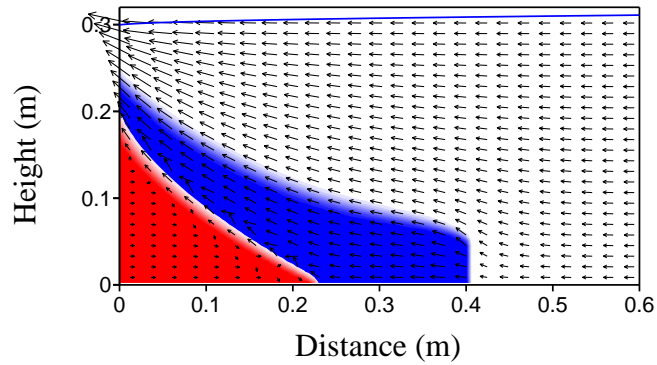
B.2 Line Injection at Different Horizontal Locations



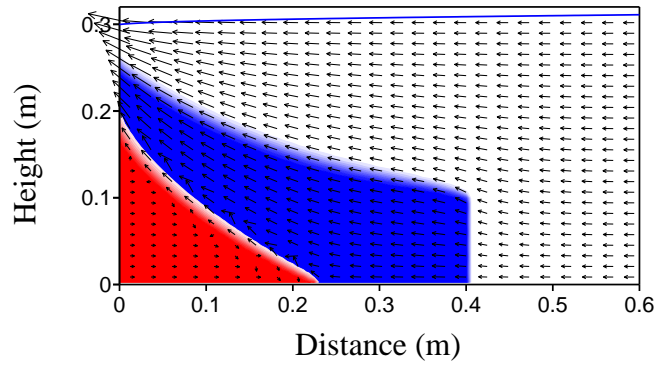
(a) 5 cm screen length at $x = 50$ cm



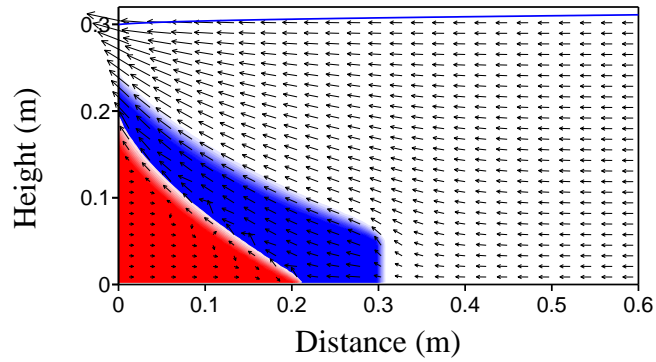
(b) 10 cm screen length at $x = 50$ cm



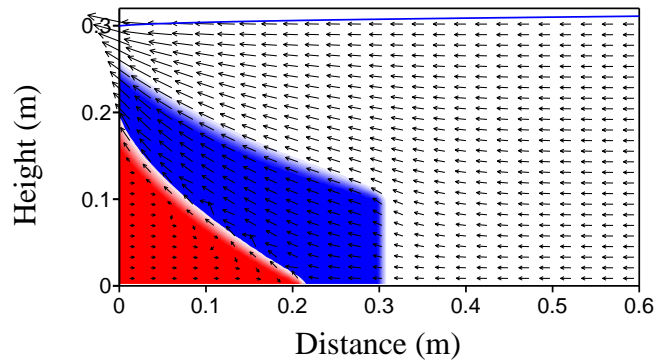
(c) 5 cm screen length at $x = 40$ cm



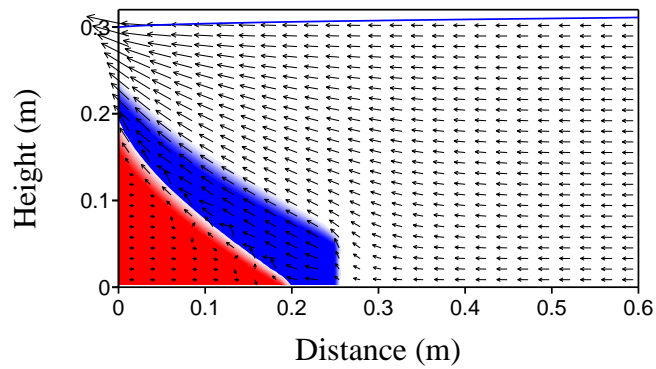
(d) 10 cm screen length at $x = 40$ cm



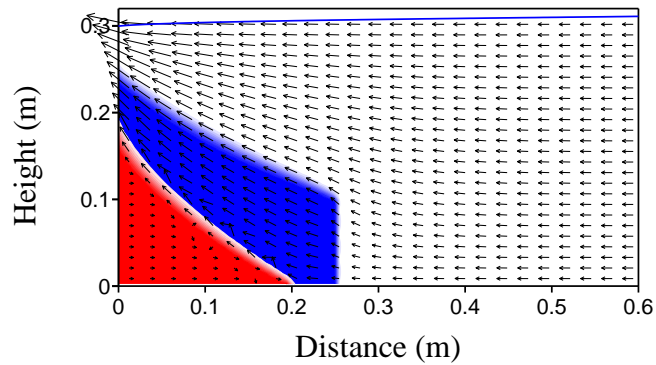
(e) 5 cm screen length at $x = 30$ cm



(f) 10 cm screen length at $x = 30$ cm



(g) 5 cm screen length at $x = 25$ cm



(h) 10 cm screen length at $x = 25$ cm

Appendix C

Japanese Abstract (日本語要旨)

海岸帯水層において淡水地下水を適切に利用するためには、海水侵入が問題となる。海岸域の人口増加に見合うだけの過剰な地下水揚水や地球温暖化による平均海水位の上昇は、海水をさらに内陸部へと侵入させることになり、淡水地下水の供給を脅かすことになる。地下止水壁と人工的な注水は、海岸帯水層における海水侵入制御手法の一つと考えられる。この手法の海水侵入制御効果について、室内実験と数値計算により検討を加えた。

地下止水壁に関しては、止水壁の貯留域に残留した海水が、内陸側からの淡水流れにより、完全に洗い出されることを実験と数値計算により明らかにした。この現象は、地下ダムが海水侵入を防ぐだけでなく、初期に塩類化している海岸帯水層における淡水の貯留と供給を改善することにも有効である。本研究により、止水壁設置位置での塩水くさびの厚さを止水壁の高さが越えていれば、残留した海水は洗い出されることが分かった。ここでの結果は、低い地下ダムを設置することにより、建設コストが節約できる可能性があることを示唆している。

また、地下止水壁を海側に近い場所で深く挿入することにより、有効に海水を海側へ押し戻すことができることを明らかにした。一方、止水壁を初期塩水くさび先端部より上流側に設置すると、止水壁の挿入に伴い、さらに海水侵入を引き起こしてしまうことを示した。止水壁の設置に伴う海水の海側への押し戻し効果は、止水壁を設置する海側からの水平距離の1次関数、及び止水壁の挿入深さの3次関数になっていることを明らかにした。本研究で検討した実験条件下での海水の押し戻し効果と止水壁設置位置との関係式を提案した。これにより、止水壁の任意の設置位置と挿入深さに対し、塩水くさび先端部の後退について定量的な検討を加えることができる。

淡水を人工的に注入する人工涵養と海水侵入制御に関する研究では、塩水くさび先端部の近傍において注水することにより、海水を海側へより有効に押し戻すことが可能であることを明らかにした。一方、注水位置が塩水くさび先端部から遠くなると効果は小さくなることから、同じ注水量であれば、海水侵入を制御するためには、地表からの涵養よりも注入井戸による涵養の方が効果的である。地表からの涵養については、最も効果的な位置は、塩水くさび先端部の直上であることを明らかにした。また、注入井戸の場合は、同一注入量の条件では、点源としての注水は、線源としての注水と同じ効果が得られることが分かった。